A technique to determine the best stellar model (mass and age) match to an observed stellar oscillation spectrum

Kevin I. T. Brown

Submitted in partial fulfilment
of the requirements for the degree of
Master of Science

Saint Mary's University
Halifax, Nova Scotia
February 2003

Your file Votre référence
ISBN: 0-612-86573-8
Our file Notre référence
ISBN: 0-612-86573-8

Table of Contents

Acknowledgements

With the completion of this thesis and my academic studies at Saint Mary's University, there are many people whom I must thank for their efforts and support on my behalf. First of all, I would like to thank my supervisor, Dr. David Guenther, for providing me with an interesting and fruitful topic for my Master of Science thesis. Dr. Guenther's instruction, comments and optimism made the field of asteroseismology a wonderful research area, one which I will continue to show keen interest. A thank you also goes to the members of my examining committee: Dr. Malcolm Butler, Dr. George Mitchell and Dr. Pierre Demarque for their time and comments on this thesis.

I would like to thank Mom, Dad and Kara for their love and support during my academic studies at Saint Mary's University. I would also like to thank Jenn for her love and support as well as her family for their company and hospitality during my stay in Halifax. I also owe a big thank you to Ray Neilson for his programming advice and assistance during my attempts to complete my own computer programs for this thesis.

My time in Halifax was a great experience and I would like to thanks the undergraduate students, graduate students and faculty members of the Astronomy & Physics department for their friendship, company and knowledge while completing my Master of Science degree at Saint Mary's University.

Abstract

Stellar non-radial oscillations (p-modes) are ideal tools to test theories of stellar evolution and to provide information about stellar properties. This thesis develops and tests a technique to determine the stellar model (which varies in mass and age only) whose pulsation spectrum best matches an observed pulsation spectrum. The best match of observed frequencies to a stellar model yields a mass and age for the observed star.

A method of direct comparison is used whereby a set of observed stellar p-modes are compared individually with p-modes calculated from stellar models. A grid of model frequencies calculated from stellar models that vary in mass and age only is required. This grid is the basis of comparison with observed stellar p-mode frequencies.

The quality of each comparison between observed frequencies and model spectra is characterized using a chi-squared best fit parameter where a low value denotes a good match. An overall minimum from the comparison of observed frequencies and model spectra identifies the best fit stellar model; therefore predicting mass and age values.

Initial debugging tests of this frequency searching technique are performed using model generated stellar p-mode frequencies. Testing indicates the requirement of high resolution in mass and age for a grid of model frequencies. This condition is necessary to provide sufficient resolution to the calculated chi-squared results. Linear interpolation of model frequency in age is utilized to increase the grid resolution in age. Tests with increased grid resolution show good results with smooth variation in calculated chi-squared values.

A single, blind analysis is conducted with four model generated sets of p-mode frequencies whose stellar model properties were unknown to me. This analysis

evaluates the ability of the technique to identify the unknown stellar properties of the artificial sets of frequencies. Tests are also performed using observed solar p-mode frequencies and observed stellar p-mode frequencies from observations of α Cen A.

Results show the frequency search technique is successful in determining the stellar model (or range of stellar models) whose pulsation spectrum best matches an observed set of frequencies. Mass and age estimates for solar-type stars can be constrained using only p-mode oscillation data. Future work using the frequency search technique will involve the generalization of the technique to include variation in the heavy metal composition, the helium abundance and the mixing length parameter.

List of Tables

List of Figures

List of Copyrighted Material

Chapter 1

Introduction

The goal of this thesis is to develop and test a technique that will determine the stellar model whose pulsation spectrum best matches an observed pulsation spectrum. This technique will search for the best match with stellar models that are varied in mass and age, with the composition and the mixing length parameter constant.

A computer program will be developed that will compare a set of observed frequencies with a constructed grid of model frequencies derived from stellar models. All frequencies will be compared individually and the comparison will be evaluated using an appropriate best fit parameter. Matches between observed and model frequencies will be determined through a defined criterion.

Debugging tests of the technique will be conducted using artificially generated observed frequencies with known stellar properties. These tests will determine if the technique works. Additional tests will be conducted using artificially generated frequencies with unknown stellar properties (a single, blind analysis), observed solar p-mode frequencies and observed stellar p-mode frequencies from α Cen A.

Solar non-radial oscillations are observed to high accuracy and have provided fundamental information about the physical characteristics and internal structure of the Sun. P-mode non-radial oscillations are predicted and known to exist on solar-type stars. Since the characteristics of p-mode oscillation depend on the physical properties

of the host star, utilizing stellar p-modes as indicators of stellar properties[1] (e.g. mass, age, luminosity, effective temperature, composition and mixing length; see § 2.1) represents a useful research tool for stellar astrophysics. This thesis develops and tests a technique where stellar, p-mode non-radial oscillations are used to constrain stellar properties; specifically the properties of mass and age.

This chapter provides the nomenclature and theoretical background for non-radial oscillations studied by this thesis.

1.1 Fundamentals of Stellar Non-radial Oscillation

Oscillations are common phenomena in nature. Familiar 1-D examples include the vibrations of a string or of a pipe organ. Such 1-D oscillations are described by sine waves. A 2-D example of oscillations is modes observed on the surface of water, induced by some vibration (driving mechanism). Stellar non-radial oscillations (p-modes) are 3-D examples of oscillations. In 3-D, the angular dependence of the non-radial oscillations are described by spherical harmonics which characterize the oscillation pattern on the stellar surface and interior.

A classical review of oscillations is found in Ledoux and Walram (1958), while Unno et al. (1989) offer a general explanation of stellar oscillations. Additional reviews of oscillations relevant to helioseismology and asteroseismology include Cox (1980), Christensen-Dalsgaard and Berthomieu (1991), Gough (1993), Brown and Gilliland (1994) and Christensen-Dalsgaard (1998; 2002). This section provides a brief

[1] Stellar properties are required to study the characteristics of individual stars, stellar populations and galaxies. Accurate stellar properties are required to construct detailed stellar models and to obtain unobservable stellar properties (e.g. age, helium composition, mixing length; see § 2.1).

discussion of the fundamentals of stellar pulsation used in helioseismology and asteroseismology.

For the case of a spherically symmetric, non-rotating star which undergoes a small perturbation to the mean state of the star, the perturbation may be described by the following equation,

$$\xi(r,\theta,\phi,t) = \xi_{nl}(r)Y_l^m(\theta,\phi)e^{-i\omega_{nlm}t}. \qquad (1.01)$$

In equation 1.01, ξ is a scalar perturbation associated with a pulsation mode (e.g. radial, pressure, or gravitational potential displacement), ω_{nlm} is the angular frequency of the propagating wave and $Y_l^m(\theta,\phi)$ are the spherical harmonics represented by,

$$Y_l^m(\theta,\phi) = (-1)^m C_{lm} P_l^m(\cos\theta)e^{im\phi}. \qquad (1.02)$$

In equation 1.02, P_l^m is an associated Legendre function of degree l and azimuthal order m, C_{lm} is a normalization constant, θ is the co-latitude, ϕ is the longitude, r is the radial coordinate and t is the time (Brown and Gilliland 1994).

In the spherical harmonic description of a small perturbation, l represents the degree of a mode and is a measure of the number of nodal lines along a meridian on the surface of a star. The value of the degree l is $l \geq 0$. The azimuthal order is represented by m, and corresponds to the number of nodal lines along the equator on the surface of a star. The value of the azimuthal order ranges from $m = -l$ to l. The radial order, n, represents the number of nodal lines from the centre of a star to the surface. Radial order is not directly observable since it deals with depth information. For p-modes, n will have values ≥ 1. Figure 1.1 presents six pictorial examples of spherical harmonics on the surface of a star for differing values of l and m.

The angular frequency of equation 1.01 is related to frequency by the relation,

$$\omega_{nlm} = 2\pi\nu_{nlm} . \qquad (1.03)$$

For a spherically symmetric star, mode frequencies are independent of m and depend only on l and n. Rotation, a magnetic field or the presence of any phenomena which breaks spherical symmetry will eliminate the independence of m (Brown and Gilliland 1994). In this thesis, all stellar models are assumed to be spherically symmetric, non-rotating, without a magnetic field, thereby eliminating m from the description of p-mode frequency.

1.2 p- and g-modes

Pulsation theory predicts two types of modes which may propagate within a stellar interior and outer envelope. These modes are p-modes and g-modes. The locations of mode propagation and the type of modes are defined by the physical properties of a stellar interior.

P-modes are sound waves, where the dominant restoring force is pressure. Such modes are found to propagate within the outer regions of stars (e.g. outer convective envelopes) where they are driven by the stochastic excitation of convection. P-modes have maximum amplitudes within outer convective envelopes. This thesis focuses on stellar p-modes.

G-modes are gravity waves, where the dominant restoring force is gravity. These modes are found to propagate within the interior regions of stars (e.g. stellar radiative cores) and are damped in convective regions. G-modes are observed on white dwarf stars and are predicted to exist in solar-type stars. If observed, g-modes would

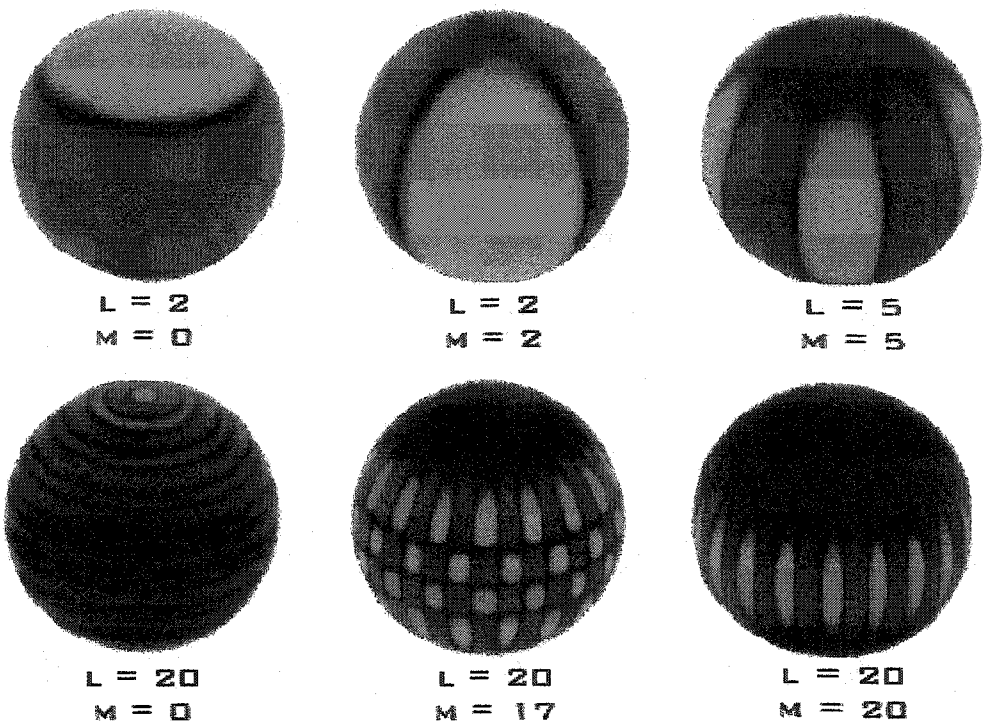

Figure 1.1: The above figures present six pictorial examples of the spherical harmonics for differing values of l and m on a stellar surface. The blue areas are regions moving towards the observer whereas the red areas are regions moving away from the observer. The axis of rotation has been titled forward to provide a clear perspective. (http://bison.ph.bham.ac.uk/)

provide valuable information about the cores of solar-type stars (Demarque and Guenther 1999).

1.3 Asymptotic Theory for p-modes

Under the assumption that the radial order is much greater than the degree (i.e. $n \gg l$), asymptotic theory of oscillation frequencies provides simplified formulae for characterizing frequency behaviour to lowest order. The use of asymptotic theory is beneficial since solar-type p-mode observations are restricted to low-l values of $l = 0$, 1, 2 and 3. Additional discussion and information about asymptotic theory and asymptotic theory for p-modes are found in Cox (1980), Tassoul (1980), Brown and Gilliland (1994), Christensen-Dalsgaard (1998; 2002), and Guenther (2002).

To second order, Tassoul (1980) characterizes p-mode frequencies for $n \gg l$ by the relation,

$$\nu_{nl} = \frac{\omega_{nl}}{2\pi} \cong \left(n + \frac{l}{2} + \frac{1}{4} + \beta\right)\Delta\nu - (AL^2 - \varepsilon)\frac{\Delta\nu^2}{\nu_{nl}} \tag{1.04}$$

where

$$\Delta\nu = \left(2\int_0^R \frac{dr}{c_s}\right)^{-1}, \tag{1.05}$$

$$A = \frac{1}{4\pi^2\Delta\nu}\left(\kappa - \int_0^R \frac{dc_s}{dr}\frac{dr}{r}\right). \tag{1.06}$$

In equations 1.04, 1.05 and 1.06, β, ε and κ are constants that depend on the structure of the stellar surface layers, R is the radius of the star, and $L^2 = l + 1/2$. A second order expansion of a p-mode frequency is required to infer stellar structure.

Equation 1.04 predicts a uniform spacing for p-mode frequencies. The large frequency spacing is defined as,

$$\Delta_{nl} \equiv \nu_{nl} - \nu_{n-1,l} \ . \tag{1.07}$$

To leading order (assuming $n \gg l$), Δ_{nl} (equation 1.07) is proportional to $\Delta\nu$ (equation 1.05). Based on this relationship, the large frequency spacing depends primarily on the run of sound speed (c_s) within the surface layers of a star. For an ideal gas, the sound speed may be characterized by the following relation,

$$c_s^2 \cong \frac{k_B T}{\mu m_H} \tag{1.08}$$

where k_B is the Boltzmann constant, μ is the mean molecular weight and m_H is the atomic weight of hydrogen. The large frequency spacing provides a measure of the time taken by a p-mode to cross the diameter of a star and is an indicator of stellar radius (Isaak and Isaak 2001). Observationally the large frequency spacing is obtained from a Fourier transform of a power spectrum of stellar oscillations. (Guenther 2002)

A second frequency spacing present in a p-mode spectra is the small frequency spacing, which is defined as,

$$\delta_{nl} \equiv \nu_{nl} - \nu_{n-1,l+2} \ . \tag{1.09}$$

The small frequency spacing (equation 1.09) is related to equation 1.04 through the relation (Tassoul 1980),

$$\delta_{nl} = \delta\nu_{nl} \cong -(4l+6)\frac{\Delta\nu}{4\pi^2 \nu_{nl}} \int_0^R \frac{dc_s}{dr}\frac{dr}{c_s} \ . \tag{1.10}$$

Equation 1.10 shows the small frequency spacing depends predominately on the derivative of sound speed within the stellar interior, resulting in sensitivity to the

structure of a stellar core. The small frequency spacing is an indicator of evolutionary state and is sensitive to helium and heavy metal abundances (Guenther 2002).

The usefulness of the large and small frequency spacing decreases with evolution off the main sequence. As evolution continues, the mode bumping of p-modes by g-modes perturbs individual frequencies to the point of contaminating the regular frequency spacing (Guenther 2002). Figure 1.2 presents a schematic of the regular frequency spacing for modes l = 0, 1, 2 and 3 in a plot of amplitude versus frequency. Indicated in figure 1.2 are the large and small frequency spacing plus the individual frequency arrangement for a p-mode spectrum.

1.4 Oscillations & Fundamental Properties

The characteristics of individual p-mode frequencies are set by the physical properties of their host star. The large and small frequency spacing, which are characteristics of a p-mode spectrum, are indicators of stellar radius and evolutionary state, respectively. For p-modes, it is useful to understand the reasons why these frequencies provide information about the properties of a star. This section discusses relationship between p-mode frequencies, stellar properties and stellar evolution.

Equations 1.04, 1.05, 1.06 and 1.09, show how stellar p-mode frequencies are inversely proportional to the run of sound speed integrated over the radius of a star. However, what characteristic of the sound speed provides information about stellar properties?

In equation 1.08, the sound speed is essentially determined by T/μ, the temperature and the mean molecular weight. For a star, the run of sound speed will

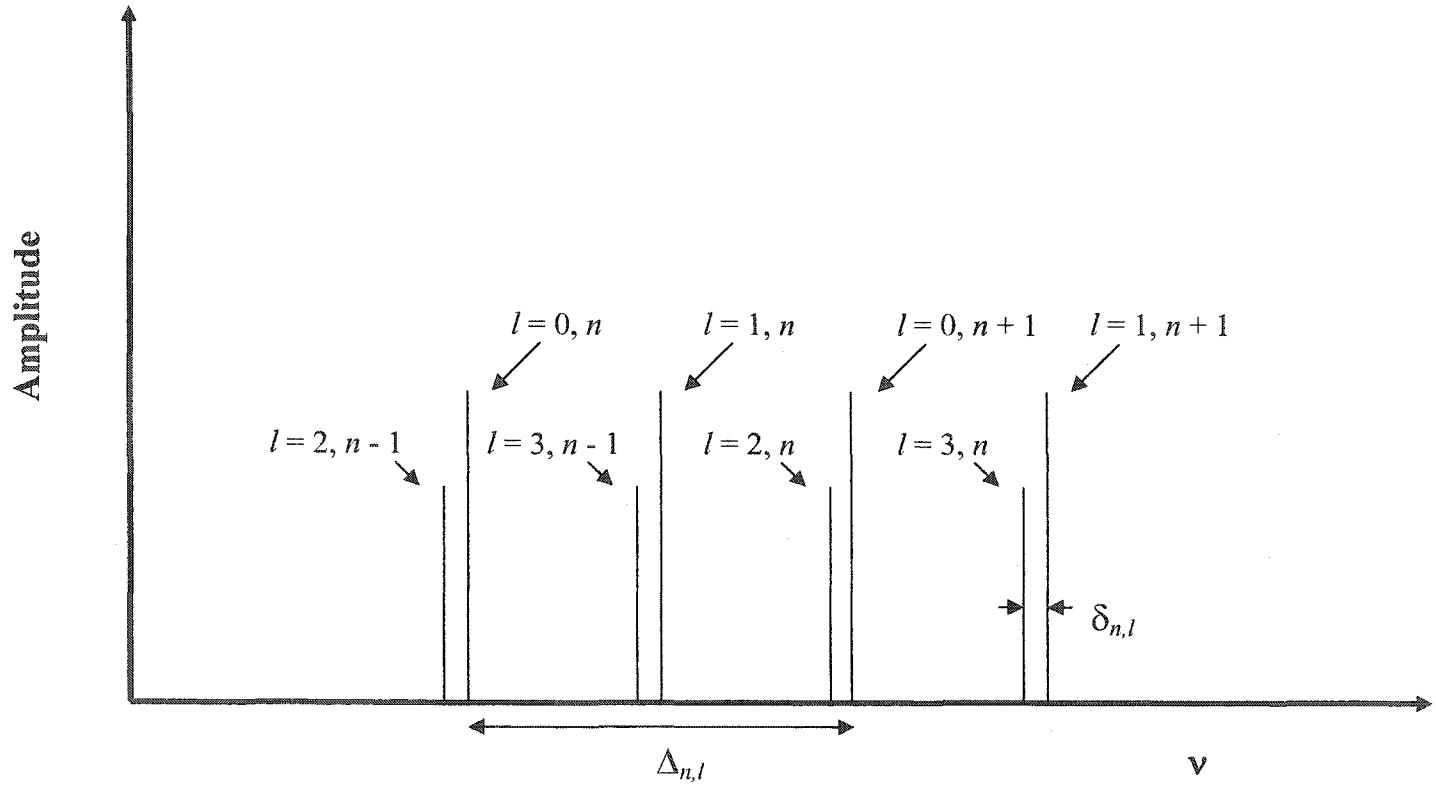

Figure 1.2: A schematic plot of amplitude versus frequency showing the regular frequency spacing for the modes l = 0, 1, 2 and 3 within a p-mode spectrum for the case of a non-rotating star. The large and small frequency spacing are indicated. The relative ordering for radial order values, n, is indicated.

decrease with radius as the temperature decreases towards the surface of a star. Applying this relationship for sound speed to equation 1.05 causes the integrand of $\int_0^R \frac{dr}{c_s}$ to increase, hence so does the contribution to the large frequency spacing, moving towards the surface. As stated in § 1.3, the large frequency spacing is related to the dynamic time scale, which is defined as,

$$t_{dyn} \cong \left(\frac{R^3}{GM} \right)^{1/2} \cong \left(G\bar{\rho} \right)^{-1/2} \tag{1.11}$$

where $\bar{\rho}$ is the mean stellar density (Christensen-Dalsgaard 1998). From equation 1.11, the large frequency spacing is related to the mean density of a star.

Over the evolutionary history of a star, interior temperature will increase with core contraction and the mean molecular weight will increase as hydrogen is fused into helium within the core. Changes in the temperature and density of the central regions will cause the sound speed to decrease. Individual p-mode frequencies will decrease in value along with the frequency spacing. The radius of the star will increase with evolution causing the large frequency spacing to decrease. The small frequency spacing is sensitive to the evolutionary changes in the central regions of the star. During later stages of evolution (e.g. the giant branch), p-mode frequencies will have lower values, with small or no uniform frequency spacing resulting in a more compact p-mode spectrum.

Efforts to use p-mode frequencies to determine stellar properties were performed by Ulrich (1986, 1988) and Christensen-Dalsgaard (1988, 1993) who explored the sensitivity of the large and small frequency spacing to changes in mass and age. Ulrich (1986, 1988) and Christensen-Dalsgaard (1988, 1993) produced the idea of an

"asteroseismic HR-diagram" and concluded that if the heavy metal composition is well known, the large and small frequency spacing provide useful estimates of mass and age. Figure 1.3 shows an example of the summarized "asteroseismic HR-diagram" in a plot of small versus large frequency spacing. In figure 1.3, solid lines denote constant mass and dashed lines denote constant central hydrogen composition[2]. Gough (1987) states that this conclusion is too optimistic and suggests that additional constraints such as individual frequencies or traditional astronomy measurements[3] are required to obtain accurate estimates of mass and age.

Brown et al. (1994) explored the use p-mode frequencies to determine stellar properties in a more complete treatment of the problem. They show the inclusion of individual p-mode frequencies substantially improves the estimation of stellar properties.

[2] The central hydrogen composition is a measure of stellar evolution or age for the asteroseismic HR-diagram.
[3] The traditional astronomy measurements suggested by Gough (1987) include photometry, astrometry and spectroscopy.

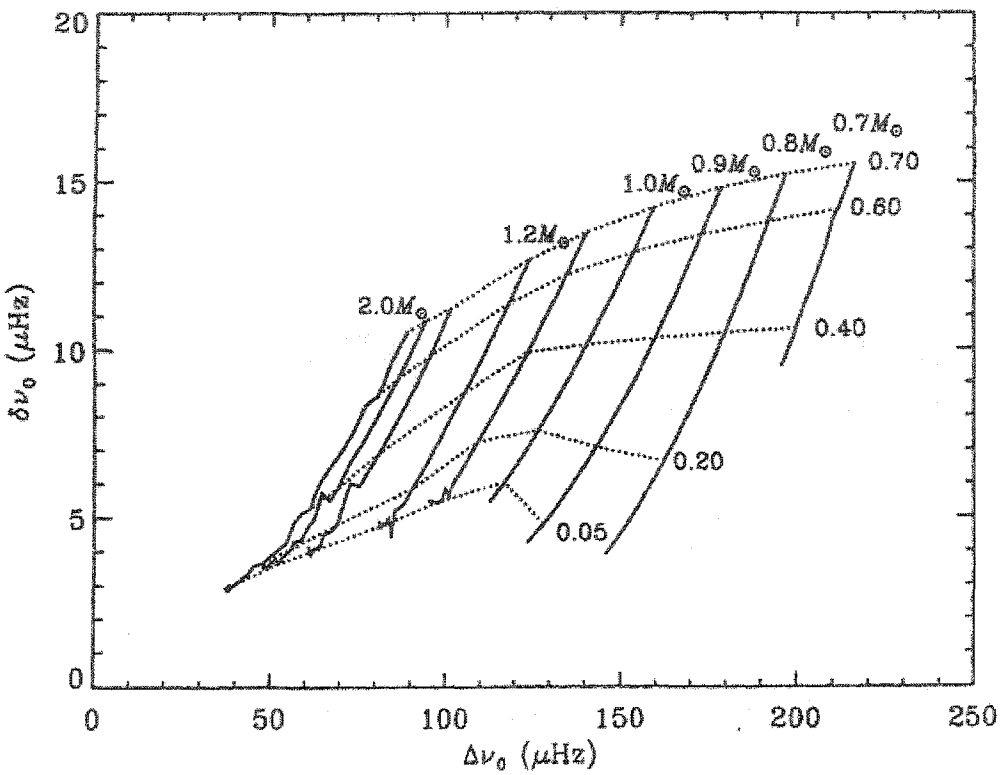

Figure 1.3: A plot of small ($\delta\nu$) versus large ($\Delta\nu$) frequency spacing showing the "asteroseismic HR-diagram" of Christensen-Dalsgaard (1993). Variation in the frequency spacing with stellar mass and age is indicated. Constant mass lines are indicated by solid lines; constant central hydrogen abundance (age) is shown by dashed lines. (With permission, from the *Annual Review of Astronomy and Astrophysics*, Volume 32, © 1994, by Annual Reviews www.annualreviews.org)

Chapter 2

Background

This chapter provides background information on stellar properties, stellar modelling and non-radial oscillation research required for this thesis.

2.1. Fundamental Properties and Stellar Modelling

Seven independent stellar properties are required to create a detailed stellar model for an individual star. These stellar properties include mass, age, luminosity (determined from distance and bolometric magnitude), heavy metal composition, helium composition, effective temperature and a mixing length parameter. This section summarizes the seven required stellar properties and the general uncertainties in their measurements.

Stellar masses are determined from astrometric observations of the orbital motions of multiple stellar systems using Kepler's third law. Masses may also be inferred using the relationship between mass and luminosity[4] (for main sequence stars only) or predicted from stellar evolution[5]. Mass measurements from well determined orbits of nearby binary systems (e.g. α Cen) have uncertainties of 5 – 10 % (Guenther and Demarque 2000).

---

[4] The mass – luminosity relationship is determined for the main sequence from observations of binary systems.

[5] This prediction is achieved by the comparison of a star's position on the HR-diagram with the predictions of stellar evolution.

Stellar luminosity is determined from the measurement of distance and bolometric magnitude. For nearby stars, distance may be determined from parallax measurements which have uncertainties of ~ 1 % or better. Bolometric magnitude is a measure of total stellar luminosity, over all wavelengths. It is calculated by applying a bolometric correction to a stellar visual magnitude, correcting for the limitations of instrumentation and the absorption of the atmosphere. The bolometric correction is calculated from stellar atmosphere fits of nearby stars. Stellar luminosities have uncertainties of 1 – 10 % for nearby stars (Guenther and Demarque 2000).

The heavy metal composition is a measure of the stellar abundance of all elements other than hydrogen and helium. The heavy metal composition for a star may be determined from a variety of techniques which include a detailed model atmosphere analysis of observed stellar spectra. Heavy metal composition measurements have uncertainties which range from 10 – 50 % (Guenther 1998).

Stellar effective temperature is the temperature of a black body that radiates with the same total luminosity per unit area as an observed star. Measurements of total luminosity and stellar radius enable the calculation of effective temperature using the Stephan-Boltzmann equation[6]. Other techniques used to evaluate effective temperature include modelling the absolute stellar energy spectrum or the use of a temperature indicator such as a colour index[7], line-depth ratios (e.g. see Gray and Brown 2001) or equivalent line-widths (e.g. see Kjeldsen et al 1995; § 2.3.1). The uncertainties in

---

[6] The Stephan-Boltzmann equation is $L = 4\pi R_{star}^2 \sigma T_{eff}^4$ where R_{star} is the stellar radius, σ is the Stephan-Boltzmann constant and T_{eff} is the stellar effective temperature.

[7] A colour index is the measured difference between stellar apparent magnitudes at two different wavelengths (e.g. B-V, U-V). Colour index provides a colour temperature, which is the temperature of a black body with the same colour index as the observed star.

effective temperature measurements are ± 20 K at best (typically ~ 50 K) (Guenther 1998).

Age is determined for the Sun from measurements of the age of the Earth and the oldest meteorites in the Solar System. Stellar ages may be inferred from stellar evolution or from qualitative correlations of age with stellar rotation, stellar activity or stellar velocities. The age estimate for the Sun has an uncertainty of ± 0.1 Gyr (Guenther and Demarque 1997).

Helium abundance (Y) and the mixing length parameter (α) are not determined from observations. Helium spectral lines are not formed at the effective temperatures present in the atmospheres of solar-type stars. The mixing length parameter is a part of the mixing length theory approximation of convection (see § 3.1). Helium abundance and the mixing length parameter are calibrated by solar models and applied to other stars.

The physical properties of the Sun are the most well determined stellar properties for any observed star. Solar mass and luminosity have uncertainties of ~ 0.1 %. The solar age is estimated to an uncertainty of ~ 1 % and the surface heavy metal composition has an uncertainty of approximately ± 5 %. The solar effective temperature is known to an uncertainty of ± 20 K, and helioseismology provides a determination of the helium abundance of the outer convective envelope to ± 0.2 % (Richard et al. 1998).

Stellar properties used to produce stellar models do not have the accuracy of solar properties and therefore are unable to produce results as detailed as current solar models. New techniques developed to determine or infer stellar properties will assist in reducing the uncertainties of stellar properties and stellar models.

2.2. Helioseismology

Helioseismology is the study and observation of global, non-radial oscillations on the surface of the Sun. Solar non-radial oscillations (p-modes) are observed to high accuracy and are diagnostic tools used to probe the solar interior, composition, dynamics and stellar evolution.

First indications of solar oscillations were observed by Plaskett (1916), who detected changes in Doppler velocity measurements of the solar surface. These observed changes were confirmed to be of solar origin by Hart (1954; 1956). Definitive observations of oscillations on the solar surface were obtained by Leighton et al. (1962). Leighton et al. (1962) observed vertical displacements on the solar surface with velocity amplitudes of ≈ 0.4 km s^{-1}, with a period of ≈ 300 seconds (5 minutes)[8]. Subsequently, the observed oscillations were described by the name, "5-minute oscillation."

The observed "5-minute oscillation" was believed to be a local phenomena occurring on the solar surface, related in some way to the observed turbulent convection occurring within the solar atmosphere. The work of Ulrich (1970) and Leibacher and Stein (1971), led to the theoretical understanding that the observed oscillations are global, surface manifestations of resonant sound waves (pressure modes or p-modes) on the solar surface. Additional elaboration on the historical development of helioseismology may be found in Christensen-Dalsgaard (2002).

Observed solar p-modes are sound waves trapped within the spherical-shell cavity of the Sun, possessing inner point turning radii that depend on the physical properties of the solar interior (Demarque and Guenther 1999). The terrestrial

[8] The 5-minute solar oscillation signal is the combination of 10^7 individual modes. Each mode has typical velocity amplitude of ~ 15 cm s^{-1} (Christensen-Dalsgaard 2002).

equivalents to solar p-modes are seismic p-waves. Solar non-radial oscillations are generally classified as "solar-type" oscillations, which are the result of stochastic excitation by turbulent convection (see Houdek et al. 1999) within the outer convective envelope. Solar-type oscillations are predicted to exist within stars on the cool side of the δ Scuti instability strip[9] where convection is expected to occur within outer stellar envelopes (Kjeldsen and Bedding 2001).

2.2.1 Results of Helioseismology

Research using the observations of helioseismology has made fundamental contributions towards understanding the Sun and testing stellar evolution. This section summarizes the observations and some key results of helioseismology.

Observations of solar non-radial oscillations identify approximately 10^7 individual modes. These p-modes have frequencies ranging from approximately 1600 μHz to 6000 μHz (e.g. see figure 2.1), and may have values of l as high as several thousand (Christensen-Dalsgaard 2002). The resolved solar disk allows the observation of p-modes with high degree, l.

Solar oscillation observations are obtained from a number of dedicated helioseismic observing facilities located throughout the world that are networked to provide continuous observation of the Sun. Networks for solar observation include BiSON (Birmingham Solar Oscillation Network; Chaplin et al. 1996) which provides disk averaged oscillation observations, and GONG (Global Oscillation Network Group;

[9] The instability strip is a narrow region of the HR diagram where the stars are characterized by pulsation. The δ Scuti instability strip is a sub-section of the instability strip characterized by evolved F-type stars found near the main sequence. δ Scuti stars exhibit both radial and non-radial oscillation. (Carroll and Ostlie 1996)

Harvey et al. 1996) which provides spatially resolved oscillation observations. Other facilities include LOWL (Tomczyk et al. 1995), IRIS (Fossat 1991), TON (Chou et al. 1995) and SOHO (Domingo et al. 1995). For additional information about helioseismic observation networks, facilities and projects see Christensen-Dalsgaard (2002) and Duvall (1995).

Current observations of solar p-modes from BiSON (Chaplin et al. 1999) are accurate up to 1 part in 10^5. An example of a disk-integrated solar power spectrum from BiSON is shown in figure 2.1. An example of a degree versus frequency ($l - \nu$) diagram is shown in figure 2.2. This plot is considered to be the most instructive presentation of observed solar p-modes. Figure 2.2 demonstrates the accuracy of observed solar p-modes and how the observed oscillation power is concentrated along ridges, fully consistent with the mode-trappings of the acoustic wave hypothesis presented by Ulrich (1970) and, Leibacher and Stein (1971) (see chapter 1).

Using accurate solar p-mode observations, helioseismic research has achieved greater understanding of the physical properties and internal structure of the Sun. Information about the structure of the solar interior is obtained through the technique of inversion whereby physical properties are obtained from observed p-modes. Reviews of inversion techniques are given by Gough and Thompson (1991) and Gough (1996). Christensen-Dalsgaard et al. (1991) show the inversion of solar p-modes provides the dependence of sound speed with depth. The maximum depth of the solar convection zone is defined by a discontinuity in sound speed where the internal temperature gradient changes from adiabatic to radiative. The base of solar convection zone is

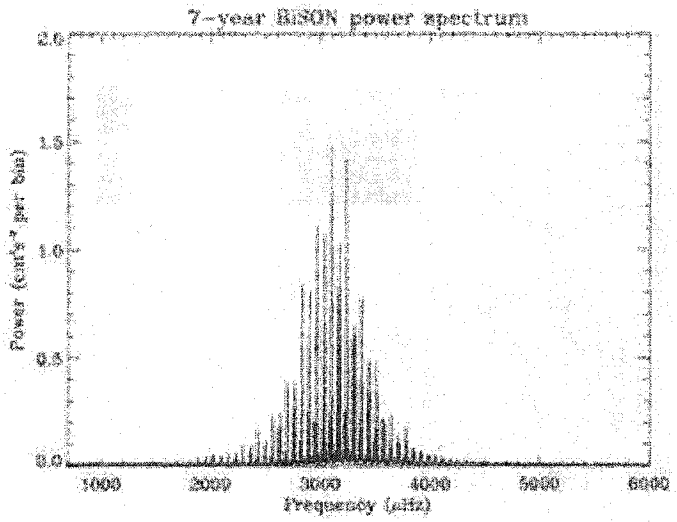

Figure 2.1: A disk-integrated solar power spectrum. This figure presents a plot of power (amplitude) versus frequency displaying the cumulative results from 7 years of BiSON observations. The shape and dominate frequencies of the solar p-mode spectrum are indicated. (http://bison.ph.bham.ac.uk/)

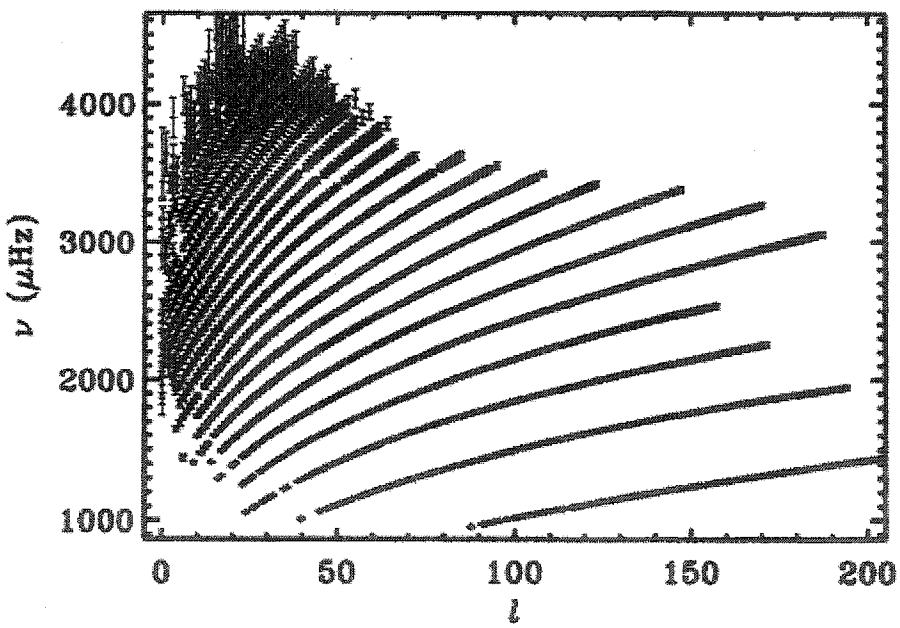

Figure 2.2: Observed frequencies of solar p-mode frequencies versus degree, *l*. The data for this plot is obtained from 144 days of Michelson Doppler Imager observations. The error bars correspond to 1000 standard deviations, with the smallest relative error being $< 3 \times 10^{-6}$. Ridges denote constant *n*. (Christensen-Dalsgaard, J. Rev. Mod. Phys., 74, 4, October (2002). © by the American Physical Society)

located at a depth of $r/R_{\odot} = 0.713 \pm 0.003$ (Christensen-Dalsgaard et al. 1991). This result was confirmed by Basu (1997).

Information about the rotation of the solar interior is determined by the inversion of intermediate and low-*l* p-mode rotational splitting. Splitting of p-modes occurs with departure from spherical symmetry (caused in this case by rotation) where p-modes are split into sets of frequencies with the same *n* and *l* values but different *m*. Rotational splitting is a function of *m*.

The analysis of p-modes exhibiting rotational splitting indicates three distinct regions of rotation within the Sun. The solar convection zone rotates differentially in solar latitude, much like the solar surface. For the solar tachocline, which is the transition between the solar convection zone and the radiative interior, rotation becomes independent of solar latitude. The radiative solar interior rotates as a solid body. (Christensen-Dalsgaard 2002)

For the outer portions of the solar convection zone, helioseismology aids in understanding the superadiabatic layer. This thin, highly turbulent layer, is currently modelled using mixing length theory (see § 3.1); however, 3-D simulations are more realistic (Nordlund and Stein 1996; Kim and Chan 1998). Helioseismic observations are required to constrain advanced model simulations of the outer solar convection zone and the superadiabatic layer (Demarque and Guenther 1999).

The inversion of p-mode frequencies also provides an independent and precise method to determine the abundance of helium within the solar convection zone. The helium abundance within the solar convection zone is determined to be $Y_{\odot} = 0.248 \pm 0.002$ (Richard et al. 1998). A determination of the solar helium abundance is important since helium is not observable within the photosphere of the Sun.

Helioseismology allows the determination of a seismic solar age. Seismic determinations of age produce results of 4.5 ± 0.1 Gyr (Guenther and Demarque 1997). This seismic age agrees with age estimates of the oldest known meteorites dated to 4.57 ± 0.04 Gyr (Tilton 1988; Bahcall et al. 1995).

P-mode observations are also capable of providing constraints for studying varying-G cosmologies. Guenther et al. (1998) use low-*l* p-mode frequencies to limit the variation of the gravitational constant over the solar lifetime. The determined limit is,

$$\approx\left(\frac{1}{G}\right)\frac{dG}{dt} < 1.6x10^{-12}\,\text{per year} \qquad (2.01)$$

and is a stronger limit than constraints determined from radar ranging and binary pulsar timing.

A fundamental success of helioseismology has been the testing of the validity of the standard solar model. The standard solar model is a numerically-constructed model of the Sun, which is constrained to the composition, luminosity and radius of the Sun, at the current solar age. Solar p-mode observations agree with the predictions of the standard solar model to better than ± 0.3 % when comparing the run of sound speed within the solar interior (Guenther and Demarque 1997). Solar neutrino fluxes observed by the Sudbury Neutrino Observatory also agree with standard solar model determinations (e.g. see Brown et al. 2003). This level of agreement demonstrates how helioseismology provides the evidence that the current physics used within the standard solar model is accurate and correct.

2.3 Asteroseismology

Asteroseismology is the extension of the tools of helioseismology to other stars. The study of stellar non-radial oscillations will expand knowledge of stellar properties and will continue to test stellar evolution.

Certain types of stars are predicted and observed to have non-radial oscillations. These types of stars are solar-type stars, white dwarfs (see Vauclair 1997; Kawaler 1998), δ Scuti stars, β Cep stars and roAp stars (Kjeldsen and Bedding 2001). This thesis focuses on the asteroseismology of solar-type stars.

The study of stellar non-radial oscillations is challenging and is distinct from the study of solar non-radial oscillations. The following points summarize the challenges for asteroseismology and the differences compared with helioseismology (see Kjeldsen and Bedding 2001):

1. Observations of stellar oscillations are limited to low-l p-modes (l = 0, 1, 2 & 3). High-l p-modes ($l \geq 4$) are not observable since stellar disks are unresolved.
2. Stellar oscillations are low-amplitude signals and solar-type stars are faint targets. Equipment used must be sensitive to low-l p-modes, must be sensitive to low amplitude signals, must be able to produce long time series observations and must be stable.
3. Stellar properties have larger uncertainties compared to solar properties. Constructed stellar models to be compared with p-mode observations will not be as accurate as solar models.
4. Solar-type stars predicted to exhibit p-mode non-radial oscillation vary in mass, age and composition. Though the Sun is the prototype for the solar-type non-

radial oscillator, other solar-type stars may prove to be more challenging to understand and to model p-mode observations.

Asteroseismology does not have the benefit of large numbers of p-mode observations. Current and future ground and space based projects will increase the available data. Ultimately, astroseismology will be used to answer more specific questions central to stellar structure and evolution which include (see Kjeldsen and Bedding 2001, Guenther 2002):

1. Determining the location of the convective core boundary[10] on the HR diagram, believed to be located around 1.1 $M_{\odot}$.
2. Locating the border between stars that possess core hydrogen-burning and stars that possess shell hydrogen-burning.
3. Testing the advanced stellar modelling details of mixing, diffusion, magnetic fields and rotation.
4. Determining stellar ages.

2.3.1 Observational techniques

To observe solar-type oscillations, astronomers have developed observational techniques which overcome the fundamental problems of detecting low amplitude signals. Individual solar p-modes possess velocity displacements of ~ 15 cm s^{-1} ($v_{osc,\odot}$ = 23.4 ± 1.4 cm s^{-1}; Kjeldsen and Bedding 1995). This velocity displacement corresponds to a wavelength shift of $\frac{\delta\lambda}{\lambda} \sim 5\times10^{-10}$, and an intensity change (caused by temperature

[10] The convective core boundary on the HR diagram represents the border between stars that possess convective cores and those which do not.

changes) of $\frac{\delta I}{I} \sim 10^{-6}$ (Guenther 1998). Observations of low amplitude signals require high sensitivity for any instrument or observational technique. Furthermore, long time series are required to achieve high frequency resolution and contiguous observations are needed to reduce aliasing[11].

There are currently three techniques used to search for solar-type non-radial oscillations in stars. They are photometry, radial velocity measurements via Doppler shifts and Balmer line equivalent widths. The following paragraphs provide a general summary of these techniques.

The photometric technique uses integrated-light (whole disk), obtained via CCD from a stellar target, to create a time series of stellar intensity fluctuations. A Fourier transform of such a time series reveals a power spectrum of any detectable stellar oscillations.

The benefits of photometry are:

1. The potential for micro-magnitude precision, which is consistent with the predicted required precision of ~ 20 - 50 μmag or $\frac{\delta I}{I} \sim 1.5 \times 10^{-6}$ for the detection of stellar pulsation signals in solar-type stars (Kjeldsen and Bedding 1995).

2. The photometric technique of detecting stellar p-modes is applicable to any star predicted to exhibit non-radial oscillations since this method involves measuring intensity variations. Spectral techniques for detecting stellar p-modes

[11] Aliasing is a problem which results from the presence of artificial frequencies within a digitized signal caused by an improper sampling rate.

require measurable spectral lines (e.g. slowly rotating stars with narrow, well defined spectral lines).

3. Photometry is sensitive to low-l p-modes.

To maximize the usefulness of photometry, observations must be conducted from space due to atmospheric scintillation. Without a large telescope at a high altitude location conducting a long time series of exposures, ground based photometry suffers from high relative intensity errors. Space based observations also achieve limited aliasing.

The second observational technique uses the Doppler shift measurement of spectral lines (radial velocity). This technique is sensitive to low-l p-modes up to $l = 3$. The benefits of radial velocity measurements are:

1. There is a large difference between the pulsation signal and convective noise in velocity measurements. This allows for high signal to noise ratios.
2. Velocity measurements are attainable on moderate size telescopes and do not require the large budgets of space based projects.
3. Insensitivity to atmospheric scintillation.

Radial velocity measurement work is limited to ground based observations. This means that radial velocity measurement observations suffer from ground based problems of non-contiguous observations which lead to aliasing.

Radial velocity measurement work requires stable, high resolution spectrographs with low background and instrumental noise. Target stars are limited to bright sources. Brown (1990) demonstrates that velocity work for measuring p-modes requires large CCDs, high resolution and the observation of many spectral lines to attain the accuracy required.

The third observational technique measures variations in the equivalent widths of Balmer lines. This technique was developed by Kjeldsen et al. (1995). Variations in the equivalent widths are the result of temperature fluctuations induced by non-radial oscillations. The relationship between equivalent width and temperature is described by,

$$\frac{\delta W}{W} \approx 6\frac{\delta T}{T}, \tag{2.02}$$

where W represents the equivalent line width (measured in parts per million, ppm). The constant of proportionality is determined from model atmosphere calculations for the Balmer lines in G and F-type stars (Kjeldsen et al. 1995; Kurucz 1979; Gray 1992).

The equivalent width technique is sensitive to low-l p-modes ($l \leq 4$), requires only moderate spectral resolution and is unaffected by atmospheric scintillation (Bedding et al. 1996). The measured signal is affected only by photon noise[12] and does not require extreme instrument stability. This technique is restricted to use with ground based telescopes and is limited to bright stellar sources.

2.3.2 Estimating Stellar Oscillations

It is useful to understand what the expected properties of non-radial oscillations will be for solar-type stars. Solar-type stars are predicted to exhibit p-mode oscillations with periods, velocity amplitudes and frequency spacing similar to the Sun. Estimates of stellar p-mode non-radial oscillation are determined by the physics of stellar oscillation and by the scaling of solar p-mode oscillation characteristics. Determinations and explanations of scaling equations are found in Christensen-Dalsgaard and Frandsen

[12] Photon noise is a signal noise due to the irregular arrival time of incoming photons. The total photon noise for a signal is the combination of target and sky photon noise.

(1983), Edmonds et al. (1992), and Kjeldsen and Bedding (1995, 2000). The following paragraphs summarize the scaling equations for solar-type p-mode oscillation.

From models calculated by Christensen-Dalsgaard and Frandsen (1983) the amplitude of solar-type p-mode oscillations, v_{osc} depends on luminosity and mass according to,

$$v_{osc} \propto \frac{L}{M}. \tag{2.03}$$

Recent work by Houdek et al. (1999) confirms the validity of this relationship for stars with approximately solar effective temperatures. Kjeldsen and Bedding (1995) determine the proportionality for scaling v_{osc} from the solar case as,

$$v_{osc} = \frac{L/L_{SUN}}{M/M_{SUN}}(23.4 \pm 1.4)\ cm\ s^{-1} \tag{2.04}$$

where $v_{osc,\odot} = 23.4 \pm 1.4$ cm s^{-1}.

The scaling of amplitudes of p-mode oscillation using equation 2.03 is widely adopted; however, Kjeldsen and Bedding (2001) point out that oscillations in F-type stars are not well predicted by the accepted relation. Kjeldsen and Bedding (2001) suggest revising equation 2.03 by using $g \propto M/R^2$ and $L \propto R^2/T_{eff}^4$ to rewrite the relationship as,

$$v_{osc} \propto T_{eff}^4/g, \tag{2.05}$$

with all quantities in solar units. In a plot of observed v_{osc} versus expected v_{osc}, Kjeldsen and Bedding (2001) present the differences between using equations 2.03 and 2.05 for the stars η Bootes, α Cen A, β Hydri, ζ Her, Procyon A and the Sun. For the G-type stars, little difference is shown between using the two scaling relations. Better agreement between observed and predicted v_{osc} for the F-type star Procyon A is shown

using equation 2.05. Kjeldsen and Bedding (2001) state that further data is required to explore the usefulness of equation 2.05.

Within a power spectrum of stellar oscillations, there exists a frequency with maximum amplitude, ν_{max}. The maximum frequency scales with the acoustic cut-off frequency[13] (ν_{ac}) for a star (Brown et al. 1991). Kjeldsen and Bedding (1995) show that ν_{max} scales via the relationship,

$$\nu_{\max} \propto \frac{g}{\sqrt{T_{eff}}}. \tag{2.06}$$

Using the solar value, $\nu_{max,\odot} \cong 3050$ μHz (Kjeldsen and Bedding 1995), scaling from the solar case is given by,

$$\nu_{\max} = \frac{M/M_{Sun}}{(R/R_{Sun})^2 \sqrt{T_{eff}/5777K}} 3050\ \mu Hz. \tag{2.07}$$

The maximum amplitude of a p-mode spectrum occurs near the radial order, n_{max}. The maximum of the solar p-mode spectrum is observed for p-modes with $n \cong 21$. Kjeldsen and Bedding (1995) present that n_{max} scales from the solar value as,

$$n_{\max} \cong \left(\frac{M/M_{Sun}}{(T_{eff}/5777K)(R/R_{Sun})} \right)^{1/2} \times 22.6 - 1.6. \tag{2.08}$$

The large frequency spacing is shown by Kjeldsen and Bedding (1995) to be directly proportional to the mean density of the star and scales via the relationship,

$$\Delta\nu \propto \left(M/R^3\right)^{1/2}. \tag{2.09}$$

---

[13] The acoustic cut-off frequency is minimum frequency of a propagating wave defined as, $\nu_{ac} = c_s/2H$, where H is the pressure scale height and c_s is the sound speed. The acoustic cut-off frequency defines the typical dynamical timescale for the stellar atmosphere. (Christensen-Dalsgaard 1998)

Equation 2.09 agrees with the model results of Ulrich (1986). The solar large frequency spacing is observed to be, $\Delta\nu_{\odot}$ = 134.92 μHz (Toutain and Frohlich 1992). Using $\Delta\nu_{\odot}$ and equation 1.09, Kjeldsen and Bedding (1995) show that the large frequency spacing scales from the solar case as,

$$\Delta\nu = \left(M/M_{Sun}\right)^{1/2}\left(R/R_{Sun}\right)^{-3/2} 134.92\ \mu Hz\ . \qquad (2.10)$$

2.4 The Current Status of Asteroseismology

A review by Kjeldsen and Bedding (1995) concluded that there was no clear evidence for the detection of stellar p-modes in stars other than the Sun. Since 1995, improvements in both observational techniques/instruments and stellar modelling have resulted in evidence for non-radial oscillations in stars (e.g. see Kjeldsen and Bedding 2001).

Ground based radial velocity measurements currently dominate stellar oscillation detections due to improvements in high-resolution spectrographs which are able to reach the desired accuracy levels (see Bouchy and Carrier 2001, 2002; Bedding et al. 2001). A review by Heasley et al. (1996), states that well chosen observation sites and networks of $\geq$ 4 m class telescopes will enable ground based work to remain a valuable source of future stellar oscillation data. Unfortunately, ground based work will never overcome the problems of weather, atmospheric scintillation, daily cycles, and low duty cycles; problems which are not encountered in space (Kjeldsen and Bedding 2001).

Space based observations are considered to be the dominant, future source of astroseismic data (Kjeldsen and Bedding 2001). Successful observations of α Ursa Major A and Arcturus with the WIRE 52mm star tracker telescope (see § 2.5.3, 2.5.6

and 2.6.1; Buzasi et al. 2000; Retter et al. 2002) demonstrate that space-based work is able to produce results. Additional space-based projects such as MOST, MONS, COROT and Eddington (see § 2.6) indicate there will be no shortage of future stellar oscillation observations.

Beyond observations, asteroseismology now has access to detailed stellar evolution models of individual stars which provide predictions such as internal structure, evolutionary status, and expected p-mode characteristics. Detailed stellar evolution models are available for α Cen A (Guenther and Demarque 2000; Morel et al. 2001; see § 2.5.1), Procyon A (Chaboyer et al. 1999; see § 2.5.2), η Bootes (DiMauro and Christensen-Dalsgaard 2001; Guenther and Demarque 1996; see § 2.5.4), as well as ε Eridani (see § 2.5.6), β Hydri (see § 2.5.5) and β Gem (MacDonald 2001).

2.5 Stellar Observations

To evaluate observations of stellar oscillation, Kjeldsen and Bedding (2001) discuss four classifications of observed results:

1. No obvious detection of stellar oscillations.
2. Detection of excess power within an observed power spectrum.
3. Large and small frequency spacing are observed.
4. Individual p-mode frequencies are observed.

The following subsections review the current status of stellar oscillation observations and results for individual solar-type stars. Summaries of observation histories, predictions and current observational results for individual stars are presented.

2.5.1 α Cen A

α Cen A (HR 5459; Sp = G2V; V = -0.003), located at 1.347 ± 0.003 pc (Hipparcos 1997), represents a prime target for asteroseismology study due to its close proximity, brightness, similarity to the Sun, well-determined stellar properties and the fact α Cen A is part of a visual binary system with a K1V companion (α Cen B; see Guenther and Demarque 2000). This star has received attention for both the observation of non-radial oscillations (e.g. see Kjeldsen et al. 1999; Bouchy and Carrier 2001, 2002; Bedding et al. 2002) and for the determination of detailed stellar models (e.g. Guenther and Demarque 2000; Morel et al. 2000; Thévenin et al. 2002). The physical properties for α Cen A are summarized in table 2.2. Using table 2.2 and the scaling equations from § 2.3.2, predictions of expected oscillation information are listed in table 2.3.

A tentative detection of stellar oscillations for α Cen A was made by Gelly et al. (1986) who observed values of v_{osc} = 150 cm s^{-1}, ν_{max} = 3400 μHz and $\Delta\nu$ = 165.5 μHz. These observations were later found to be inconsistent with upper limits obtained by Brown and Gilliland (1990) and Edmonds (1993) of v_{osc} < 70 - 80 cm s^{-1} and v_{osc} < 50 - 60 cm s^{-1} respectively. Observations conducted by Pottasch et al. (1992) obtained a value for v_{osc} of 3 - 5 times the solar value (70 – 120 cm s^{-1}), ν_{max} = 2900 μHz and $\Delta\nu$ = 110.6 μHz.

Kjeldsen and Bedding (1995) presented a summary of α Cen A observations and placed an upper limit to the value of v_{osc} for α Cen A at 2 - 3 times solar (45 – 70 cm s^{-1}). Later observations by Kjeldsen et al. (1999) report detection of oscillations using the Balmer-line equivalent width technique and reset the v_{osc} upper limit for α Cen A to 1.4 times solar (~ 33 cm s^{-1}). To this point in time, detections consisted of excess

Table 2.1: The physical properties of α Cen A.

Name	Value	Source
Mass ($M_\odot$).....	1.09 ± 0.01	Demarque et al. (1986)
	1.084 ± 0.008	Guenther and Demarque (2000), Yale π
	1.102 ± 0.008	Guenther and Demarque (2000), Soderhjelm π
	1.124 ± 0.008	Guenther and Demarque (2000), Hipparcos π
	1.10	Guenther and Demarque (2000)
	1.105 ± 0.007	Pourbaix et al. (2002)
$L/L_\odot$	1.45 ± 0.07	Demarque et al. (1986)
	1.557 ± 0.063	Guenther and Demarque (2000), Yale π
	1.574 ± 0.063	Guenther and Demarque (2000), Soderhjelm π
	1.595 ± 0.063	Guenther and Demarque (2000), Hipparcos π
	1.575 ± 0.063	Guenther and Demarque (2000)
	1.519 ± 0.018	Thévenin et al. (2002)
T_{eff}	5770 ± 50 K	Neuforge-Verhechke and Magain (1997)
	5790 ± 30 K	Morel et al. (2000)
$R/R_\odot$	1.21 ± 0.02	Demarque et al. (1986)
	1.258	Guenther and Demarque (2000)
	1.230	Thévenin et al. (2002)

π - parallax

Table 2.2: The predicted oscillation values for α Cen A.

v_{osc} (cm s^{-1})	ν_{max} (μHz)	Δν (μHz)	δν (μHz)	Source
----------	-----	107.9	---------	Edmonds et al. (1993)[b]
31.1 ± 2.0	2300	105.8 ± 2.7	---------	Kjeldsen and Bedding (1995)[a]
----------	-----	101 ± 3	4.6 ± 0.4	Guenther and Demarque (2000)[b]

[a] – Indicates scaled prediction.
[b] – Indicates model result.

power, an upper limit to v_{osc} and determined spacing values with no detected individual p-mode frequencies.

Additional p-mode observations were reported by Schou and Buzasi (2000) using the WIRE satellite; however, the first evidence of individual p-mode oscillations in α Cen A is presented by Bouchy and Carrier (2001, 2002). Using the radial velocity observations obtained with the CORALIE spectrograph on the 1.2m Euler Swiss telescope at La Silla Observatory, Bouchy and Carrier (2001, 2002) report the identification of 28 p-mode frequencies, with $v_{osc} \approx 31$ cm s^{-1}, $\nu_{max} = 2360$ μHz, $\Delta\nu = 105.5 \pm 0.1$ μHz and $\delta\nu = 5.6 \pm 0.7$ μHz. These values are in agreement with predicted values listed in table 1.3. An example of a power spectrum for α Cen A is shown in figure 1.3 based on the observations performed by Bouchy and Carrier (2002).

The identifications/observations of Bouchy and Carrier (2001, 2002) represent an important accomplishment for asteroseismic observations. Confirmation of the identifications of Bouchy and Carrier (2001; 2002) were made by Bedding et al. (2002). Now, the observation of α Cen A from space is a future goal. The satellites MOST (§ 2.6.2) and COROT (§ 2.6.4) will be unable to observe α Cen A due to the inclination of their respective orbits, however, observations with MONS (§ 2.6.3) are planned (Christensen-Dalsgaard 2001).

2.5.2 Procyon A (α Canis Minor A)

Procyon A (HR2943; Sp = F5IV-V; V = 0.34), located at 3.50 ± 0.01 pc (Hipparcos 1997), is a bright nearby star which is the primary of a visual binary system with a white dwarf secondary. For asteroseismology, Procyon A is of interest since it's

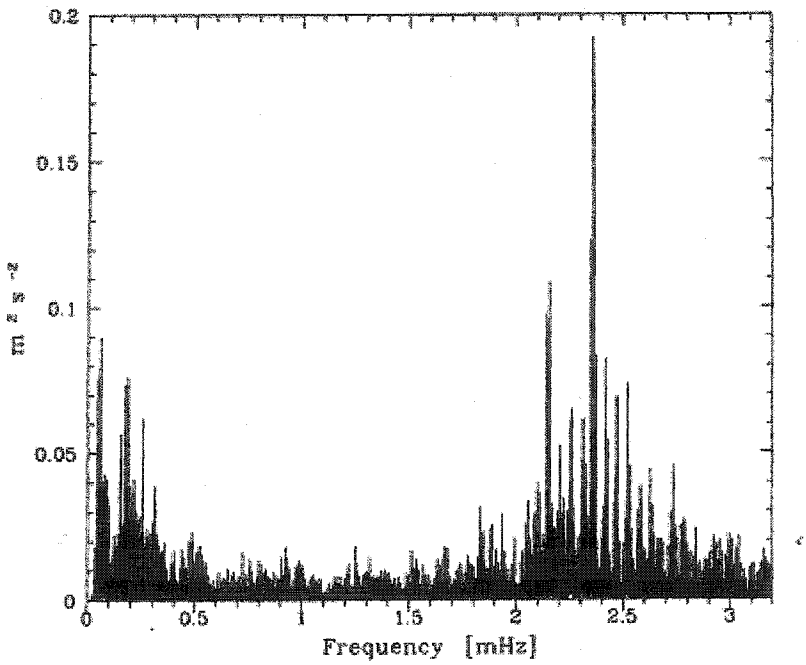

Figure 2.3: A power spectrum of α Cen A radial velocity observations. This figure presents a plot of power (amplitude) versus frequency for radial velocity measurements of α Cen A performed by Bouchy and Carrier (2002). This plot shows a p-mode power spectrum similar in characteristics to the solar p-mode power spectrum. (With permission, from *Astronomy & Astrophysics*, Volume 390, © 2002, by Astronomy & Astrophysics)

HR-diagram position predicts the presence of a thin convective zone[14], and g-modes may be observable as a result of a thin convective zone[15]. There is also uncertainty if Procyon A still possesses a hydrogen-burning core or if the star has evolved into a shell hydrogen-burning state. Asteroseismic observations will clarify this uncertainty (Chaboyer et al. 1999).

The physical properties of Procyon A are interesting due to a past discrepancy between the observed astrometric mass and the mass predicted from stellar evolution. Astrometric observations of the Procyon system placed the mass of Procyon A at 1.75

[14] With the presence of a convective zone, p-modes are predicted to exist.
[15] A thin convective zone may not completely damp-out g-modes, making their detection possible.

$M_\odot$ (Irwin et al. 1992), whereas stellar models coupled with the observed position of Procyon A on the HR-diagram predicted a mass of 1.5 $M_\odot$ (Guenther and Demarque 1993). This discrepancy was resolved by astrometric observations conducted using the Wide Field Planetary Camera 2 (WFPC2) on the Hubble Space Telescope which obtained a mass of 1.470 ± 0.045 $M_\odot$ for Procyon A (Girard et al. 1996). Further physical properties of Procyon A are $L/L_\odot$ = 7.22 ± 0.35 (Chaboyer et al. 1999), T_{eff} = 6500 ± 100 K (Guenther and Demarque 1993) and $R/R_\odot$ = 2.09 ± 0.02 (Chaboyer et al. 1999). Predicted oscillation values based on these physical parameters are listed in table 2.3.

Table 2.3: The predicted oscillation values for Procyon A.

v_{osc} (cm s^{-1})	ν_{max} (μHz)	Δν (μHz)	δν (μHz)	Source
111 ± 17	1000	54 ± 6	----------	Kjeldsen & Bedding (1995)[a] (1.5$M_\odot$)
~ 115	~ 970	~ 54.2	----------	From physical properties[a]
----------	-------	≈ 54	≈ 5	Chaboyer et al. (1999)[b]

[a] – Indicates scaled result.
[b] – Indicates model result.

Early observations of oscillations on Procyon A includes Gelly et al. (1986) who reported observation of $v_{osc} \approx 70$ cm s^{-1}, ν_{max} = 1200 μHz and Δν = 79.4 μHz from radial velocity measurements. Other early results include $v_{osc} < 100$ cm s^{-1} (Libbrecht 1988) and $v_{osc} < 400$ cm s^{-1} (Innis et al. 1991). Observations performed by Brown et al. (1991) and Bedford et al. (1993) report v_{osc} = 50 - 60 cm s^{-1}, ν_{max} = 850 μHz and Δν ≈ 71 μHz as well as $v_{osc} \approx 30$ - 100 cm s^{-1}, ν_{max} = 950 μHz and Δν = 70.6 μHz respectively. A review by Kjeldsen and Bedding (1995) argued that the observations of both Gelly et al. (1986) and Brown et al. (1991) are explainable as noise.

Good evidence for oscillations on Procyon A is provided by Martic et al. (1999) and confirmed by Barban et al. (1999). Using the ELODIE fiber-fed cross-dispersed echelle spectrograph on the 1.93m telescope at Observatoire de Haute Provence to obtain radial velocity measurements, Martic et al. (1999) report the observation of a power excess between 500 - 1500 μHz, $v_{osc} \cong 50$ - 60 cm s^{-1}, $\nu_{max} \approx 1000$ μHz and $\Delta\nu \approx$ 55 μHz. Space based observations of Procyon A are to be conducted by MOST.

2.5.3 α Ursa Major A

α Ursa Major A, hereafter α UMa A (HR 4301; Sp = K0III, V = 1.79), located at 38 pc (Hipparcos 1997), is a bright, well studied visual binary system consisting of the K0III primary and an inferred F7V secondary (see, e.g., the Smithsonian Astrophysical Observatory Star Catalogue). This star is quite different from the Sun. α UMa A is a moderately luminous red giant star with an internal structure consisting of an inert helium core, shell hydrogen-burning, and a deep convective envelope (Guenther et al. 2000). For asteroseismology, α UMa A is a target of opportunity to answer the uncertainty concerning the nature of oscillations on giant stars[16]; are the oscillations stochastically excited by the deep convection like in the Sun, or are the oscillations due to mode instability (Dziembowski et al. 2001)? There is also the uncertainty of what modes are produced in giant stars. A detailed model of α UMa A is provided by Guenther et al. (2000).

The physical properties of α UMa A are, $M = 4.25 \pm 0.25\ M_{\odot}$, $L/L_{\odot} = 316.2 \pm$ 38.6 (Guenther et al. 2000), $T_{eff} = 4660 \pm 25$ K (Taylor 1999), and $R/R_{\odot} \approx 25 - 28$ (Bell

[16] Some K giant stars are reported to exhibit periodic variability at levels of ≈ 100 m s^{-1} (Hatzes and Cochran 1994a, b; Edmonds and Gilliland 1996)

1993; Buzasi et al. 2000). Predicted oscillation values for α UMa A are listed in table 2.4.

Table 2.4: The predicted oscillation values for α UMa A.

v_{osc} (cm s^{-1})	ν_{max} (μHz)	Δν (μHz)	δν (μHz)	Source
---	---	2 – 3	---	Guenther et al. (2000)[b]
~ 1700	~ 23	~ 2.2	---	From physical properties[a]

[a] – Indicates a scaled result.
[b] – Indicates a model result.

Buzasi et al. (2000), using the WIRE satellite, reports the identification of 10 oscillation modes which are cautiously suggested to be radial, and solar-like in nature. These observed oscillations range between 1 μHz to 30 μHz and possess a mean spacing of 2.94 μHz. The range of oscillation values as well the observed spacing agrees with both the predicted values (table 2.4) and the model calculations of α UMa A performed by Guenther et al. (2000) who interpret the observed frequencies as radial (e.g. $l = 0$) p-mode oscillations of low radial order, n.

The observations of Buzasi et al. (2000) represent the first space based astroseismology observations and prove the future usefulness of space based observation projects.

2.5.4 η Bootes

η Bootes, hereafter η Boo (HR 5235; Sp = G0IV; V = 2.68), located at 11.3 ± 0.1 pc (Hipparcos 1997) is a well studied nearby star which has produced mixed asteroseismic results. This star is part of an unresolved spectroscopic binary system

with a distant companion. Detailed stellar and pulsation models of η Boo are available from Christensen-Dalsgaard et al. (1995), Guenther and Demarque (1996), and Di Mauro and Christensen-Dalsgaard (2001).

The physical properties of η Boo are, M = 1.55 ± 0.03 $M_\odot$ (Guenther and Demarque 1996), $L/L_\odot$ = 9.02 ± 0.22 (Bedding et al. 1997), T_{eff} = 6050 ± 50 K (Bell and Gustafsson 1989), and $R/R_\odot$ = 2.74 ± 0.04 (Bedding et al. 1997). Predicted oscillation values for η Boo are listed in table 2.5.

Table 2.5: The predicted oscillation values for η Boo.

v_{osc} (cm s^{-1})	ν_{max} (μHz)	Δν (μHz)	δν (μHz)	Source
160	---------	36 ± 3	----------	Kjeldsen et al. (1995)[a]
136.2	644	37.0	----------	From physical properties[a]
-------	---------	--------	2-4	Christensen-Dalsgaard (1988)[b]

[a] – Indicates a scaled result.
[b] – Indicates a model result.

Observations of η Boo were conducted by Kjeldsen et al. (1995) using the Balmer-line equivalent width technique with the data collected from the Low Dispersion Spectrograph on the 2.5m Nordic Optical Telescope at La Palma. Kjeldsen et al. (1995) claim identification of 13 oscillation modes with $\nu_{max} \approx 850$ μHz, Δν = 40.3 ± 0.3 μHz and δν = 3.1 ± 0.3 μHz. Radial velocity observations were conducted by Brown et al. (1997) to confirm the results of Kjeldsen et al. (1995) using the AFOE spectrograph on the 1.5m Tillinghast telescope at Mt. Whipple. Brown et al. (1997) failed to detect any evidence of the frequencies reported by Kjeldsen et al. (1995).

Recent observations of η Boo conducted by Kjeldsen et al. (2002) confirms the identifications reported by Kjeldsen et al. (1995). Kjeldsen et al. (2002) conducted Balmer line equivalent width observations using the ALFOSC (Andalucia Faint Object Spectrograph and Camera) on the 2.5m Nordic Optical Telescope on La Palma as well as radial velocity measurements using the Hamilton Echelle Spectrometer on the 0.6m Coude Auxiliary Telescope (CAT) at Lick Observatory. These observations confirm the earlier identifications and produced new measurements of $\Delta\nu = 40.06 \pm 0.02$ μHz and $\delta\nu = 3.85 \pm 0.28$ μHz. These spacing values are consistent with the predicted values of table 2.5.

Space based observations are planned for η Boo using MOST and MONS.

2.5.5 β Hydri

β Hydri (HR 98; Sp = G2IV; V = 2.82) is the closest G-type subgiant to the Sun, located at 7.48 ± 0.03 pc (Hipparcos 1997). This star is of prime asteroseismic interest due to its similarity to the solar spectral type, the opportunity to conduct post-main sequence evolution research, the close proximity and brightness. Dravins et al. (1993a, b, c) provide information covering overall properties and characteristics of β Hydri. MacDonald (2001) discusses in detail the evolutionary status and pulsation analysis of β Hydri.

The physical properties of β Hydri are, $M \cong 1.10\ M_{\odot}$, $L/L_{\odot} \cong 3.50$ (Dravins et al. 1993a, 1998), $T_{eff} = 5800 \pm 100$ K (Dravins et al. 1998) and $R/R_{\odot} = 1.86$ (based on Dravins et al. 1998 values). Predicted oscillation values for β Hydri are listed in table 2.6.

Table 2.6: The predicted oscillation values for β Hydri.

v_{osc} (cm s^{-1})	ν_{max} (μHz)	Δν (μHz)	δν (μHz)	Source
64 ± 7	1100	64 ± 5	---------	Kjeldsen and Bedding (1995)[a]
74.5	970	55.8	---------	From Dravins et al. (1998) values[a]

[a] – Indicates scaled result.

Observations of β Hydri for solar-type oscillations begin with Frandsen (1987). This work did not achieve the desired noise levels and an upper limit of $\frac{\delta L}{L} \sim 5 \times 10^{-5}$ for intensity oscillations was reported. Edmonds and Cram (1995) conducted further observations and again upper limits of $v_{osc} < 150$ - 200 cm s^{-1} and $\frac{\delta L}{L} \sim 2 \times 10^{-5}$ were reported.

Clear evidence for stellar oscillations in β Hydri is reported by Bedding et al. (2001). Using the radial velocity measurement technique and the University College London Echelle Spectrograph on the 3.9m Anglo-Australian Telescope, Bedding et al. (2001) claim detection of a power spectrum with a $v_{osc} \approx 50$ cm s^{-1}, $\nu_{max} \approx 1000$ μHz and $\Delta\nu = 56.2$ μHz. These results are confirmed by Carrier et al. (2001) who report values of $v_{osc} \approx 40$ cm s^{-1}, $\nu_{max} \approx 1000$ μHz and $\Delta\nu = 58$ μHz.

With evidence for stellar oscillations on β Hydri, determinations of individual frequencies are a task for future observations. Space based observations of β Hydri are planned using MOST.

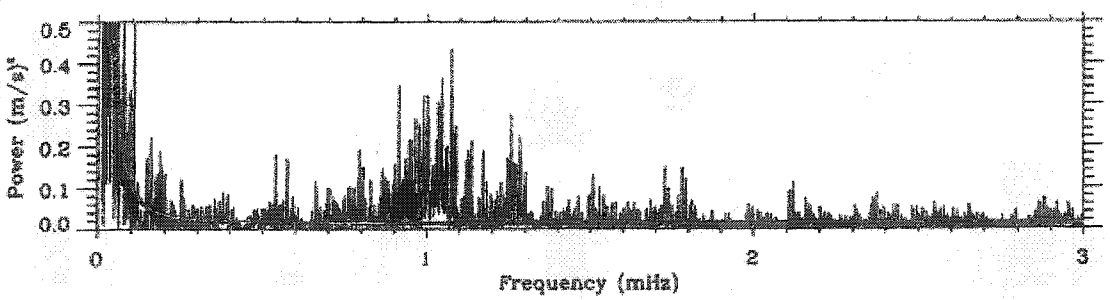

Figure 2.4: A power spectrum of β Hydri radial velocity observations. This figure presents a plot of power versus frequency for β Hydri based on radial velocity measurements conducted by Bedding et al. (2001). (With permission, from *The Astrophysical Journal*, Volume 549, © 2001, by The Astrophysical Journal)

2.5.6 Other Stars

§ 2.5.1 to 2.5.5 discuss stars which have received a great deal of asteroseismic interest and observational time. This section discusses briefly other stars which have received attention and the results which are reported.

One of the brightest stars in the northern hemisphere is Arcturus (α Boo; HR 5340; Sp = K1.5III; V = -0.04) located at 11.26 ± 0.09 pc (Hipparcos 1997). Arcturus, like α UMa A, is in the red giant stage of evolution and therefore is of interest to asteroseismology in order to study the oscillation properties of giant stars.

The physical properties of Arcturus are M = 0.7 ± 0.3 $M_{\odot}$ (Bonnell and Bell 1993), $L/L_{\odot} \cong 111$ (Hipparcos 1997), $T_{eff} = 4290 \pm 30$ K (Griffen and Lynas-Gray 1999) and $R/R_{\odot} \cong 19$ (Hipparcos 1997). Predicted oscillation values are listed in table 2.7.

Belmonte et al. (1990a) presented radial velocity measurements which indicate strong evidence for possible solar-type oscillations in Arcturus. Their observations indicate $v_{osc} \approx 6000$ cm s^{-1}, $\nu_{max} \approx 4.3$ μHz and $\Delta\nu \approx 5$ μHz. The values for the observed

v_{osc} and ν_{max} are comparable with scaled estimates; however the value of $\Delta\nu$ is much higher than predictions.

Table 2.7: The predicted oscillation values for Arcturus.

V_{osc} (cm s^{-1})	ν_{max} (μHz)	$\Delta\nu$ (μHz)	$\delta\nu$ (μHz)	Source
6200 ± 2800	4	0.9 ± 0.2	----------	Kjeldsen and Bedding (1995)[a]
~ 3700	~ 7	~ 1.4	----------	From physical properties[a]

[a] – Indicates a scaled result.

Retter et al. (2002), observing Arcturus using the WIRE satellite, report the detection of possibly 10 modes with oscillation values of $v_{osc} \cong 6000$ cm s^{-1}, $\nu_{max} \cong 4.11$ μHz and $\Delta\nu \cong 0.8$ μHz. These results are consistent with the values of table 2.7. Retter et al. (2002) conclude that the observed modes are p-modes, but are unclear as to the origin of the modes.

ε Eridani (HR 1084; Sp = K2V; V = 3.73), like α Cen A, is one of the closest solar neighbours located at 3.218 ± 0.009 pc (Hipparcos 1997). This star is of interest to astroseismology due to its proximity, prediction of solar-type oscillations and the need for better constrained physical properties.

The physical properties of ε Eridani are broad in range and are listed in table 2.8. A detailed evolution and pulsation analysis of ε Eridani is shown by MacDonald (2001). Predicted oscillations values are listed in table 2.9.

The only observations available for ε Eridani thus far are obtained from Ca II H & K measurements of Noyes et al. (1984). The signal detected was several hundred times higher than expected and contained no recognizable p-mode signature. Noyes et

al. (1984) reported a ν_{max} = 1700 μHz which is inconsistent with predictions and a $\Delta\nu$ = 172 μHz which agrees with predictions, but was determined from a few observed peaking in the power spectrum. New observations are required to test predicted model results and to constrain the physical properties of ε Eridani. ε Eridani is a planned target star for both MOST and MONS.

Table 2.8: The physical properties of ε Eridani.

Name	Value	Source
Mass ($M_\odot$)	0.80	Guenther and Demarque (1986)
	0.78	Soderblom and Dappen (1989)
	0.85 ± 0.05	Drake and Smith (1993)
	0.78 ± 0.02	MacDonald (2001)
$L/L_\odot$	0.36 ± 0.02	Guenther and Demarque (1986)
	0.33 ± 0.03	Soderblom and Dappen (1989)
	0.33 ± 0.03	Drake and Smith (1993)
T_{eff}	5180 ± 50 K	Drake and Smith (1993)
$R/R_\odot$	0.71 ± 0.04	Kjeldsen and Bedding (1995)

Table 2.9: The predicted oscillation values for ε Eridani.

v_{osc} (cm s^{-1})	ν_{max} (μHz)	$\Delta\nu$ (μHz)	$\delta\nu$ (μHz)	Source
9.1 ± 1.1	5300	204 ± 18	----------	Kjeldsen and Bedding (1995)[a]
----------	---------	170.5	----------	Guenther and Demarque (1986)[b]
----------	---------	213	----------	Soderblom and Dappen (1989)[b]

[a] – Indicates a scaled result.
[b] – Indicates a model result.

ζ Hercules (HR 6212; Sp = G0IV; V = 2.90) is a bright visual and spectroscopic binary system, located at 10.79 ± 0.07 pc (Hipparcos 1997). Stellar evolution and pulsation information for ζ Hercules is found in Morel et al. (2001).

The physical properties of ζ Hercules are M = 1.45 ± 0.01 $M_{\odot}$, $L/L_{\odot}$ = 6.55 ± 0.30, T_{eff} = 5820 ± 50 K and $R/R_{\odot}$ = 2.52 (Morel et al. 2001). Predicted oscillation information for ζ Hercules include $v_{osc} \approx 100$ cm s^{-1}, $\nu_{max} \approx 700$ μHz and $\Delta\nu = 41$ μHz. Morel et al. (2001) predicts $\Delta\nu \approx 42$ μHz. Observations of ζ Hercules conducted by Martic et al. (2001) indicate a $\nu_{max} \approx 675$ μHz, $\Delta\nu = 43.1$ μHz and $\delta\nu = 3$ μHz (Kjeldsen and Bedding 2001). These results are consistent with the predicted values.

A final star to discuss is HD 155543 (Sp = F2V, V = 6.95), located at 83.8 ± 5.8 pc (Hipparcos 1997). The physical properties of the star using Hipparcos data are M = 1.35 ± 0.05 $M_{\odot}$ (Belmonte et al. 1990b), $L/L_{\odot}$ = 9.9 (Hipparcos 1997), T_{eff} = 6700 ± 200 K (Belmonte et al. 1990b) and $R/R_{\odot}$ = 2.34 (Hipparcos 1997). Predicted oscillation values are listed in table 2.10.

Table 2.10: The predicted oscillation values for HD 155543.

v_{osc} (cm s^{-1})	ν_{max} (μHz)	$\Delta\nu$ (μHz)	$\delta\nu$ (μHz)	Source
64 ± 18	1900	92 ± 20	---------	Kjeldsen and Bedding (1995)[a]
~ 172	~ 700	~ 44	---------	From physical properties[a]

[a] – Indicates a scaled result.

In table 2.10, there is a large change in the predicted oscillation values based on the use of Hipparcos (1997) data. Belmonte et al. (1990b) reported observing a power excess with oscillation values of $\nu_{max} \sim 2000 - 2800$ μHz and $\Delta\nu \cong 97.6$ μHz. These

results are roughly consistent with the Kjeldsen and Bedding (1995) predictions, but completely disagree with the predictions determined using the current estimates of the physical properties.

2.6 Space Based Projects

The following subsections summarize operational, scheduled or planned space-based stellar oscillation observation projects.

2.6.1 WIRE (Wide field InfraRed Explorer)

The WIRE satellite is the first satellite to detect stellar oscillations from space (see § 2.5.3, 2.5.6). Launched in March 1999 into a sun-synchronous 96 minute orbit, WIRE was originally designed to perform an infrared survey of the sky. Suffering a rapid coolant loss after deployment, WIRE was reworked to utilize the onboard, 52mm aperture star camera, to conduct space based observations of stellar oscillations.

WIRE uses the photometric technique (see § 2.3.1) to observe stellar oscillations and is capable of observing stellar targets for up to 40 minutes per orbit with exposure times of 0.1 second duration. The satellite successfully detected solar-type oscillations on α UMa A (Buzasi et al. 2000) and Arcturus (Retter et al. 2002).

For further information on the current status and results for WIRE see http://www.ipac.caltech.edu/wire/.

2.6.2 MOST (Microvariability and Oscillation of STars)

The MOST (Matthews et al. 2000) satellite is a Canadian micro-satellite project designed to study and search for oscillations on a combination of solar-type, metal poor subdwarfs, roAp, and wolf-rayet stars. This project, which is headed by Dr. Jaymie Matthews (UBC), has been built and is scheduled for launch in April 2003.

The MOST satellite is a 65 cm x 65 cm x 30 cm, 60 kg satellite which will use the photometric technique via a 15 cm aperture to observe stellar oscillations. MOST will be located in a circular orbit at an altitude of 785 km and possess a contiguous observational zone of ~54 degrees. The satellite will spend up to 40 days on targets, but will be confined to observable range of declination -18 degrees to +38 degrees.

For further information on MOST see http://www.astro.ubc.ca/MOST/.

2.6.3 MONS (Measuring Oscillations in Nearby Stars)

The MONS (Kjeldsen et al. 2000) satellite is a Danish-led project designed to search for both stellar oscillations and extra-solar planets. MONS will be placed into an elliptical orbit with altitudes ranging from 600 to 40000 km, allowing MONS to view the entire sky. This satellite will possess a 40 cm telescope and will initially conduct observations of 20 nearby stars.

MONS is scheduled for launch in 2005. For further information see http://astro.ifa.au.dk/MONS. Note added in proof: MONS funding has been cancelled.

2.6.4 COROT (COnvection, Rotation and Planetary Transits)

The COROT (Baglin et al. 1998) satellite is a French/European project designed a search for stellar oscillations and extra-solar planets via observed transits using the photometric technique.

COROT is scheduled for launch in 2004. For further information see http://www.astrsp-mrs.fr/www/corot.html.

2.6.5 Eddington

The Eddington mission is an ESA project designed to search of stellar oscillations and extra-solar planets using photometry. Eddington will possess a 1.2m telescope and will be deployed at the L_2 Lagrange point.

Eddington is scheduled for launch no earlier than ~ 2008. For further information see http://astro.esa.int/SA-general/Projects/Eddington/.

Chapter 3

Computation and Testing

3. Introduction

This chapter presents the results of testing a technique to determine the stellar model whose pulsation spectrum best matches an observed pulsation spectrum. Hereafter, this technique will be referred to as the frequency search technique. A grid of pulsation spectra calculated from stellar models, varied in mass and age, is constructed. Frequencies from an observed pulsation spectrum are compared individually with the model frequencies from a grid of model pulsation spectra (a model frequency grid).

This chapter tests the frequency search technique using model generated p-mode frequencies (test spectra) with known (debugging tests) and unknown (a single, blind test) mass and age values. Chapters 4 and 5 will test the frequency search technique on observed p-mode frequencies.

3.1 Yale Stellar Evolution Code with Rotation (YREC)

Pulsation frequencies for this thesis are derived from detailed stellar models calculated using the Yale stellar evolution code, YREC (Yale Stellar Evolution Code with Rotation; Prather 1976; Pinsinnneault 1988; Guenther et al. 1992a, 1992b; Guenther, Kim and Demarque 1996). The YREC code solves the equations of stellar evolution (Clayton 1968) using the Henyey relaxation technique to produce a stellar

model. Opacities used in YREC are obtained from OPAL98 tables (Iglesias and Rodgers 1996) for T > 6000 K and from Alexander and Ferguson (1994) for opacities below T = 15000 K. For the transition temperature range, a weighted average from a linear ramp function is used (Guenther 2002). Current equations of state tables from Lawrence Livermore National Laboratory are also used (Rogers 1986; Rogers, Swenson and Iglesias 1996). The latest nuclear reaction cross-section values from Bahcall et al. (2001) are implemented within the YREC nuclear energy generation routine (see also Brown et al. 2003).

To calculate stellar model oscillation frequencies which are numerically accurate, approximately 600 to 750 shells are used to model the interior of a main sequence star. The required number of shells increase with evolution (age) and an equal number of shells are required for both the outer stellar envelope and atmosphere. To model a stellar atmosphere, YREC may use a grey atmosphere[17] in the Eddington approximation, a Krishna Swamy (1966) empirical fit to the observed solar T-τ relation[18], or other models including Kurucz and Harvard atmospheres.

YREC may also model the gravitational settling of helium and heavy metals. Gravitational settling within stellar models was proposed by Michaud (1970), was proved important for stars with large convection zones by Michaud (1986), and was shown to produce better agreement between observed solar oscillations and the standard solar model (Däppen and Gough 1986; Antia and Basu 1994; Guenther and Demarque

[17]The Eddington grey atmosphere is typically implemented when using YREC to model stars other than the Sun.

[18] The Krishna Swamy (1966) empirical fit to the observed T-τ relation for the Sun is typically implemented when using YREC to compute a model of the Sun or a standard solar model.

1997). The inclusion or non-inclusion of gravitational settling within the stellar models of this thesis is discussed in § 3.3, chapters 4 and 5.

Convection within YREC is modeled using mixing length theory[19] (Böhm-Vitense 1958). Mixing length theory characterizes convection by assuming that convective energy is carried in a convective bubble a distance defined as the mixing length l, after which the bubble instantaneously dissipates. This mixing length is proportional to the pressure scale height, H_p, shown in the following equation,

$$l = \alpha H_p . \tag{3.01}$$

The term α is the mixing length parameter. H_p is given by,

$$H_p = -\frac{dr}{d\ln P} . \tag{3.02}$$

and mixing length parameter is determined through the calibration of a standard solar model and have values of ~ 1.5 to ~ 2.0 depending on opacities, equation of state and atmospheric models.

Further information concerning the current use of YREC is found in MacDonald (2001) and Guenther (2002).

3.2 The Pulsation Code

The calculation of model oscillation frequencies from YREC stellar models is performed using a non-radial, non-adiabatic pulsation code provided by Guenther (1994). Using this pulsation code, an adiabatic frequency spectrum is calculated for the modes of degree $l = 0$, 1 & 2, and radial order, $1 \leq n \leq 30$. The pulsation code is capable

[19] Mixing length theory is considered to be a very crude approximation of convection. 3-D convection simulations are more desirable, but are computationally intensive.

of determining modes of high order (e.g. $l \gg 1$), however, since only $l = 0, 1, 2$ & 3 modes are observable in stars, only low-l modes are calculated.

Further discussion on the calculation of oscillation frequencies from YREC stellar evolution models using the pulsation code may be found in Guenther (1994).

3.3. Forming a Model Frequency Grid

A grid composed of stellar model pulsation spectra is used as the basis of the frequency search technique. This grid is created around a "central model" about which the properties of mass and age are varied to form the model frequency grid. The stellar models are constructed using the stellar evolution code, YREC (see § 3.1). Pulsation frequencies for the stellar models are calculated using the non-radial pulsation code discussed in § 3.2.

The central model chosen for the model frequency grid is a calibrated solar model that does not include the gravitational settling of helium or heavy metals[20]. Stellar atmospheres are modelled using a grey atmosphere in the Eddington approximation. The central model is determined by evolving a 1 $M_{\odot}$, solar Zero Age Main Sequence (ZAMS)[21] model to the current age of the Sun, calibrated to the solar radius and luminosity to 1 part in 10^6. This calibration is accomplished by varying mixing length parameter and the helium abundance within YREC until the desired accuracy in solar radius and luminosity is reached. Table 3.1 lists the determined parameters for the calibrated solar model.

---

[20] The gravitational settling of helium and heavy metals was excluded from the calculation of a calibrated solar model to obtain a grid of model frequencies from basic stellar models.

[21] All ZAMS models used in this thesis are obtained by evolving a Lane-Emden gas sphere with the appropriate mass from the Hayashi track to the ZAMS point using the YREC code (Guenther 2002).

Table 3.1: The determined properties for the calibrated solar model.

Parameter	Value
Mass	$1.0\ M_{\odot}$
Age	4.55 Gyr
X_{ZAMS}	0.70409
Y_{ZAMS}	0.27591
Z_{ZAMS}	0.02
$L_{\odot}$	3.851×10^{26} W
T_{eff}	5780 K
α	1.9064

Using the calibrated solar model values of X_{ZAMS} (hydrogen abundance), Y_{ZAMS} (helium abundance), Z_{ZAMS} (heavy metal abundance) and mixing length parameter, a grid of stellar models is created by calculating stellar evolutionary tracks within the mass range of 0.8 $M_{\odot}$ to 3.0 $M_{\odot}$, in increments of 0.1 $M_{\odot}$, for a total of 22 tracks. The stellar models are evolved in age from appropriate ZAMS models to the base of the giant branch in approximately 140 to 250 time steps per evolutionary track. Age values at the base of the giant branch for the 22 tracks range from $\approx$ 26 Gyr for 0.8 $M_{\odot}$ to $\approx$ 315 Myr for 3.0 $M_{\odot}$. The mass resolution for this grid of 22 models is 0.1 $M_{\odot}$. Additional stellar evolutionary tracks are added at 0.95 $M_{\odot}$, 0.99 $M_{\odot}$, 1.01 $M_{\odot}$ and 1.05 $M_{\odot}$ to test mass resolution effects.

The stellar model mass range of 0.8 $M_{\odot}$ to 3.0 $M_{\odot}$ spans the convective boundary between hot and cool stars. Stars on the cool side of the boundary will have convection within their outer envelopes and will manifest p-mode oscillations. The manifestation of p-mode oscillations will also depend on the evolutionary state of a star.

For the 26 stellar evolutionary tracks, approximately 50 to 120 models per track are extracted at equal spacing along the track. Pulsation frequencies are calculated for $l = 0$, 1 and $n = 1$ to 30. The extracted models set the basic frequency resolution in age for the model pulsation spectra from each individual track.

The pulsation spectra derived from the 26 evolutionary tracks forms the calibrated solar model frequency grid used for the testing of the frequency search technique.

3.4. The SEARCH Program

A computer program was developed to implement the frequency search technique. This program finds the model pulsation spectrum from a model frequency grid (varied in mass and age) that most closely matches an observed pulsation spectrum. The program, hereafter known as SEARCH, was written using a FORTRAN 77 code and is listed in Appendix A.

The SEARCH program compares the individual frequencies of an observed pulsation spectrum with the individual frequencies of a model pulsation spectrum within a model frequency grid. Model frequencies that best correspond to the observed frequencies are found. Matches between the model and observed frequencies are quantified by a matching criterion. The quality of fit for a set of matches between a model and observed spectrum is evaluated using a chi-squared (χ^2) best fit parameter. This comparison between an observed and model pulsation spectrum is performed for all model pulsation spectra of a model frequency grid.

The performance of the SEARCH program is enhanced by the application of frequency interpolation in age and a defined matching criterion. Frequency interpolation in age is included to improve the resolution of χ^2 results from the SEARCH program. A linear interpolation of frequencies is performed between consecutive model pulsation spectra of constant mass within a model frequency grid. The number of frequencies interpolated between consecutive model pulsation spectra is set as a variable parameter within the SEARCH program.

A definition of what constitutes a match between observed and model frequencies is incorporated into the SEARCH program. The matching criterion states that an observed p-mode frequency is matched only when the absolute difference between ν_{obs} and ν_{model} is a minimum and is ≤ 25 % of the large spacing frequency appropriate to the compared model pulsation spectrum.

The output for the SEARCH program is a χ^2 value for each mass and age (stellar model) of a model frequency grid. Additional output may include the model pulsation spectrum (from the model frequency grid) that most closely matches the observed pulsation spectrum.

3.5. χ^2

The SEARCH program uses a χ^2 best fit parameter to evaluate the quality of fit of identified frequency matches between an observed and model pulsation spectrum. χ^2 measures the dispersion of actual and expected values, providing an indication of whether or not two sets of data are related. In the SEARCH program, χ^2 is defined by the relation,

$$\chi^2 = \sum_{j=1}^{N} \frac{\left(\nu_{Obs}(j) - \nu_{Model}(j)\right)^2}{\sigma_{Obs}^2(j) + \sigma_{Model}^2(j)}, \qquad (3.03)$$

where N is the total number of identified matches between observed and model frequencies (for a given model spectrum), ν_{obs} and ν_{model} are the observed and model frequencies respectively, σ_{Obs} and σ_{Model} are the corresponding uncertainties in the observed and model frequencies respectively.

Values for σ_{Obs} and σ_{Model} are required. The observed frequency uncertainties are obtained from observations whereas the value for the model frequency uncertainties must be estimated. Pulsation frequencies calculated using the non-radial pulsation code are known to be numerically accurate to ± 0.1 μHz (Guenther 2002). Uncertainties in the physics of stellar models leads to uncertainties in the calculation of model frequencies which may be estimated by comparing standard solar model frequencies[22] directly with observed solar p-mode frequencies from BiSON (see table 4.2; Chaplin et al. 1999). The comparison of low-l values reveals that the discrepancy between the standard solar model and observed solar frequencies is approximately ± 0.01 μHz for low frequencies increasing to approximately ± 10 μHz for higher frequencies. This increase in the discrepancy from low to high frequency is known to be caused by the relatively crude modelling of the outer layers of the Sun. For values of n = 1 to 20, the average discrepancy is ≈ 1 μHz, and for values of n = 21 to 25, the average discrepancy is ≈ 7 μHz.

A normalized χ^2 is calculated based on following relation,

[22] The standard solar model frequency values discussed here are determined from YREC and the non-radial pulsation code. See Brown et al. (2003).

$$\chi^2_N \equiv \frac{1}{N}\chi^2, \tag{3.04}$$

where χ^2_N is the normalized χ^2 and N is the number of identified matches between observed and model frequencies. The normalized χ^2 is an output of the SEARCH program.

There are two cases which explain the basic statistical significance of the normalized χ^2 values. Case 1 involves the situation where observed and model frequencies are matched to values $\leq \left(\sigma^2_{Obs} + \sigma^2_{Model}\right)^{1/2}$. In this case, the normalized χ^2 will have values less than or equal to ≈ 1. Case 2 involves the situation where the observed and model frequencies are matched to values $\gg \left(\sigma^2_{Obs} + \sigma^2_{Model}\right)^{1/2}$. In this case, the normalized χ^2 will have values $\gg 1$.

3.6. General Testing Results

The following sections presents debugging test results of the frequency search technique using artificially generated frequencies (test spectra) with known mass and age values. Testing the frequency search technique using test spectra evaluates the results, performance and limitations of the technique.

Input for the SEARCH program consists of a model frequency grid calculated from stellar models plus an observed pulsation spectrum and corresponding observed frequency uncertainties. The SEARCH program will first find any matches between observed and model pulsation frequencies then will calculate a normalized χ^2 for the overall comparison of the observed and model spectra.

There are questions to be tested concerning the SEARCH program and the practical application of the frequency search technique. The questions to be tested and answered are:

1. Will the ability of the SEARCH program to match observed and model frequencies vary over the mass and age range of a model frequency grid? How should the results of the SEARCH program be analyzed? What information will the normalized χ^2 provide?
2. Is frequency interpolation in age (and mass) required in a model frequency grid? If so, what amount of frequency (or mass) interpolation is required?
3. What effects do observed frequency uncertainties have on the matching results of the SEARCH program?
4. What is the effect of varying the total number of observed frequencies to be matched on the matching results of the SEARCH program?
5. Are additional constraint parameters required to identify the best stellar model (mass and age) match to an observed pulsation spectrum? If so, what constraint parameters are useful?

The following sections will explore these questions in the evaluation of the frequency search technique and SEARCH program.

3.6.1. Normalized χ^2 versus Age

Five artificially generated sets of frequencies (test spectra) with differing mass and age values are obtained from the calibrated solar model frequency grid. These five spectra test the ability of the SEARCH program to obtain a match to the observed

frequency spectrum over the mass and age range of the calibrated solar model frequency grid. The SEARCH program should, in principle, find the original stellar models of the five test spectra perfectly. Table 3.2 lists an example of one of the five test spectra used in this section[23].

The results of the SEARCH program are presented in a 2-D plot of normalized χ^2 versus age. Each point in such a plot corresponds to a calculated normalized χ^2 at a specific mass and age. A line connects all data points of constant mass in the normalized χ^2 versus age plot.

Prior to discussing the analysis results using the five artificially generated sets of frequencies, figures 3.1 through 3.4 present schematic figures which illustrate the fundamentals of the SEARCH program results presented in the normalized χ^2 versus age plots. Figure 3.1 shows a schematic of the basic SEARCH results for the comparison of an observed p-mode spectrum with model spectra obtained from a single evolutionary track (a single mass). Two main features are identified: unmatched or poorly matched model results with high normalized χ^2 values and a narrow (in age), parabola-like feature (labelled feature 1) denoting the best-fit model for a constant mass.

Figure 3.2 shows a schematic of the SEARCH program results for the comparison of an observed p-mode spectrum with model spectra obtained from two evolutionary tracks (two masses). Unmatched and poorly matched model results are evident along with two best-fit features (feature 1) for each mass. Note that for each evolutionary track evaluated (model mass value) there will be a best-fit model result (feature 1).

[23] Tables and figures are located at the end of this chapter.

Figure 3.3 shows a schematic of the SEARCH program results of comparing an observed p-mode spectrum with model spectra obtained from five evolutionary tracks (five masses). Note that each mass will have a best-fit result (feature 1) and that the spacing between the best-fit results will depend on the frequency resolution in mass of the model spectra.

Figure 3.4 shows a blow-up of the statistically significant results shown in the schematic of figure 3.3. The minima of the five best-fit results (feature 1) are shown and correspond to the mass and age values of the best matching model spectrum. There will be a feature 1 result, identified as the figure minimum, which possesses the lowest normalized χ^2 value. The minima of each individual feature 1 result form a broad (in age), parabolic-like shape (labelled feature 2) centred about the figure minimum.

Figures 3.5 through 3.9 show the SEARCH program results for each of the five test spectra. Mass and age values for the five test spectra are listed in inset boxes within the figures. A frequency interpolation in age of 100 points between consecutive model spectra from the calibrated solar model frequency grid and a test frequency uncertainty of $\pm$ 1 μHz are used for all SEARCH runs using the five test spectra[24].

The identified mass and age values for the figure minima of figures 3.5 through 3.9 show the SEARCH program is capable of matching the five test spectra with their respective source model spectra. The normalized χ^2 values for the identified figure minima range from approximately 10^{-5} to 10^{-8}, which approximates the numerical accuracy of the SEARCH program.

---

[24] The reasons for the value settings of interpolation and test frequency uncertainty will be explained in § 3.6.2 and § 3.6.3 respectively.

In figures 3.5 through 3.9, there is a difference in the shape of feature 2 between the matching results of lower and higher mass test spectra. Higher mass results have smaller age spacing between the narrow, constant mass parabolic-shapes (feature 1) and the broad distribution of the normalized χ^2 minima (feature 2) is more defined in higher mass plots. The trend from low to high mass is the result of a shorter time span from ZAMS to the base of the giant branch in higher mass stars. A higher frequency resolution in mass is automatically achieved for high mass stellar pulsation models.

3.6.2. Interpolation

Frequency interpolation in age for a model frequency grid was added to the SEARCH program to improve the resolution of the normalized χ^2 results. Figures 3.5 to 3.9 show that a high frequency resolution in age is required to produce sufficient resolution in the normalized χ^2 results for the identification of the age of the best fit model for a constant mass. This section tests the required amount of frequency interpolation in age to produce optimal matching results.

Figures 3.10 and 3.11 show the SEARCH program results using the same test spectrum (from figure 3.6) with two differing amounts of frequency interpolation in age. The test frequency uncertainty is $\pm$ 1 μHz. In figure 3.10 and 3.11, a frequency interpolation in age of 10 and 100 points between consecutive model spectra in the calibrated solar model frequency grid are used respectively. Both figures have the same arrangement of normalized χ^2 minima of constant mass (see figure 3.6); however, figure 3.6 shows more scatter in the distribution of the normalized χ^2 minima of constant mass

(feature 2). Figure 3.11 shows a smooth, broad, parabolic distribution to the constant mass minima (feature 2) with little to no scatter.

Additional testing of interpolation indicates a frequency interpolation in age of 100 points is required to produce sufficient resolution in normalized χ^2 to identify a minimum for a constant mass. Frequency interpolation in age of 100 points increases the age resolution of the calibrated solar model frequency grid to $\approx$ 11 Myr for 0.8 $M_\odot$ and to $\approx$ 0.15 Myr for 3.0 $M_\odot$ along the main sequence. Near the giant branch, the age resolution is increased to $\approx$ 0.2 Myr for 0.8 $M_\odot$ and to $\approx$ 4000 years for 3.0 $M_\odot$.

Frequency interpolation in mass was not incorporated into the SEARCH program for this thesis, but is a useful future enhancement.

3.6.3. Observed Frequency Uncertainty

This section tests the effects of variation in the observed frequency uncertainties on the frequency search technique matching results[25]. Figures 3.6, 3.12, 3.13 and 3.14 show normalized χ^2 versus age results using the same test spectrum (from figure 3.6) with test frequency uncertainties of $\pm$ 1, $\pm$ 2, $\pm$ 3 and $\pm$ 5 μHz respectively. A frequency interpolation in age of 100 points is used in the results of all four figures.

The observed trend in the four figures resulting from the increase the test frequency uncertainty is a broadening of the parabolic distribution of the constant mass minima (feature 2). This causes the figure minimum to be less defined with increasing test frequency uncertainty. This trend is the result of an increase in the denominator of equation 3.03, thereby causing a reduction in the normalized χ^2 values. Low test

[25] For this test, the observed frequency uncertainties correspond to the test frequency uncertainties associated with the artificially generated test frequencies.

frequency uncertainties or uncertainties of the same order as the model frequency uncertainties result in higher confidence in the matching results (normalized χ^2 values) of the frequency search technique.

3.6.4. Total Number of Observed Frequencies

This section tests the effects of variation in the total number of observed frequencies to be matched. Figures 3.6, 3.15, 3.16 and 3.17 show normalized χ^2 versus age results using 32, 20, 10 and 5 artificially generated observed frequencies based on the test spectra used in figure 3.6.

The four figures show no apparent trend or variation in the normalized χ^2 versus age matching results based on the use of varying numbers of observed frequencies. However, a valid observation is the more frequencies which a figure minimum is based on, the more confidence can be placed on the matching results.

3.6.5 Non-Pulsation Constraints

The pulsation constraints provided by normalized χ^2 in determining the stellar model (mass and age) that best matches an observed pulsation spectrum may be insufficient to provide a definitive result. Realistically, normalized χ^2 will provide a range of stellar models (masses and ages) that match observations. Additional constraints may be useful in further constraining the matching results obtained using normalized χ^2.

A non-pulsation constraint is the effective temperature of the observed star. Stellar effective temperatures are observable quantities. Comparing an observed

effective temperature (and corresponding uncertainty) with the effective temperatures of stellar models constrained by normalized χ^2 results enables the elimination of unphysical stellar models (masses and ages).

The use effective temperature as a non-pulsation constraint will be incorporated into the testing in § 3.7, chapters 4 and 5.

3.7. Unknown Model Results

The following sections perform a single, blind analysis of the frequency search technique using four model generated pulsation spectra (test spectra) obtained from models of unknown mass and age values. These four unknown test spectra were calculated independently from the calibrated solar model frequency grid. The four test spectra labelled, models A, B, C and D, were provided by Guenther (private communication). The unknown stellar models were calculated with the same stellar physics used in the construction of the calibrated solar model frequency grid; however, the unknown models may have heavy metal values which differ from the calibrated solar model frequency grid and larger individual frequency uncertainties. The calibrated solar model frequency grid is used as the model frequency grid for the frequency search technique testing using the test spectra from models A, B, C and D. The results of this testing will be compared with the actual stellar model values (mass and age) of models A, B, C and D, provided later.

3.7.1 Model A Results

Table 3.3 lists the l = 0, 1 test spectra from the unknown stellar models A, B, C and D. For model A, 36 test frequencies are provided. A review of the model A test frequencies indicates the frequencies alternate between l = 0 or 1 with no missing modes. The model A frequency uncertainties are ± 1 μHz.

Figure 3.18 shows the SEARCH program results using the model A test frequencies in a plot of normalized χ^2 versus age. The best results are identified by three minima which are labelled with the corresponding mass, age, effective temperature and normalized χ^2 values[26]. The minimum for figure 3.18 corresponds to a stellar model with a mass of 0.90 $M_\odot$ and an age of 2.633 Gyr. The normalized χ^2 value for this minimum is 0.09. Table 3.4 lists the model pulsation spectrum that most closely matches the model A test spectrum as well as the differences between the matched test and model frequencies. Model and test frequencies agree to within ~ 0.01 μHz to ~ 0.7 μHz for this figure minimum.

A secondary minimum corresponds to the stellar model with a mass of 0.95 $M_\odot$ and an age of 2.633 Gyr. The normalized χ^2 value for this minimum is 0.55. The normalized χ^2 values for the minima at 0.90 $M_\odot$ and 0.95 $M_\odot$ indicates the model spectra corresponding to these points match the model A test spectra to $< \left(\sigma_{Obs}^2 + \sigma_{Model}^2\right)^{1/2}$ (which is ~ 1.4 μHz for model A).

To differentiate between the two minima, the non-pulsation constraint of effective temperature is incorporated into this analysis. The effective temperature for model A is given to be 5500 ± 250 K. Comparing this effective temperature range with

[26] Best results will be limited by the resolution of the grid.

the stellar model effective temperature for the minima of figure 3.18 eliminates the minimum corresponding to 0.80 $M_{\odot}$, leaving the two possible stellar models at 0.90 $M_{\odot}$ and 0.95 $M_{\odot}$. The best match to the model A test spectrum is the stellar model with a mass of 0.90 $M_{\odot}$ and an age of 2.633 Gyr.

The actual properties of model A are 0.92 $M_{\odot}$, 2.77 Gyr and Z = 0.02 (see figure 3.14; Guenther, private communication). The stellar model (M = 0.90 $M_{\odot}$, age = 2.633 Gyr) constrained by normalized χ^2 agrees with the actual values of model A to 0.02 $M_{\odot}$ in mass and to 0.11 Gyr in age. The heavy metal composition of the model frequency grid and model A also agree.

A higher resolution in mass of the model frequency grid would have attained a better match.

3.7.2. Model B Results

Table 3.3 lists 37 l = 0, 1 test frequencies from model B. A review of the test frequencies indicates the spectrum is complete, with no missing modes, and alternates between l = 0 or 1. The model B frequency uncertainty is ± 1 μHz and the effective temperature is given to be 6000 ± 250 K for model B.

Figure 3.19 shows the SEARCH program results using the model B test frequencies in a plot of normalized χ^2 versus age. Three minima and their respective information are identified. The minimum for figure 3.19 corresponds to a stellar model with a mass of 0.90 $M_{\odot}$ and an age of 4.326 Gyr. The normalized χ^2 value for this minimum is 0.62. Table 3.5 lists the most closely matched model spectrum as well as the differences between the matched test and model frequencies. Model and test

frequencies for this match agree to within ~ 0.1 μHz to ~ 3.0 μHz. A secondary minimum is identified corresponding to the stellar model with a mass of 0.95 $M_{\odot}$ and an age of 1.102 Gyr. The normalized χ^2 value for this minimum is 1.11. The normalized χ^2 values for the two minima at 0.90 and 0.95 $M_{\odot}$ indicates the model spectra corresponding to these points match the model B test spectra to $\leq \left(\sigma_{Obs}^2 + \sigma_{Model}^2\right)^{1/2}$ (which is ~ 1.4 μHz for model B).

Model effective temperatures for the figure 3.19 minima do not agree with the given effective temperature range of model B. The results of figure 3.19 cannot be constrained using effective temperature.

The actual properties of model B are 0.92 $M_{\odot}$, 2.03 Gyr and Z = 0.01 (see figure 3.15; Guenther, private communication). The stellar model (M = 0.90 $M_{\odot}$, age = 4.362 Gyr) constrained by normalized χ^2 agrees with the actual values for model B to 0.02 $M_{\odot}$ in mass and to 2.3 Gyr in age. The value of heavy metal composition for model B and the calibrated solar model frequency grid do not agree.

A higher resolution in mass for the model frequency grid would have been beneficial to the analysis. The inability to constrain the results of figure 3.19 using effective temperature may be an indicator for a discrepancy between the properties of the model frequency grid and the model star, especially with the value of heavy metal composition.

3.7.3. Model C Results

Table 3.3 lists 25 l = 0, 1 test frequencies from the unknown model C. A review of the test frequencies indicates there are missing modes within the set of either l = 0 or

1, resulting in an uneven number of l = 0 or 1 frequencies. The model C frequency uncertainty is ± 1 μHz and the effective temperature is given to be 7000 ± 100 K for model C.

Figure 3.20 shows the SEARCH program results using the model C test frequencies, in a plot of normalized χ^2 versus age. Four minima are identified along with their respective information. The figure minimum corresponds to a stellar model with a mass of 1.40 $M_\odot$ and an age of 0.265 Gyr. The normalized χ^2 for this minimum is 0.295. Table 3.6 lists the model spectrum that best matches test spectrum along with the differences between the matched test and model frequencies. The model C test frequencies are matched to within ~0.03 μHz to ~1.5 μHz. The normalized χ^2 value for the minimum at 1.40 $M_\odot$ indicates the model spectrum of this point matches the test spectrum for model C to $<\left(\sigma^2_{Obs} + \sigma^2_{Model}\right)^{1/2}$ (which is ~ 1.4 μHz for model C).

The model effective temperatures for the identified minima in figure 3.20 do not agree with the given effective temperature range for model C. These minima cannot be constrained using the observed effective temperature.

The actual properties for model C are 1.43 $M_\odot$, 0.38 Gyr and Z = 0.02 (see figure 3.16; Guenther, private communication). The stellar model (M = 1.40 $M_\odot$, age = 0.265 Gyr) constrained by normalized χ^2 agrees with the actual values for model C to within 0.03 $M_\odot$ in mass and to 0.12 Gyr in age. The heavy metal composition for model C and for the calibrated solar model frequency grid agrees.

These results suggest that a higher resolution in mass would provide a closer agreement and enable the use of a non-pulsation constraint.

3.7.4. Model D Results

Table 3.3 lists 14 l = 0, 1 test frequencies from model D. A review of the test frequencies indicates no missing modes and a pattern of alternation between l = 0 or 1. The model D frequency uncertainty is ± 3 μHz and the effective temperature is 5600 ± 200 K for model D.

Figure 3.21 shows the SEARCH program results for the model D test frequencies in a plot of normalized χ^2 versus age. Five minima are identified with their respective information. The minimum of figure 3.21 corresponds to a stellar model with a mass of 0.95 $M_\odot$ and an age of 2.88 Gyr. The normalized χ^2 value for this minimum is 0.259. Table 3.7 lists the model spectrum that best matches the test spectrum along with the differences between the matched test and model frequencies. The model D test frequencies are matched to within ~0.3 μHz to ~3.3 μHz. All five minima possess normalized χ^2 values which indicates the model spectra corresponding to these points match the model D test spectra to $< \left(\sigma^2_{Obs} + \sigma^2_{Model}\right)^{1/2}$ (which is ~ 3 μHz for model D).

The application of effective temperature constraints indicates that the model effective temperatures for all five identified minima agree with the given effective temperature for model D.

The actual properties for model D are 0.92 $M_\odot$, 6.07 Gyr and Z = 0.02 (see figure 3.21; Guenther, private communication). For the five minima of figure 3.21, the agreement with the actual values for model D range from 0.02 $M_\odot$ to 0.09 $M_\odot$ in mass and from 0.18 Gyr to 6.0 Gyr in age.

The results for model D provide no definitive figure minimum. This uncertain result is due to several key reasons which are:

1. A higher observed frequency uncertainty means that it is easier to obtain a low normalized χ^2 based on a match between the observed and model frequencies.
2. A low frequency resolution in mass.
3. A low number of observed frequencies.

3.8 Overall Testing Results

The evaluation of the frequency search technique through testing using model generated test spectra with known and unknown stellar properties (mass and age) produces some overall results. The overall results for chapter 3 are:

1. High frequency resolution in mass is required for a constructed model frequency grid. A mass resolution of at least 0.01 $M_{\odot}$ is required.
2. High frequency resolution in age is required to provide the necessary resolution in normalized χ^2 results to identify individual minima for constant masses. The testing conducted in this chapter required a frequency interpolation in age of 100 points.
3. Low observed frequency uncertainties are desirable in order to provide confident normalized χ^2 results.
4. Large numbers of observed frequencies are desirable. More matched observed frequencies increases the confidence in a normalized χ^2 result.
5. An accurate determination of the heavy metal composition of an observed star is required for the calculation of the central model of a model frequency grid.

6. An additional constraint is beneficial to an observed and model frequency analysis. Effective temperature provides an observable and useful constraint parameter.
7. An important observation from the general testing results of the frequency search technique is illustrated in figure 3.22. Figure 3.22 illustrates the possibility of an observed spectrum being well-matched to multiple model spectra (i.e. multi-valued). Such a situation would require an additional constraint to determine the best-fit model to the observed spectrum. This scenario did not arise during the tests conducted in this thesis.

Table 3.2: 20 artificially generated $l = 0$, 1 p-mode frequencies extracted from the stellar model with a mass of 0.80 $M_{\odot}$ and an age of 20.0271 Gyr (from a CSM frequency grid).

ν (μHz)	l	n
1234.380	1	7
1320.704	0	7
1384.636	1	8
1467.646	0	8
1531.365	1	9
1611.846	0	10
1674.343	1	10
1753.151	0	11
1816.016	1	11
1893.253	0	12
1957.469	1	12
2033.993	0	13
2098.669	1	13
2174.420	0	14
2239.392	1	14
2313.448	0	15
2379.021	1	15
2451.975	0	16
2518.068	1	16
2590.919	0	17

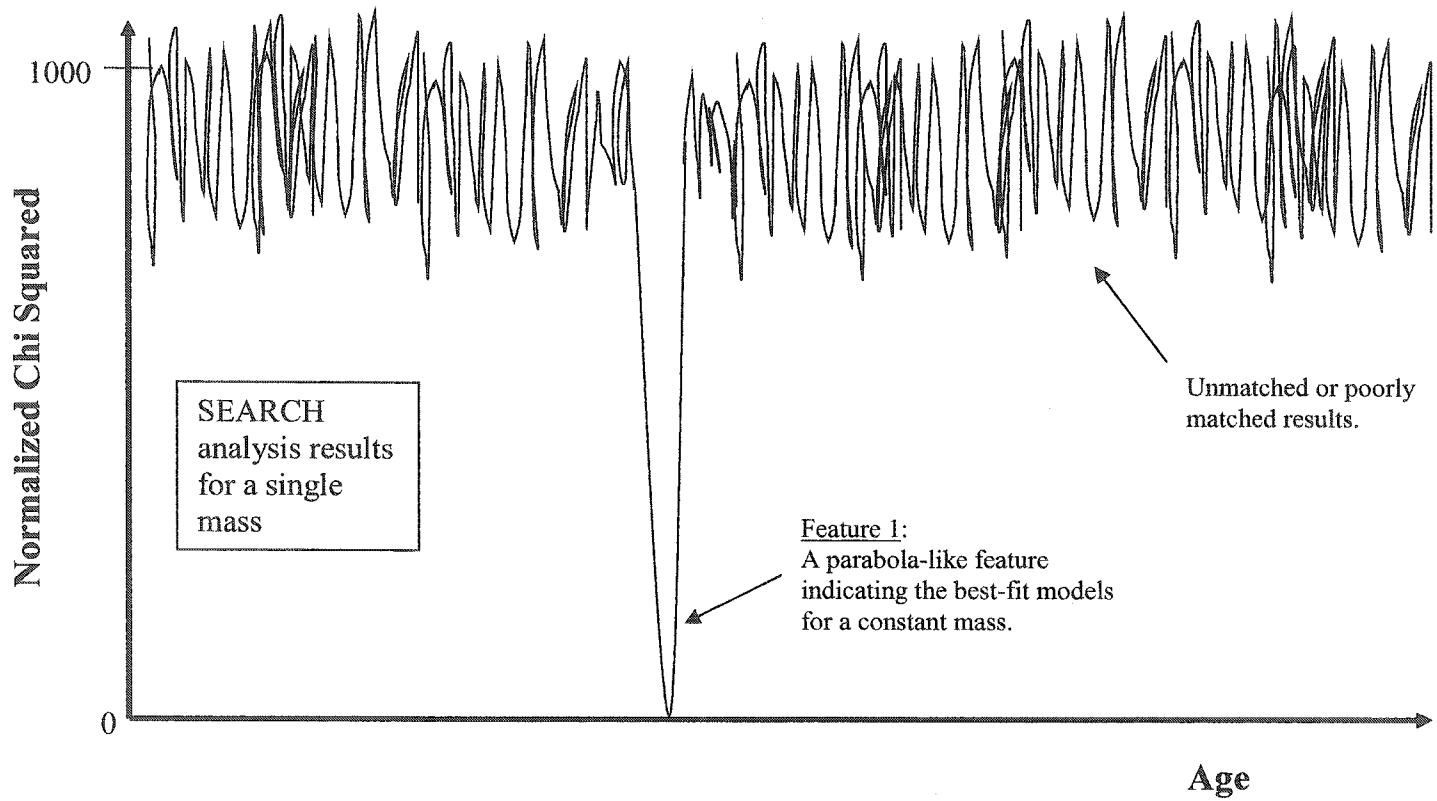

Figure 3.1: A schematic plot of normalized χ^2 versus age showing the SEARCH program result for the comparison of an observed p-mode spectrum with model spectra obtained from a single evolutionary track (a single mass). The analysis results will consist of unmatched or poorly matched models and a best-fit model result for a constant mass indicated by feature 1.

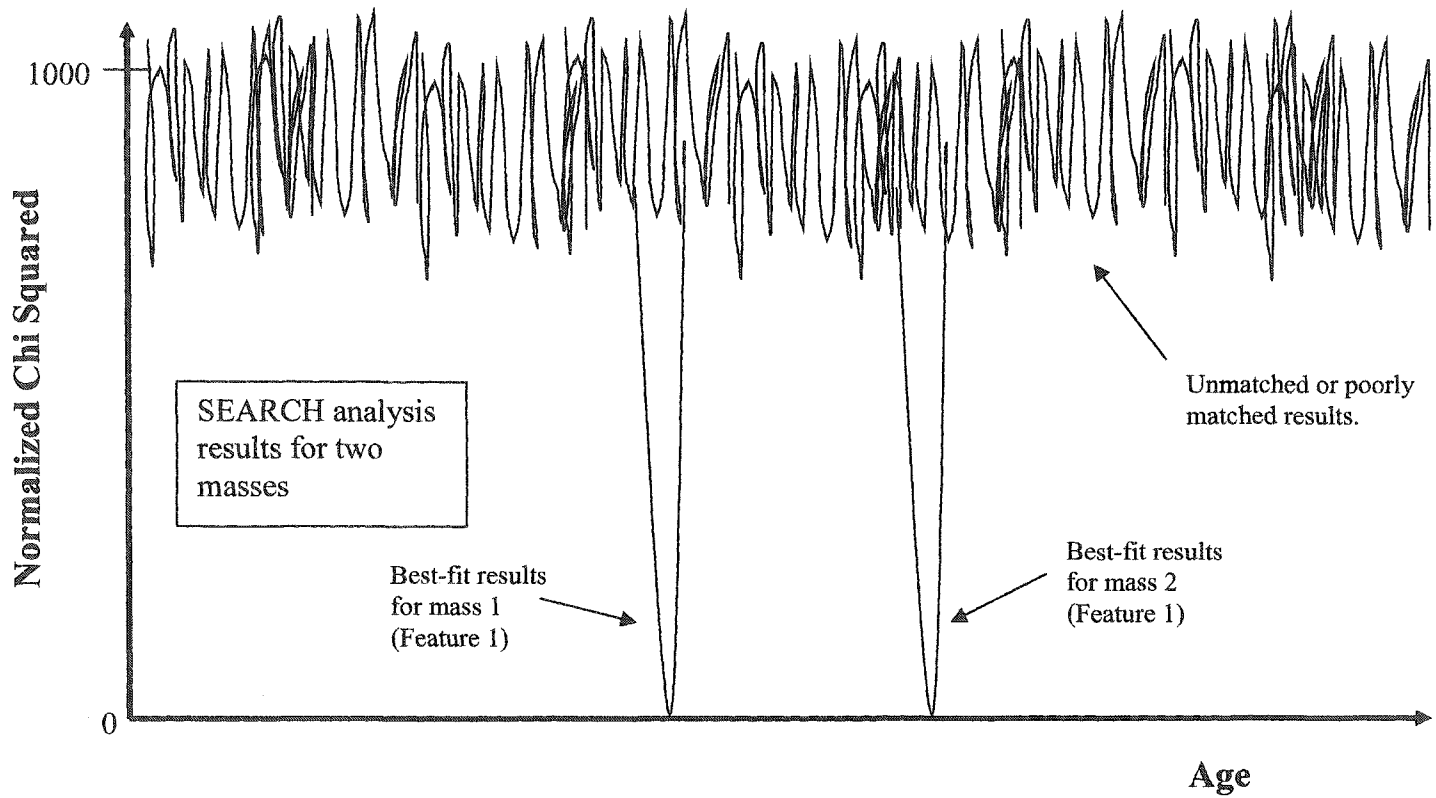

Figure 3.2: A schematic plot of normalized χ^2 versus age showing the SEARCH program result for the comparison of an observed p-mode spectrum with model spectra obtained from two evolutionary tracks (two masses). The analysis results will consist of unmatched or poorly matched models and best-fit model results for a constant mass indicated by feature 1.

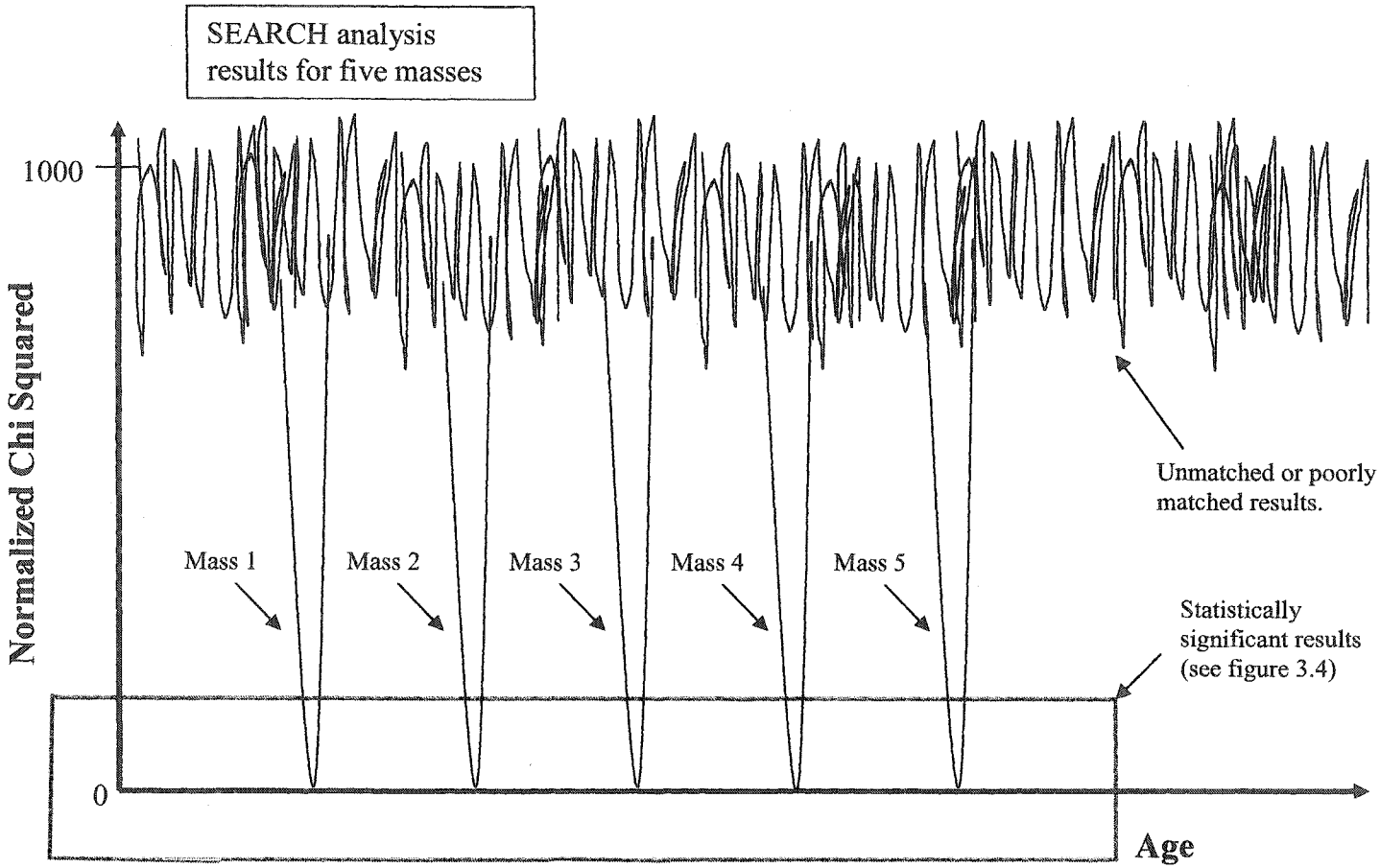

Figure 3.3: A schematic plot of normalized χ^2 versus age showing the SEARCH program result for the comparison of an observed p-mode spectrum with model spectra obtained from five evolutionary tracks (five masses). The analysis results will consist of unmatched or poorly matched models and best-fit model results for a constant mass indicated by feature 1. The statistically significant results of figure 3.3 are indicated by the grey box and will be shown/explained in figure 3.4.

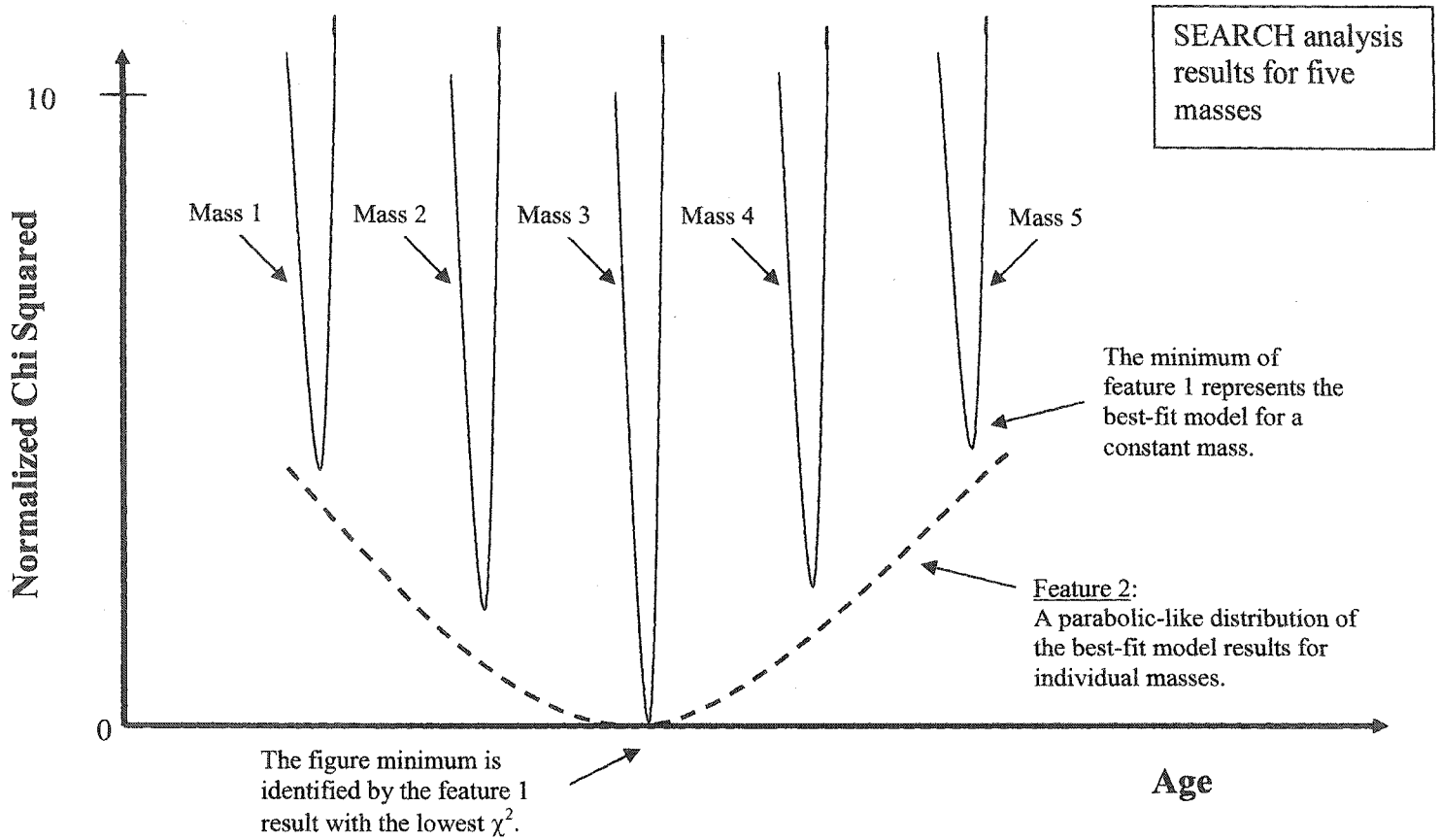

Figure 3.4: A schematic plot of normalized χ^2 versus age showing the statistically significant SEARCH program results (from the schematic of figure 3.3) for the comparison of an observed p-mode spectrum with model spectra obtained from five evolutionary tracks (five masses). Identified are the figure minimum (best overall fit), the minima of feature 1 (best-fit results for individual masses) and the distribution of the best-fit results for individual masses (feature 2).

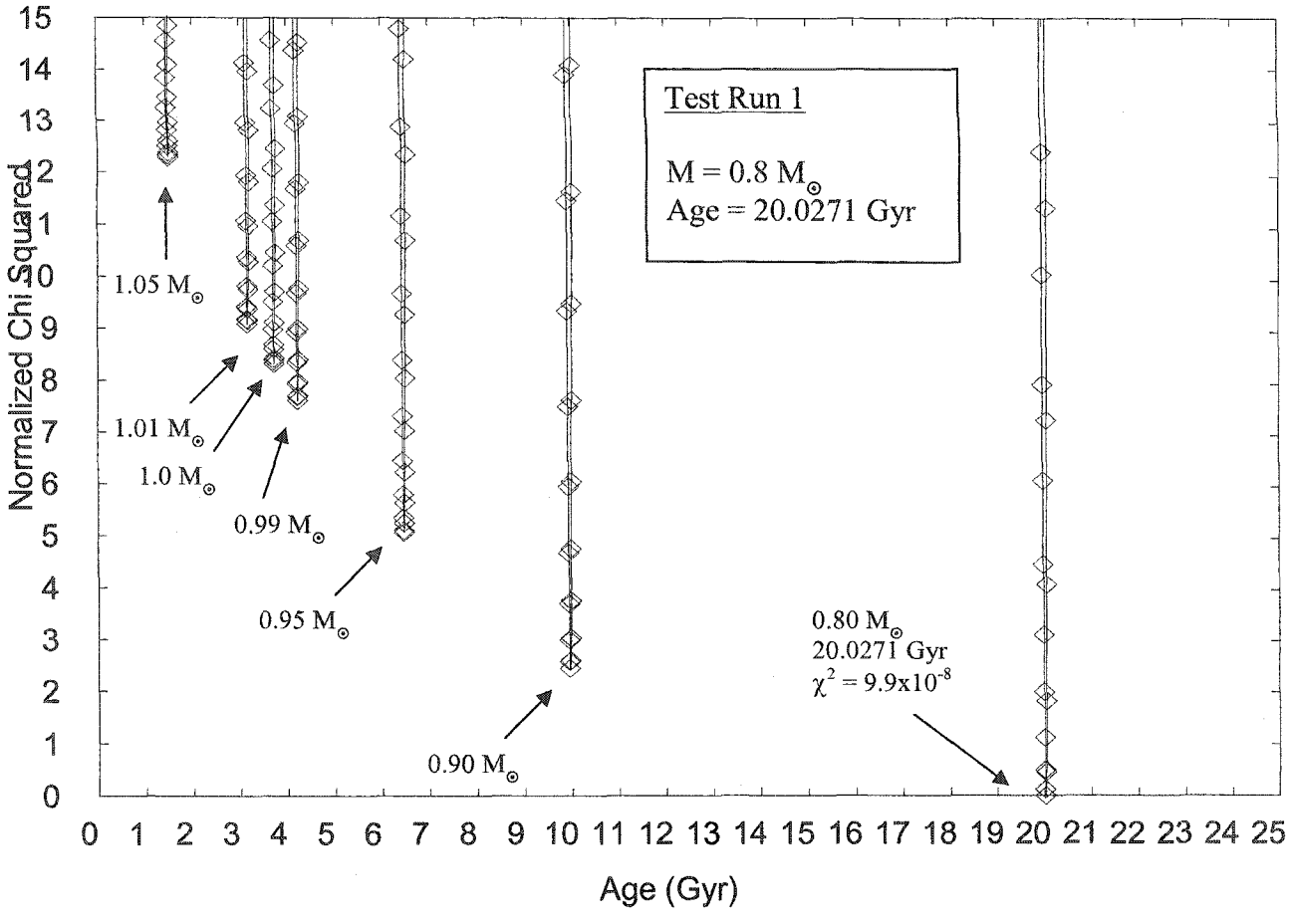

Figure 3.5: Normalized χ^2 versus age SEARCH program results using 20 $l = 0, 1$ frequencies corresponding to M = 0.80 $M_\odot$ and 20.0271 Gyr. A figure minimum is labelled at 0.80 $M_\odot$ and 20.0271 Gyr with a normalized χ^2 value of 9.9×10^{-8}. Mass values for additional minima are labelled. The frequency interpolation in age is set to 100 points and the σ_{obs} is set to ± 1 μHz. The two characteristic features present in the normalized χ^2 versus age plots are identified.

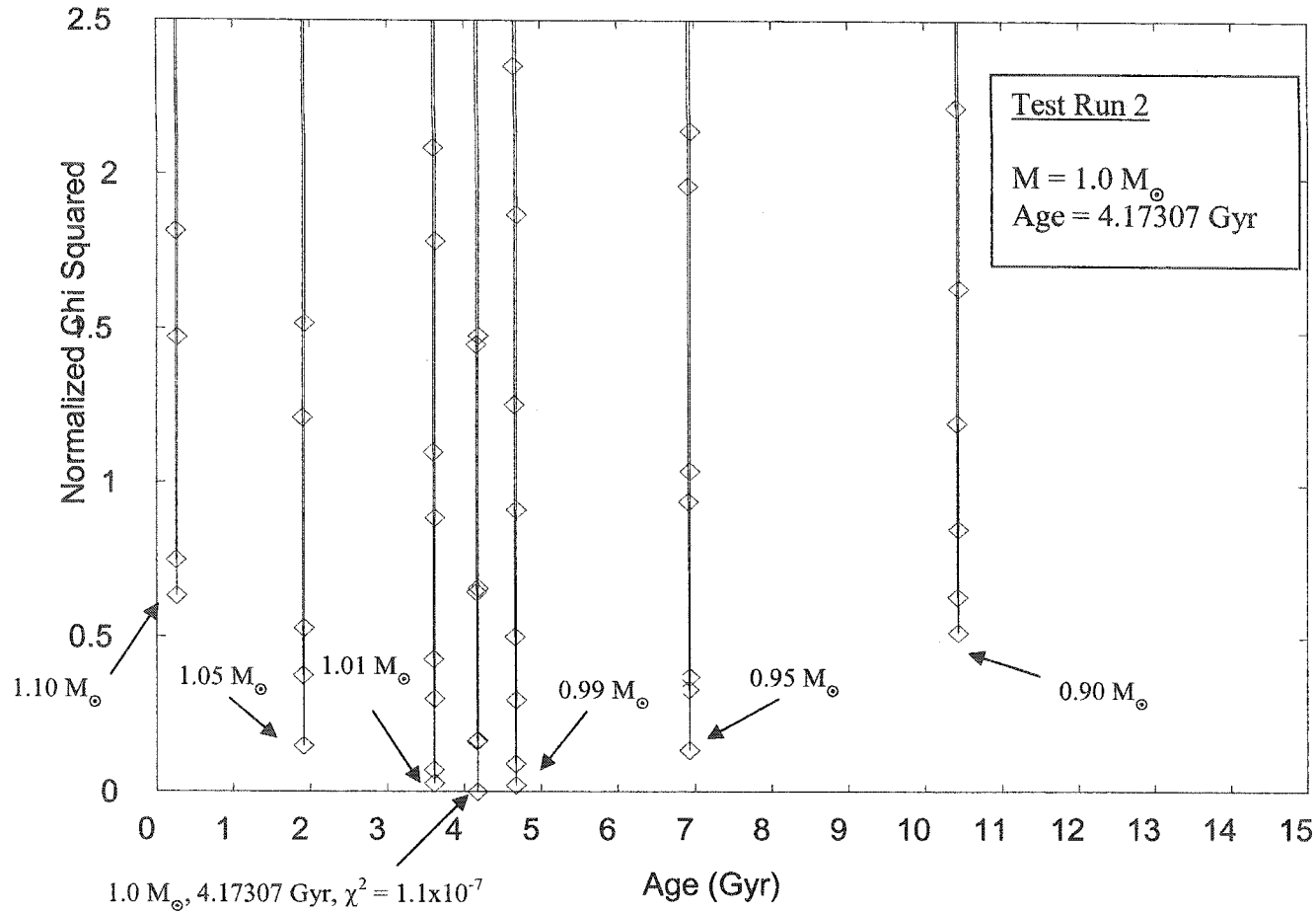

Figure 3.6: Normalized χ^2 versus age SEARCH program results using 32 $l = 0, 1$ frequencies corresponding to M = 1.0 $M_\odot$ and 4.17307 Gyr. A figure minimum is labelled at 1.0 $M_\odot$ and 4.17307 Gyr with a normalized χ^2 value of 1.1×10^{-7}. Mass values for additional minima are indicated. The frequency interpolation in age is set to 100 points and the σ_{obs} is set to $\pm$ 1 μHz.

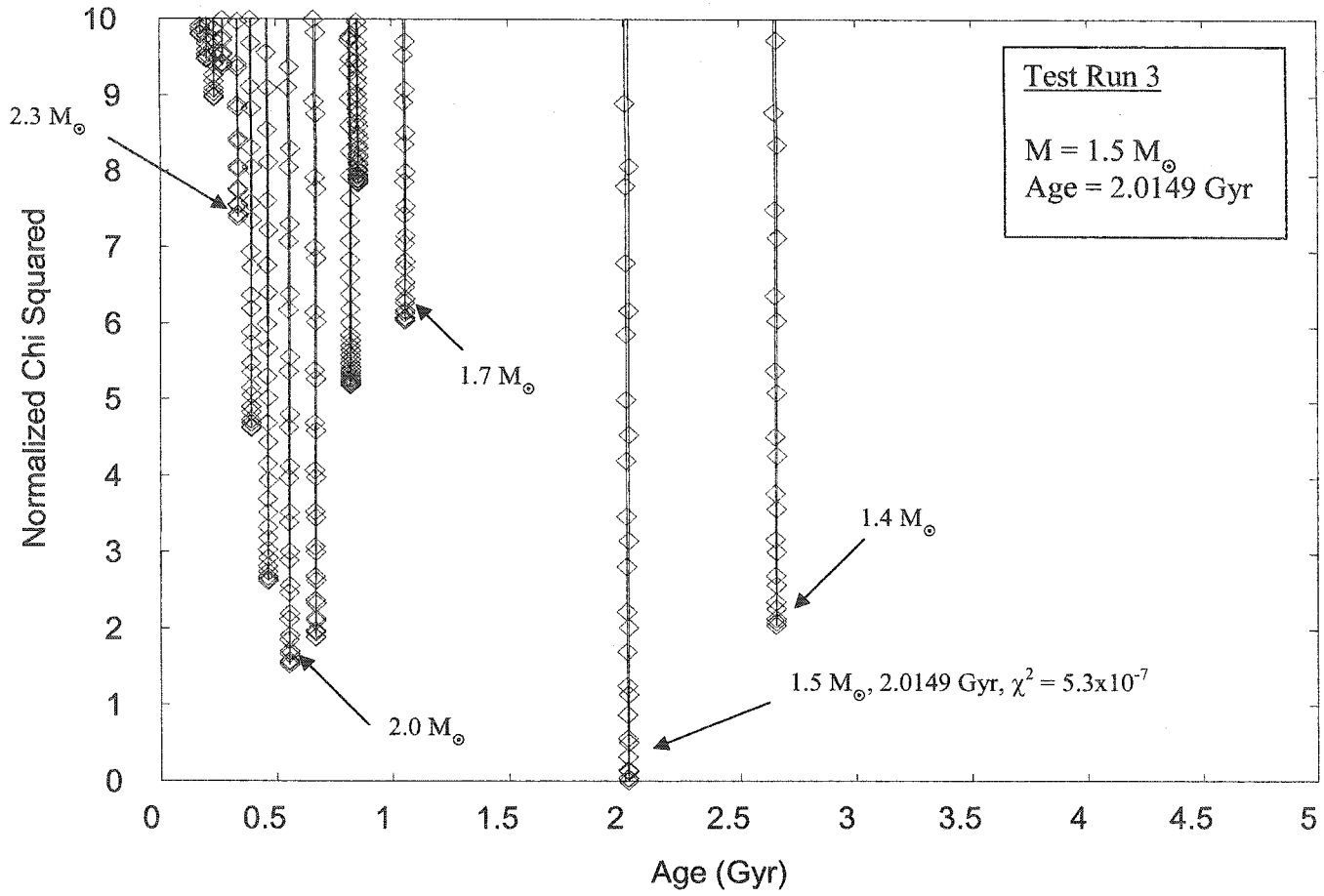

Figure 3.7: Normalized χ^2 versus age SEARCH program results using 28 $l = 0, 1$ frequencies corresponding to M = 1.5 $M_\odot$ and 2.0149 Gyr. A figure minimum is labelled at 1.5 $M_\odot$ and 2.0149 Gyr with a normalized χ^2 value of 5.3×10^{-7}. Mass values for additional minima are identified. The frequency interpolation in age is set to 100 points and the σ_{obs} is set to ± 1 μHz.

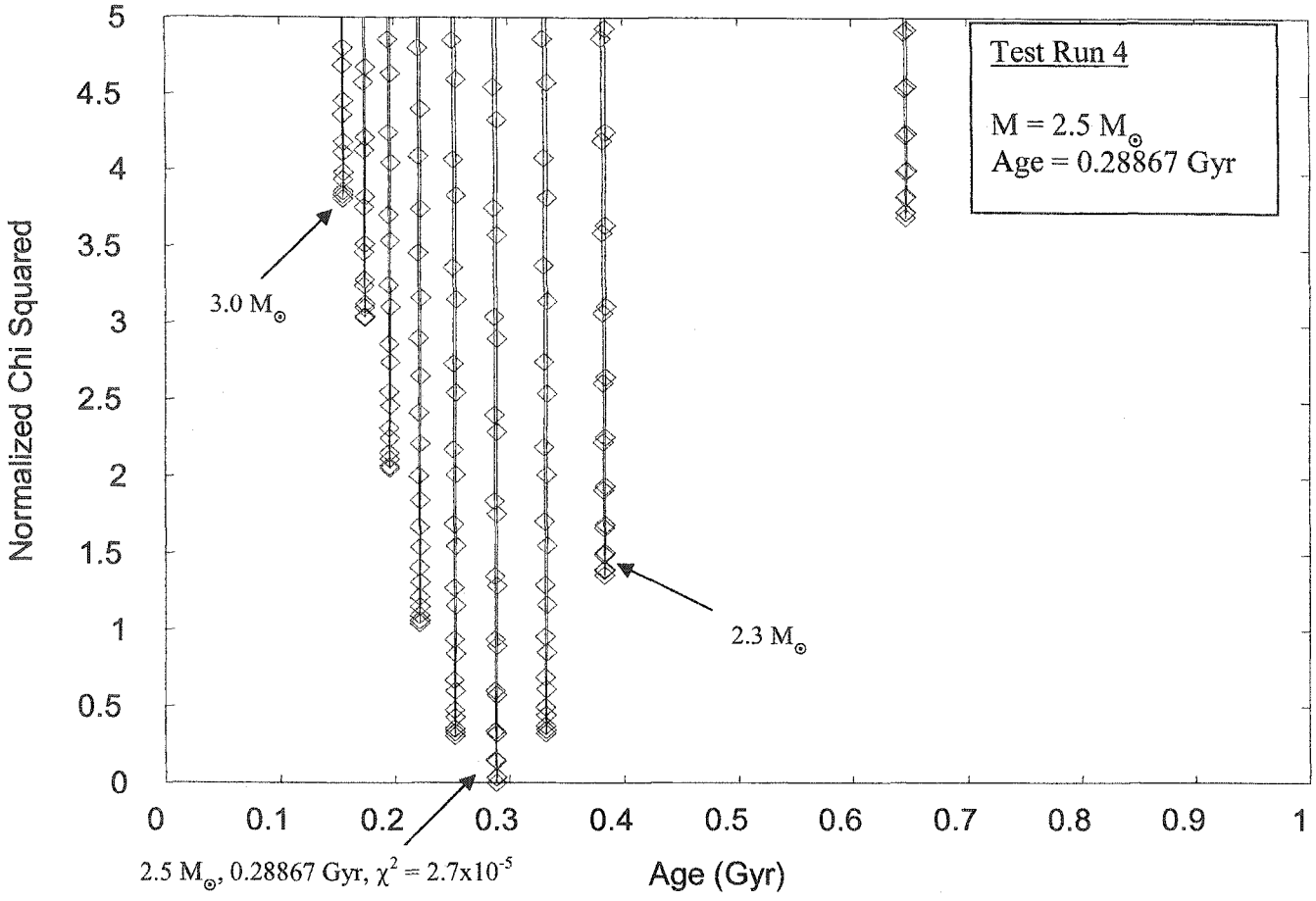

Figure 3.8: Normalized χ^2 versus age SEARCH program results using 31 $l = 0, 1$ frequencies corresponding to $M = 2.5\ M_\odot$ and 0.28867 Gyr. A figure minimum is labelled at $2.5\ M_\odot$ and 0.28867 Gyr with a normalized χ^2 value of 2.7×10^{-5}. Mass values for additional minima are identified. The frequency interpolation in age is set to 100 points and the σ_{obs} is set to $\pm$ 1 μHz.

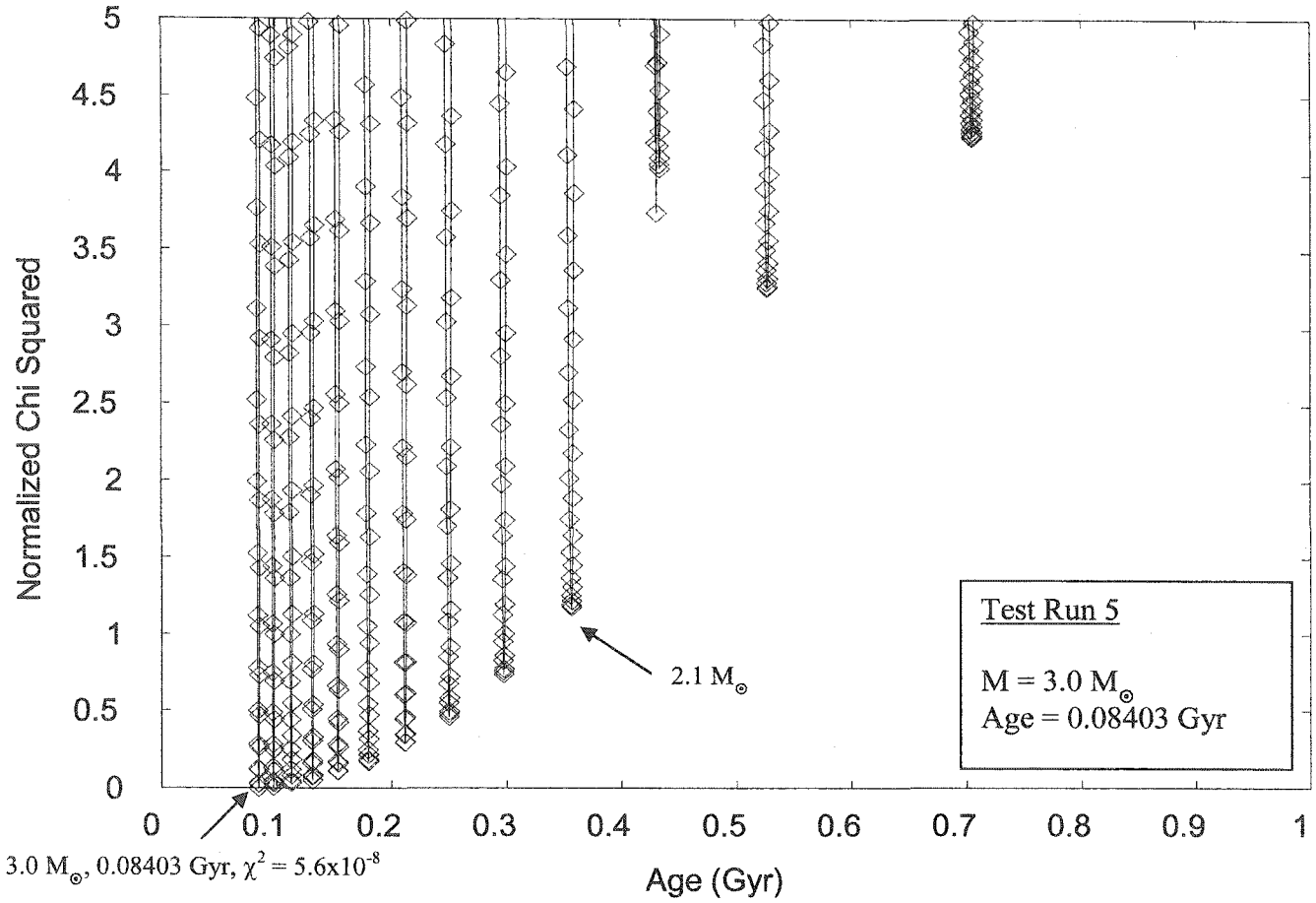

Figure 3.9: Normalized χ^2 versus age SEARCH program results using 20 $l = 0$, 1 frequencies corresponding to M = 3.0 $M_\odot$ and 0.08403 Gyr. A minimum is labelled at 3.0 $M_\odot$ and 0.08403 Gyr with a normalized χ^2 value of 5.6×10^{-8}. Mass values for additional minima are indicated. The frequency interpolation in age is set to 100 points and the σ_{obs} is set to $\pm$ 1 μHz.

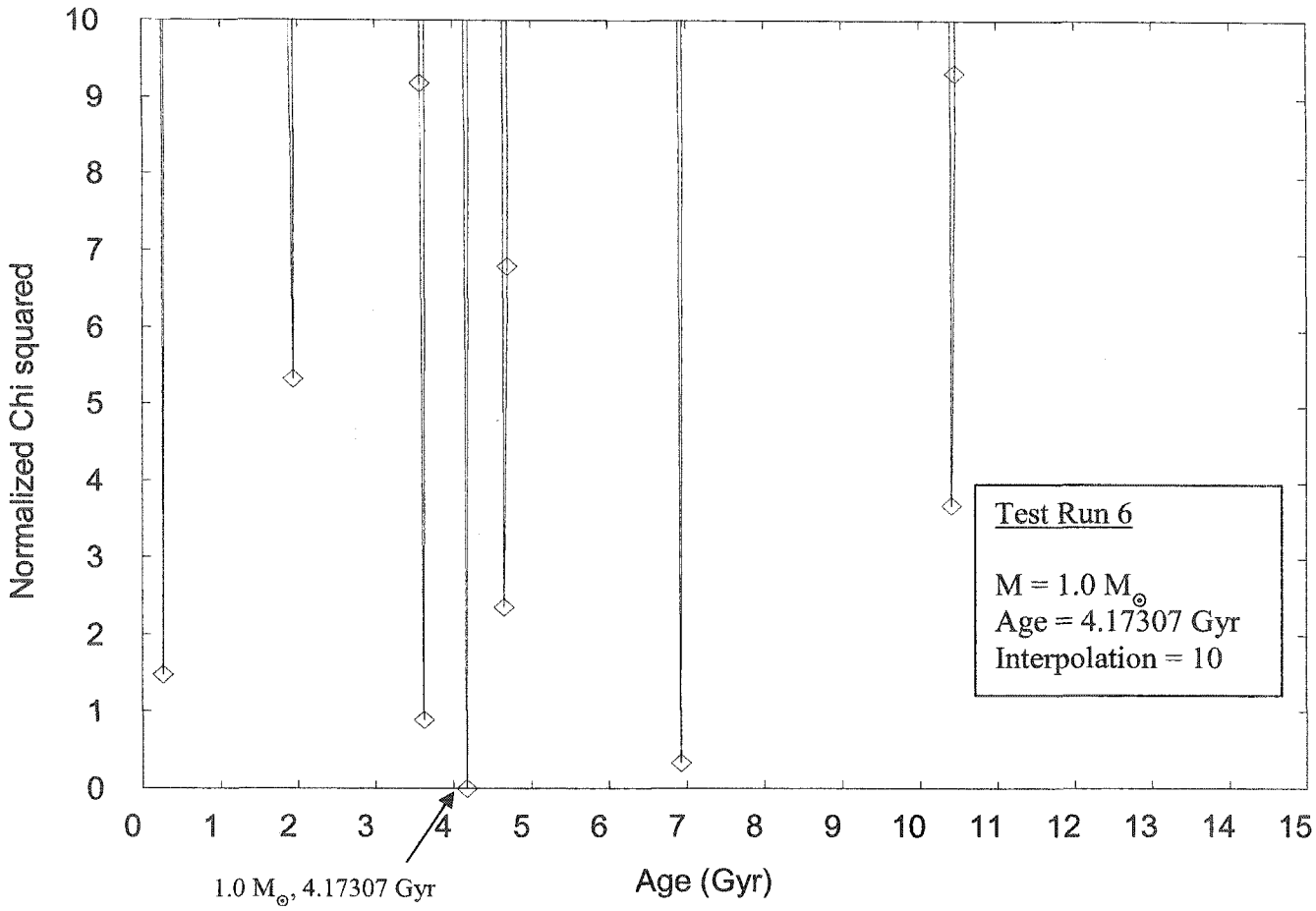

Figure 3.10: Normalized χ^2 versus age SEARCH program results using a frequency interpolation in age set to 10 points. This test uses 32 $l = 0$, 1 frequencies corresponding to M = 1.0 $M_\odot$ and 4.17307 Gyr (see figure 3.2). The σ_{obs} value is set to ± 1 μHz. Large scatter the resulting minima are indicated. A figure minimum at M = 1.0 $M_\odot$ and 4.17307 Gyr is identified.

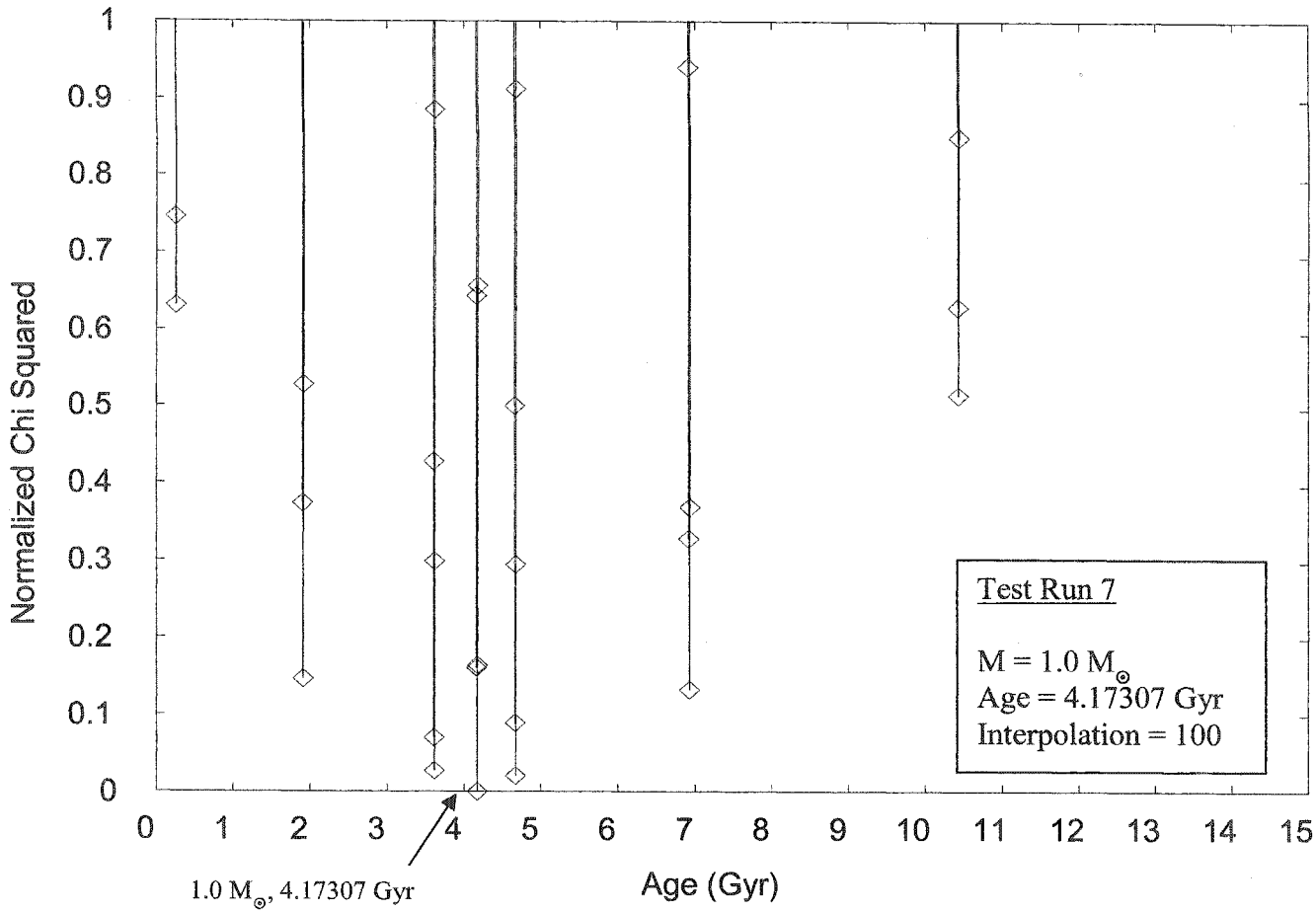

Figure 3.11: Normalized χ^2 versus age SEARCH program results using a frequency interpolation in age of 100 points. This test uses 32 $l = 0$, 1 frequencies corresponding to M = 1.0 $M_\odot$ and 4.17307 Gyr (see figure 3.2). The σ_{obs} value is set to ± 1 μHz. The shape of the resulting minima shows little to no scatter which is an improvement to the results of figure 3.6. A figure minimum at M = 1.0 $M_\odot$ and 4.17307 Gyr is indicated.

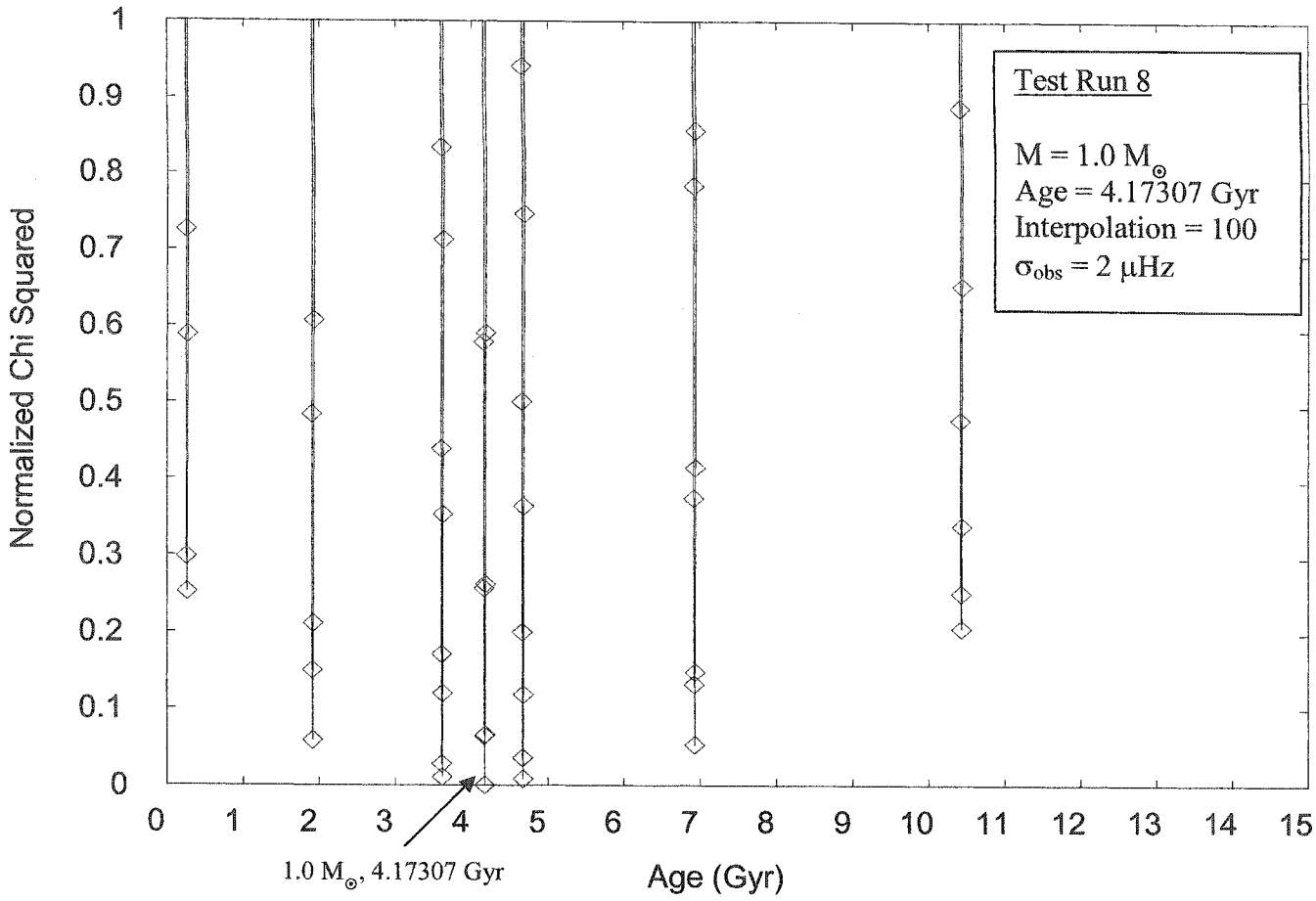

Figure 3.12: Normalized χ^2 versus age SEARCH program results using a σ_{obs} value of ± 2 μHz. This test uses 32 $l = 0$, 1 model frequencies corresponding to M = 1.0 $M_\odot$ and 4.17307 Gyr (see figure 3.2) with a frequency interpolation in age set to 100 points. The figure minimum at 1.0 $M_\odot$ and 4.17307 Gyr as well as the minima arrangement is consistent with figure 3.2.

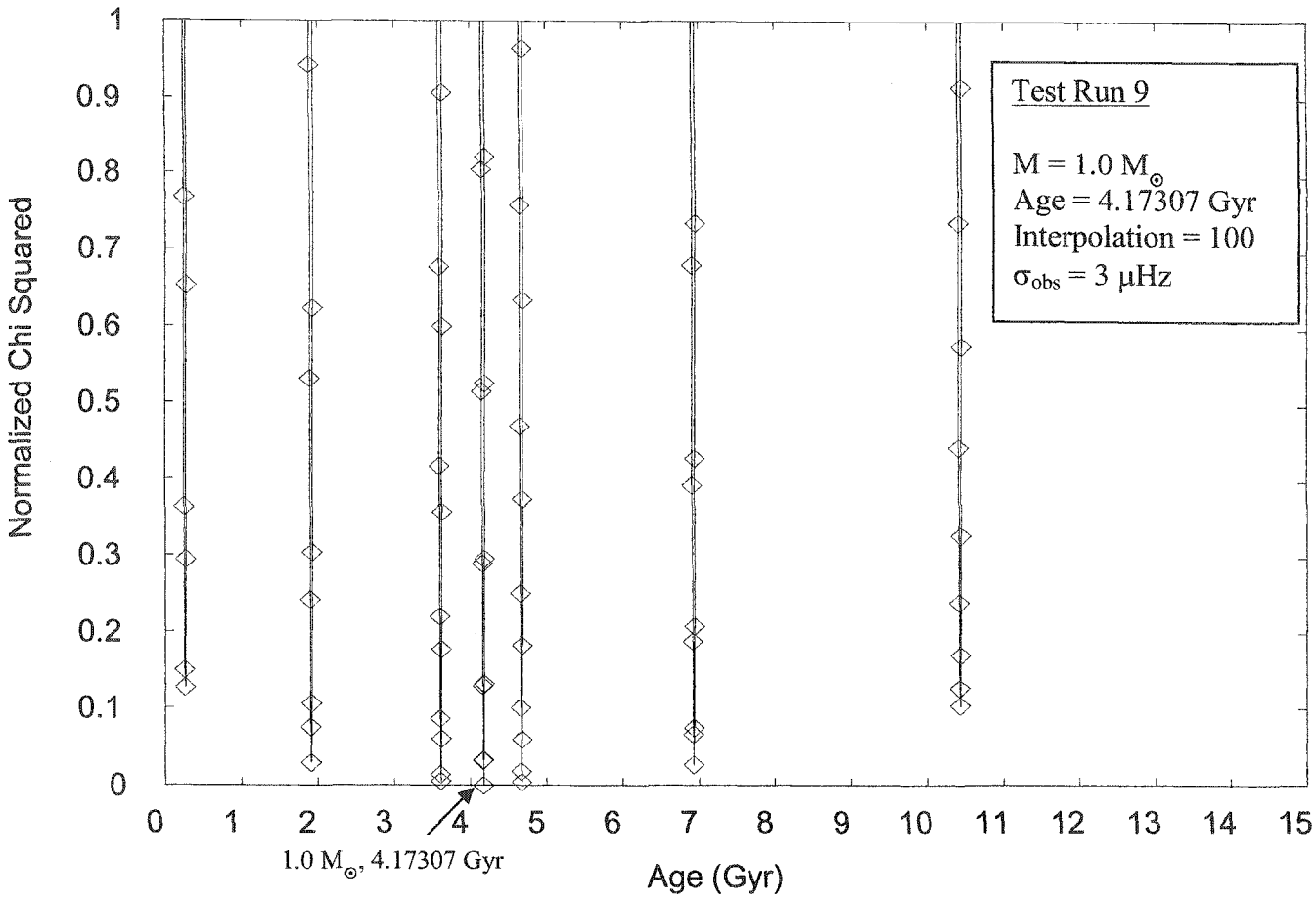

Figure 3.13: Normalized χ^2 versus age SEARCH program results using a σ_{obs} value of ± 3 μHz. This test uses 32 $l = 0$, 1 model frequencies corresponding to M = 1.0 $M_\odot$ and 4.17307 Gyr (see figure 3.2) with a frequency interpolation in age set to 100 points. The figure minimum at 1.0 $M_\odot$ and 4.17307 Gyr as well as the minima arrangement is consistent with figure 3.2.

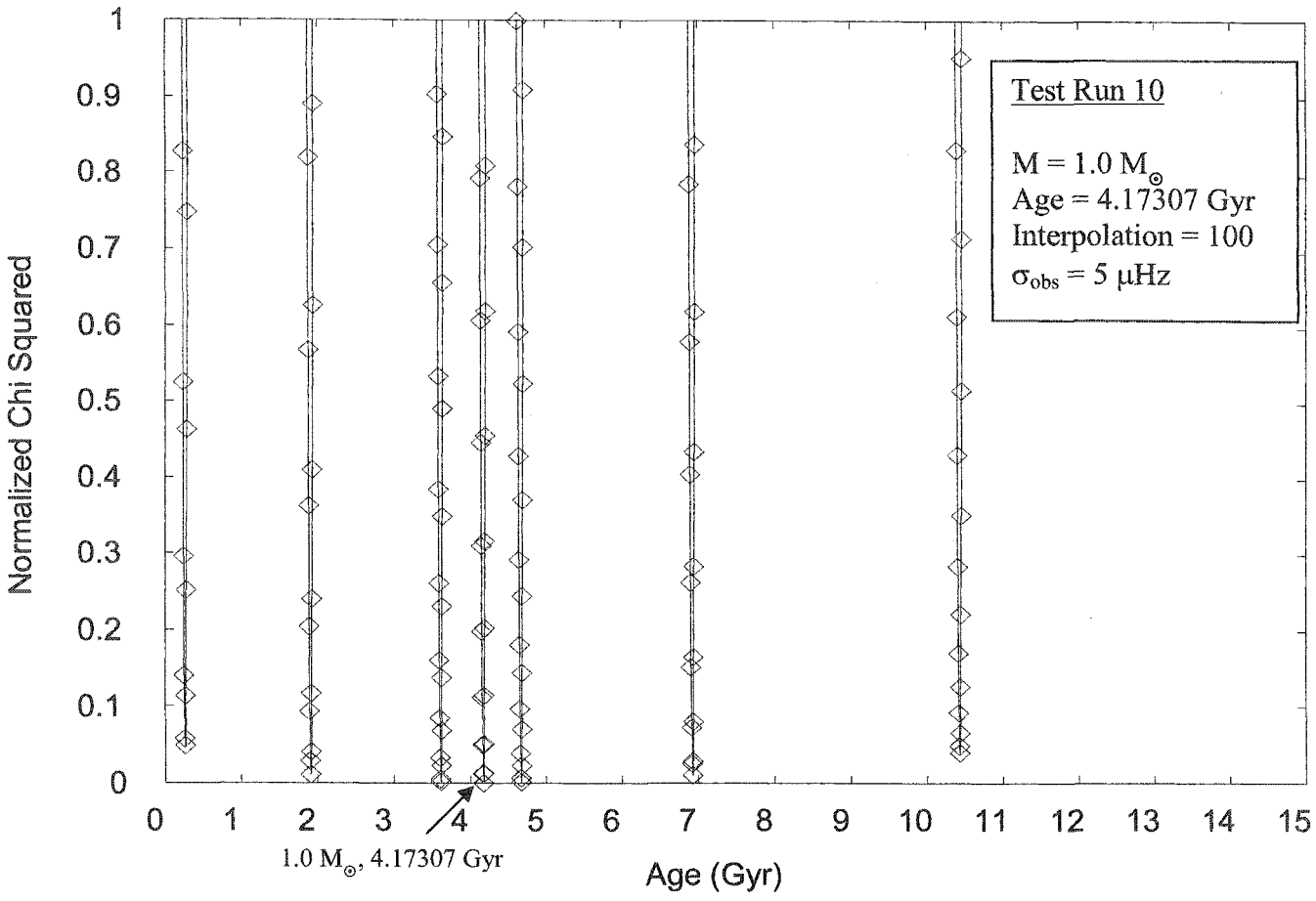

Figure 3.14: Normalized χ^2 versus age SEARCH program results using a σ_{obs} value of ± 5 μHz. This test uses 32 $l = 0$, 1 model frequencies corresponding to M = 1.0 $M_\odot$ and 4.17307 Gyr (see figure 3.2) with a frequency interpolation in age set to 100 points. The figure minimum at 1.0 $M_\odot$ and 4.17307 Gyr as well as the minima arrangement is consistent with figure 3.2.

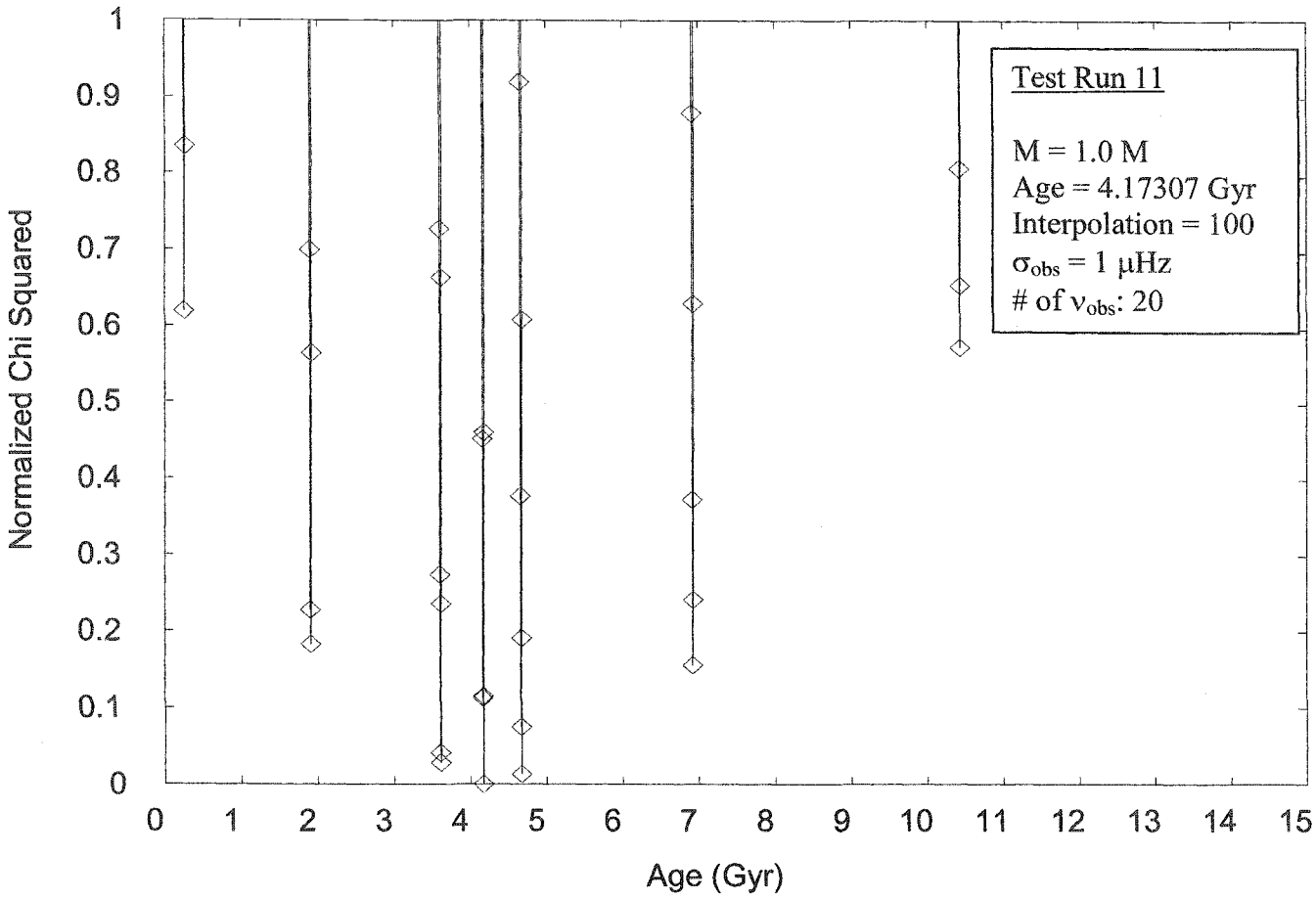

Figure 3.15: Normalized χ^2 versus age SEARCH program results using 20 $l = 0$, 1 model frequencies corresponding to M = 1.0 $M_\odot$ and 4.17307 Gyr (see figure 3.2). The frequency interpolation in age is set to 100 points and the σ_{obs} is set to ± 1 μHz. The figure minimum at 1.0 $M_\odot$ and 4.17307 Gyr as well as the minima arrangement is consistent with figure 3.2.

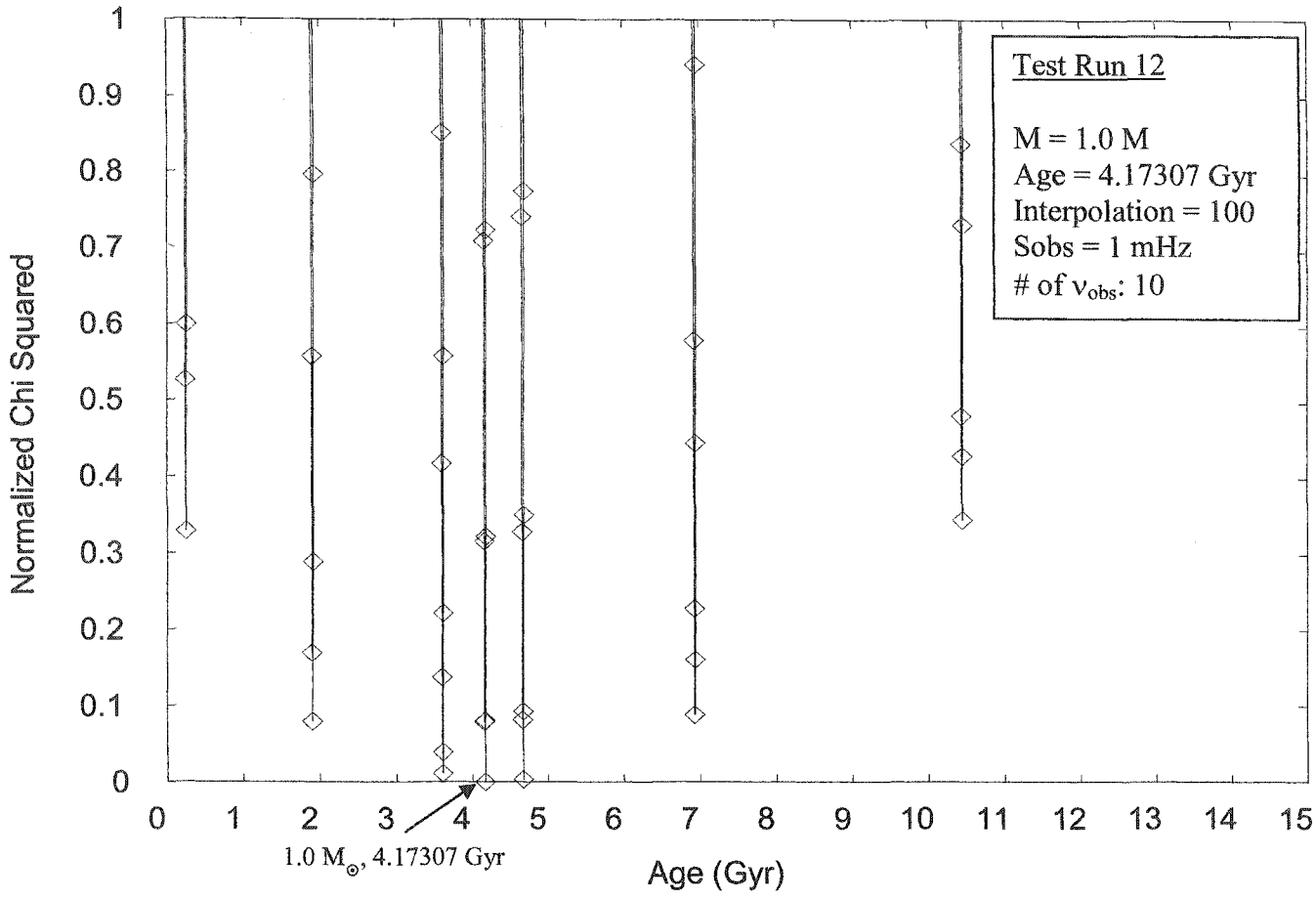

Figure 3.16: Normalized χ^2 versus age SEARCH program results using 10 $l = 0$, 1 model frequencies corresponding to M = 1.0 $M_\odot$ and 4.17307 Gyr (see figure 3.2). The frequency interpolation in age is set to 100 points and the σ_{obs} is set to ± 1 μHz. The figure minimum at 1.0 $M_\odot$ and 4.17307 Gyr as well as the minima arrangement is consistent with figure 3.2.

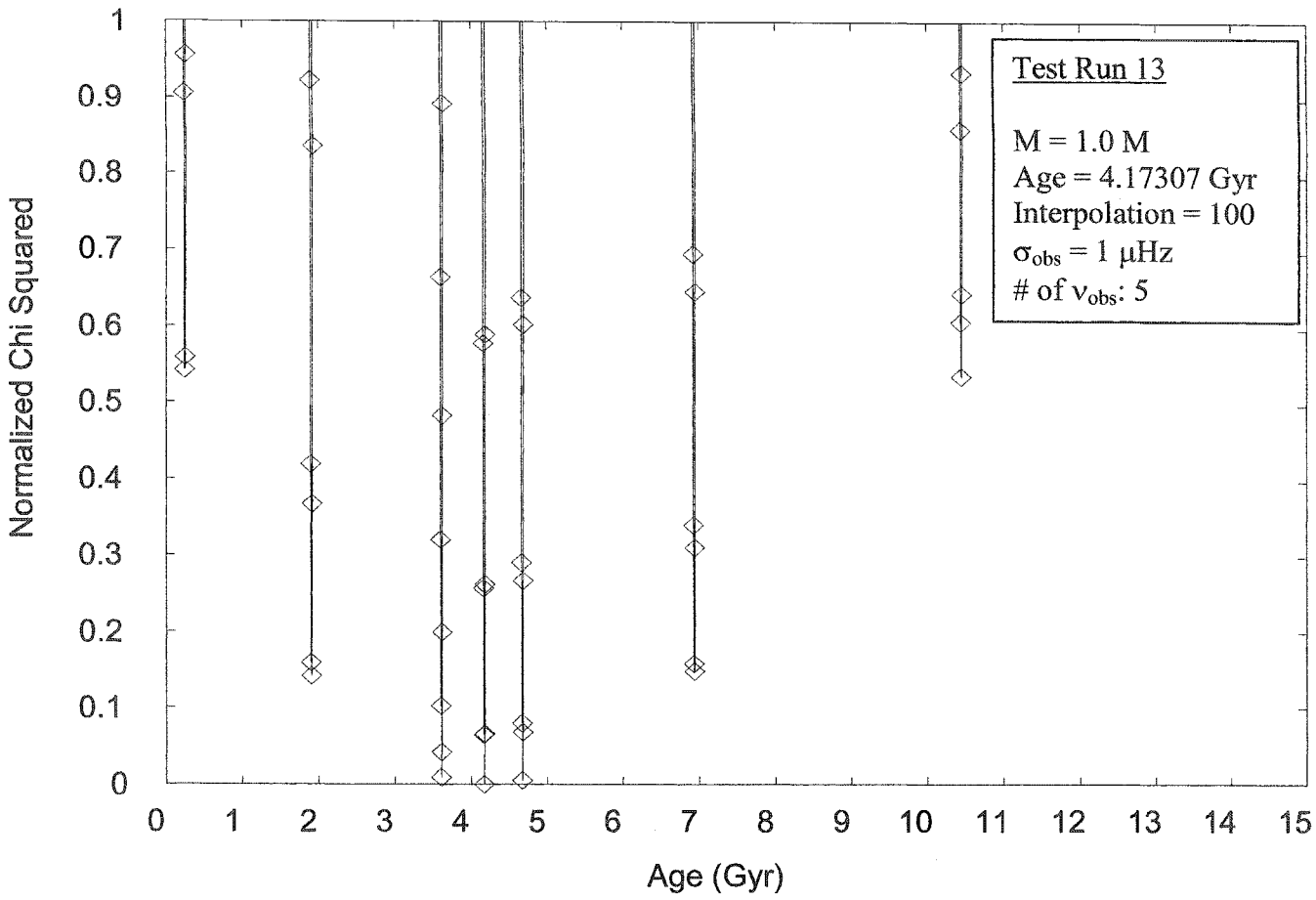

Figure 3.17: Normalized χ^2 versus age SEARCH program results using 5 $l = 0$, 1 model frequencies corresponding to M = 1.0 $M_\odot$ and 4.17307 Gyr (see figure 3.2). The frequency interpolation in age is set to 100 points and the σ_{obs} is set to ± 1 μHz. The figure minimum at 1.0 $M_\odot$ and 4.17307 Gyr as well as the minima arrangement is consistent with figure 3.2.

Table 3.3: Frequencies from the unknown models A, B C and D, provided by Guenther (private communication).

Model A (μHz)	Model B (μHz)	Model C (μHz)	Model D (μHz)
663.517512	646.016795	384.690922	1313.640
754.745759	731.176477	410.274505	1392.279
857.391611	828.470381	465.781212	1480.936
946.924943	916.490574	504.452919	1559.432
1046.62807	1010.73802	554.065606	1650.191
1136.93848	1096.80878	598.341223	1729.808
1237.18917	1193.83331	645.37635	1819.292
1323.91695	1277.87602	690.72798	1893.707
1424.92159	1373.44015	736.789113	1983.474
1511.69276	1457.25539	829.148675	2058.446
1610.95221	1553.79033	874.942633	2142.154
1696.83733	1635.71868	922.370372	2216.567
1796.47412	1731.41479	1015.49489	2304.206
1880.78789	1813.243	1109.20417	2380.441
1978.29472	1907.28051	1154.19781	
2062.06568	1986.95735	1203.75965	
2157.36558	2079.49819	1297.53433	
2239.13852	2157.97743	1389.15299	
2333.19829	2248.06029	1479.32781	
2414.28269	2325.7755	1569.32491	
2506.84015	2415.66046	1660.30012	
2588.19182	2493.20654	1753.1733	
2680.84667	2582.82635	1847.40731	
2762.03242	2661.1828	1941.72614	
2854.60732	2750.6803	2035.57735	
2936.11276	2828.67433		
3027.71058	2917.78981		
3108.88773	2995.66191		
3200.0428	3083.62472		
3280.71084	3161.21424		
3371.26248	3249.10473		
3452.36643	3326.76097		
3542.75614	3414.60439		
3624.15455	3493.12316		
3715.08123	3581.33268		
3796.97185	3660.15292		
	3748.62031		

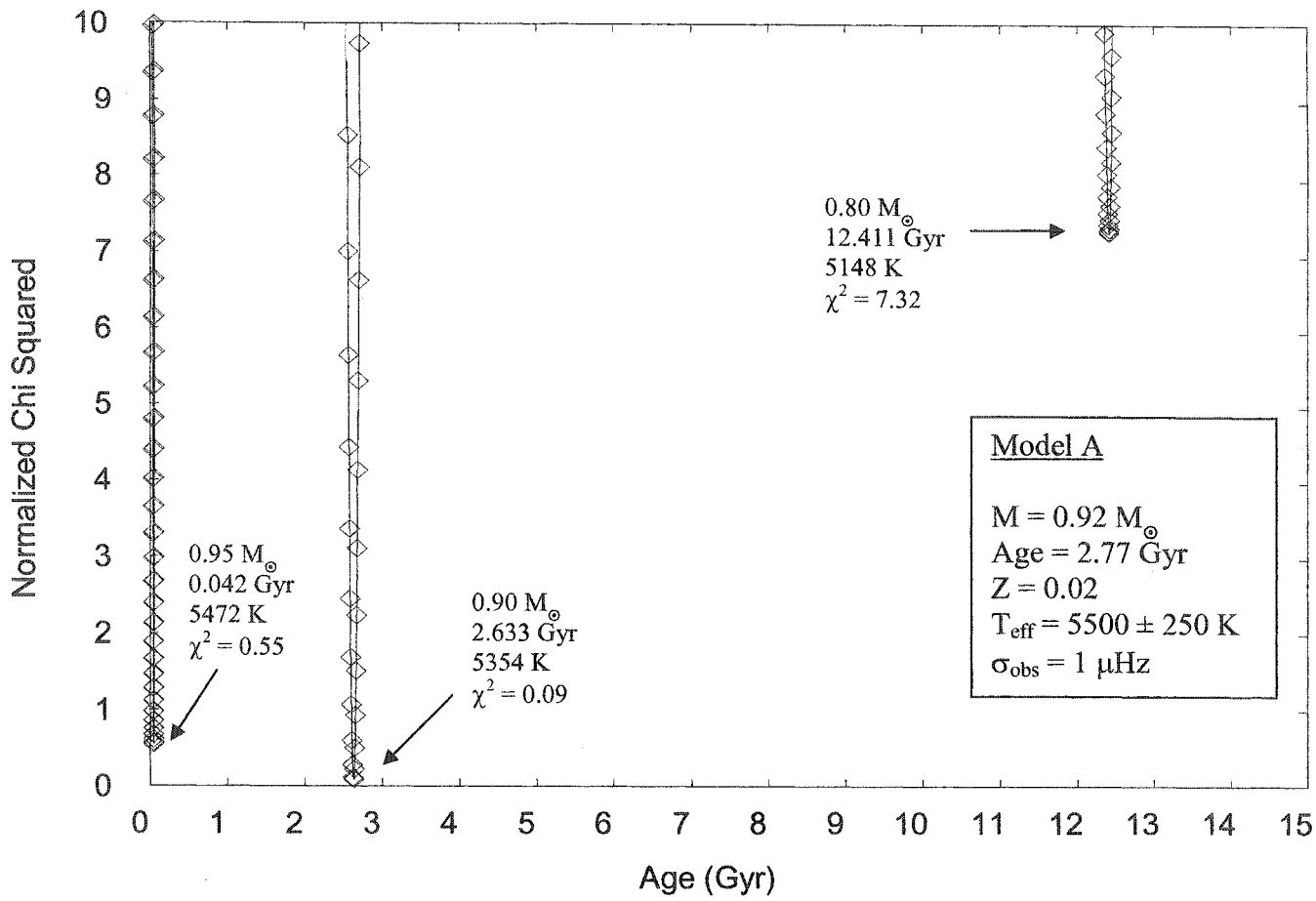

Figure 3.18: Normalized χ^2 versus age SEARCH program results using 36 $l = 0, 1$ frequencies from the unknown model A (see table 3.3). Three minima are identified along with mass, age, T_{eff} and normalized χ^2 values. The figure minimum is located at 0.90 $M_\odot$ and 2.633 Gyr. The inset box lists the actual mass, age, Z, T_{eff} and σ_{obs} values for model A. The frequency interpolation in age level is set to 100 points.

Table 3.4: Model A matched frequency results for the minimum at 0.90 $M_{\odot}$ and 2.633 Gyr. Listed are observed frequencies, model frequencies, model l and n values, and matching differences between observed and model frequencies.

ν_{obs} (μHz)	ν_{model} (μHz)	l	n	$\Delta_{obs-model}$ (μHz)
663.518	663.363	0	3	0.155
754.746	755.051	1	3	0.305
857.392	857.530	0	4	0.138
946.925	947.340	1	4	0.415
1046.628	1046.933	0	5	0.305
1136.938	1137.422	1	5	0.483
1237.189	1237.614	0	6	0.425
1323.917	1324.467	1	6	0.550
1424.922	1425.439	0	7	0.518
1511.693	1512.292	1	7	0.599
1610.952	1611.531	0	8	0.579
1696.837	1697.423	1	8	0.586
1796.474	1797.010	0	9	0.536
1880.788	1881.241	1	9	0.454
1978.295	1978.649	0	10	0.354
2062.066	2062.260	1	10	0.194
2157.366	2157.451	0	11	0.086
2239.139	2239.061	1	11	0.077
2333.198	2333.091	0	12	0.108
2414.283	2414.080	1	12	0.203
2506.840	2506.717	0	13	0.123
2588.192	2588.034	1	13	0.158
2680.847	2680.808	0	14	0.039
2762.032	2761.934	1	14	0.098
2854.607	2854.579	0	15	0.028
2936.113	2935.945	1	15	0.168
3027.711	3027.532	0	16	0.179
3108.888	3108.513	1	16	0.375
3200.043	3199.632	0	17	0.411
3280.711	3280.106	1	17	0.605
3371.262	3370.676	0	18	0.586
3452.366	3451.639	1	18	0.727
3542.756	3542.119	0	19	0.637
3624.155	3623.439	1	19	0.716
3715.081	3714.488	0	20	0.593
3796.972	3796.285	1	20	0.687

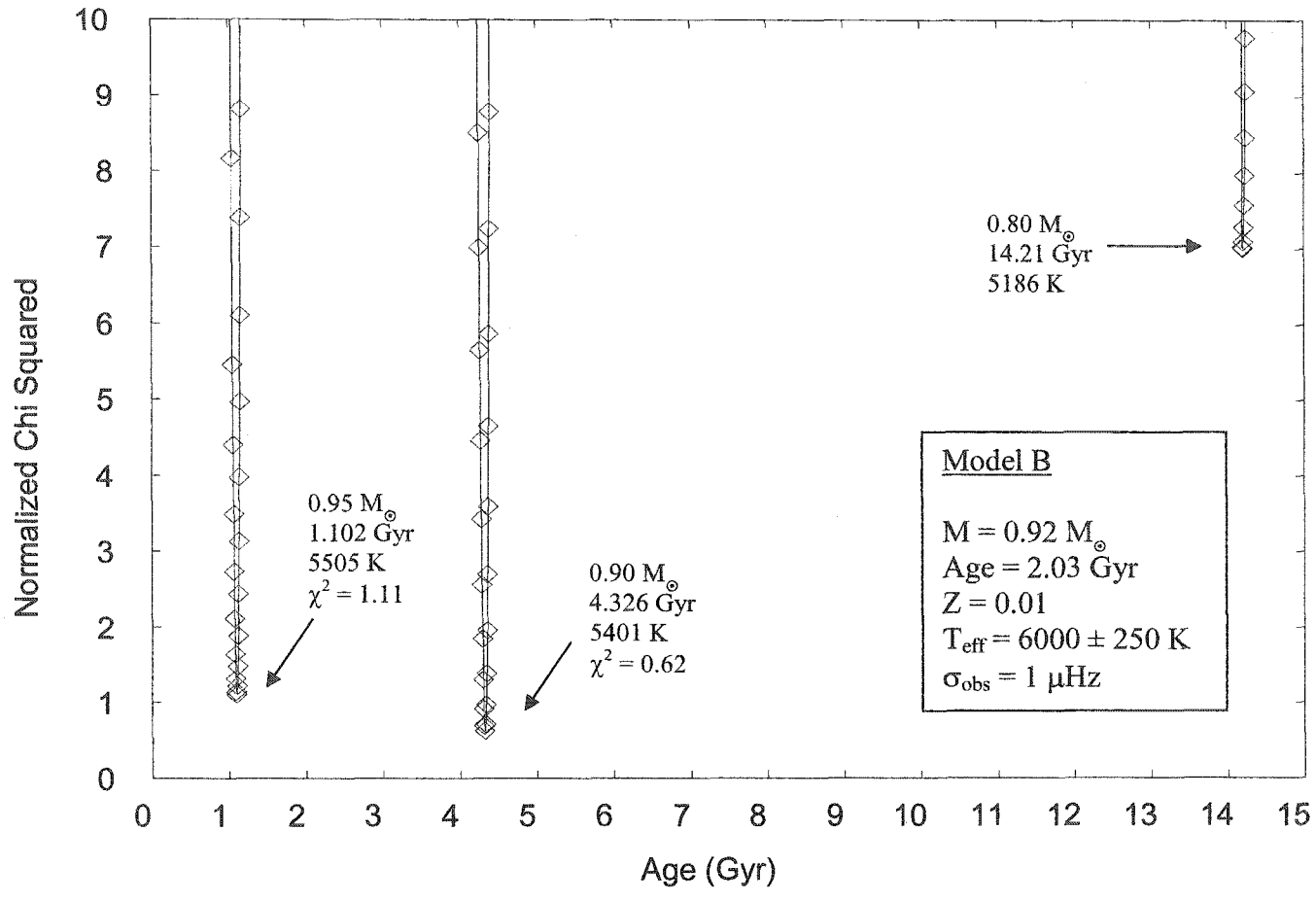

Figure 3.19: Normalized χ^2 versus age SEARCH program results using 37 $l = 0$, 1 frequencies from the unknown model B (see table 3.3). Three minima are labelled along with mass, age, T_{eff} and normalized χ^2 values. The figure minimum is located at 0.90 $M_\odot$ and 4.326 Gyr. The inset box lists the actual mass, age, Z, T_{eff} and σ_{obs} values for model B. The frequency interpolation in age level is set to 100 points.

Table 3.5: Model B matched frequency results for the minimum at 0.90 $M_{\odot}$ and 4.326 Gyr. Listed are observed frequencies, model frequencies, model l and n values, and matching differences between observed and model frequencies.

ν_{obs} (μHz)	ν_{model} (μHz)	l	n	$\Delta_{obs-model}$ (μHz)
646.017	643.05	0	2	2.967
731.176	729.1387	1	3	2.038
828.470	828.9688	0	4	0.498
916.491	914.2028	1	4	2.288
1010.738	1010.904	0	5	0.166
1096.809	1097.426	1	5	0.617
1193.833	1194.17	0	6	0.337
1277.876	1277.543	1	6	0.333
1373.440	1375.107	0	7	1.667
1457.255	1458.526	1	7	1.270
1553.790	1554.258	0	8	0.467
1635.719	1637.04	1	8	1.322
1731.415	1732.912	0	9	1.497
1813.243	1814.029	1	9	0.786
1907.281	1907.775	0	10	0.495
1986.957	1988.324	1	10	1.367
2079.498	2079.647	0	11	0.149
2157.977	2158.396	1	11	0.418
2248.060	2248.633	0	12	0.573
2325.776	2326.785	1	12	1.009
2415.660	2415.761	0	13	0.101
2493.207	2494.452	1	13	1.246
2582.826	2583.451	0	14	0.625
2661.183	2661.984	1	14	0.801
2750.680	2750.901	0	15	0.221
2828.674	2829.581	1	15	0.907
2917.790	2917.391	0	16	0.399
2995.662	2995.815	1	16	0.154
3083.625	3083.153	0	17	0.471
3161.214	3161.132	1	17	0.082
3249.105	3248.137	0	18	0.968
3326.761	3326.641	1	18	0.120
3414.604	3413.521	0	19	1.083
3493.123	3492.486	1	19	0.637
3581.333	3579.893	0	20	1.440
3660.153	3659.17	1	20	0.983
3748.620	3746.454	0	21	2.166

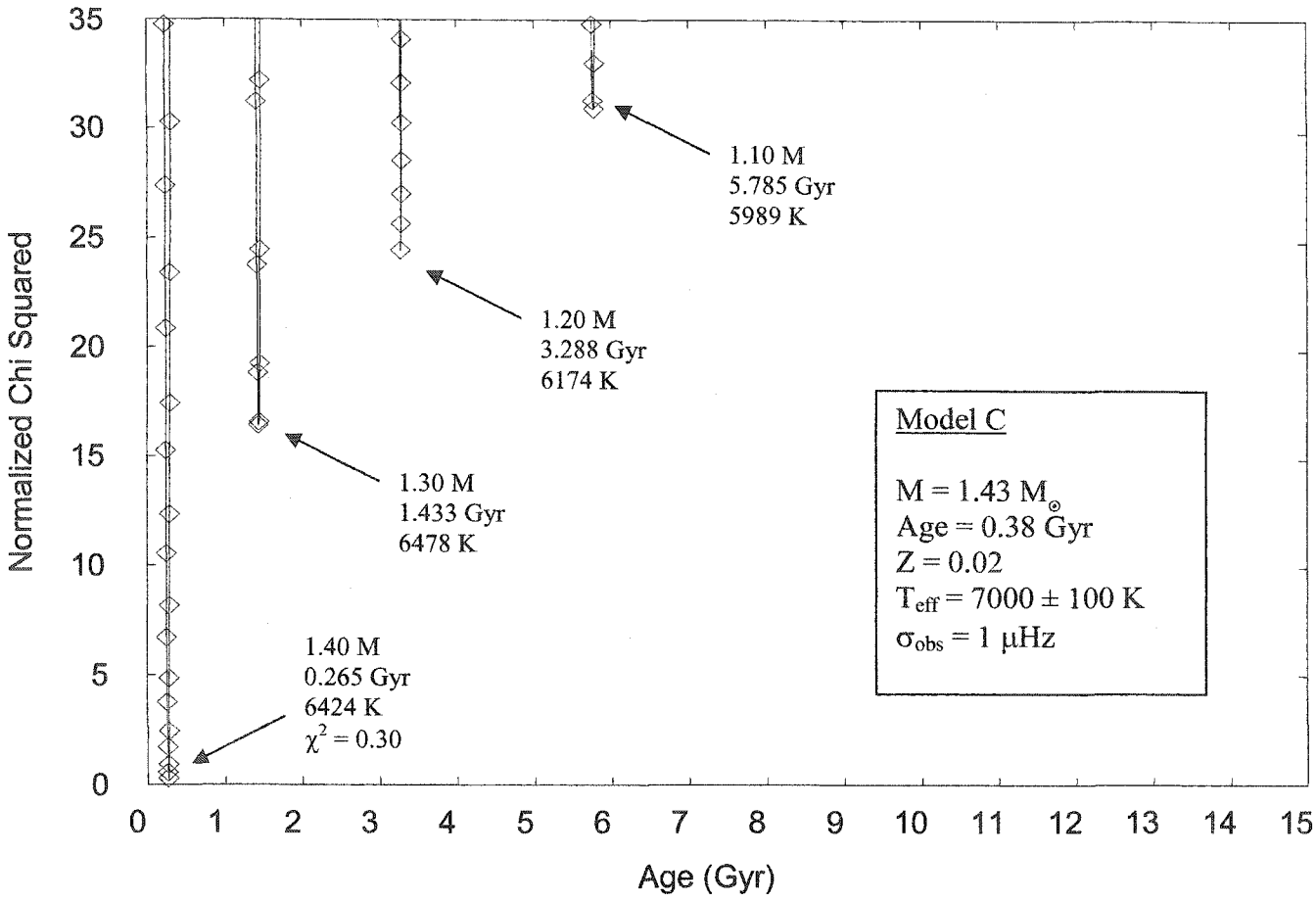

Figure 3.20: Normalized χ^2 versus age SEARCH program results using 25 $l = 0$, 1 frequencies from the unknown model C (see table 3.3). Three minima are labelled along with mass, age, T_{eff} and normalized χ^2 values. The figure minimum is located at 1.40 $M_\odot$ and 0.265 Gyr. The inset box lists the actual mass, age, Z, T_{eff} and σ_{obs} values for model C. The frequency interpolation in age is set to 100 points.

Table 3.6: Model C matched frequency results for the minimum at 1.40 $M_{\odot}$ and 0.265 Gyr. Listed are observed frequencies, model frequencies, model l and n values, and matching differences between observed and model frequencies.

ν_{obs} (μHz)	ν_{model} (μHz)	l	n	$\Delta_{obs-model}$ (μHz)
384.691	386.221	0	2	1.530
410.275	411.499	1	3	1.225
465.781	466.483	0	3	0.702
504.453	504.873	1	4	0.420
598.341	598.706	1	5	0.365
645.376	645.759	0	6	0.382
690.728	691.304	1	6	0.576
736.789	737.149	0	7	0.360
829.149	828.996	0	8	0.153
874.943	874.712	1	8	0.231
922.370	921.993	0	9	0.377
1015.495	1015.328	0	10	0.166
1109.204	1108.856	0	11	0.348
1154.198	1153.735	1	11	0.463
1203.760	1203.146	0	12	0.613
1297.534	1297.145	0	13	0.390
1389.153	1389.118	0	14	0.035
1479.328	1479.184	0	15	0.144
1569.325	1569.141	0	16	0.184
1660.300	1660.165	0	17	0.135
1753.173	1752.770	0	18	0.403
1847.407	1846.828	0	19	0.579
1941.726	1941.384	0	20	0.342
2035.577	2035.431	0	21	0.146

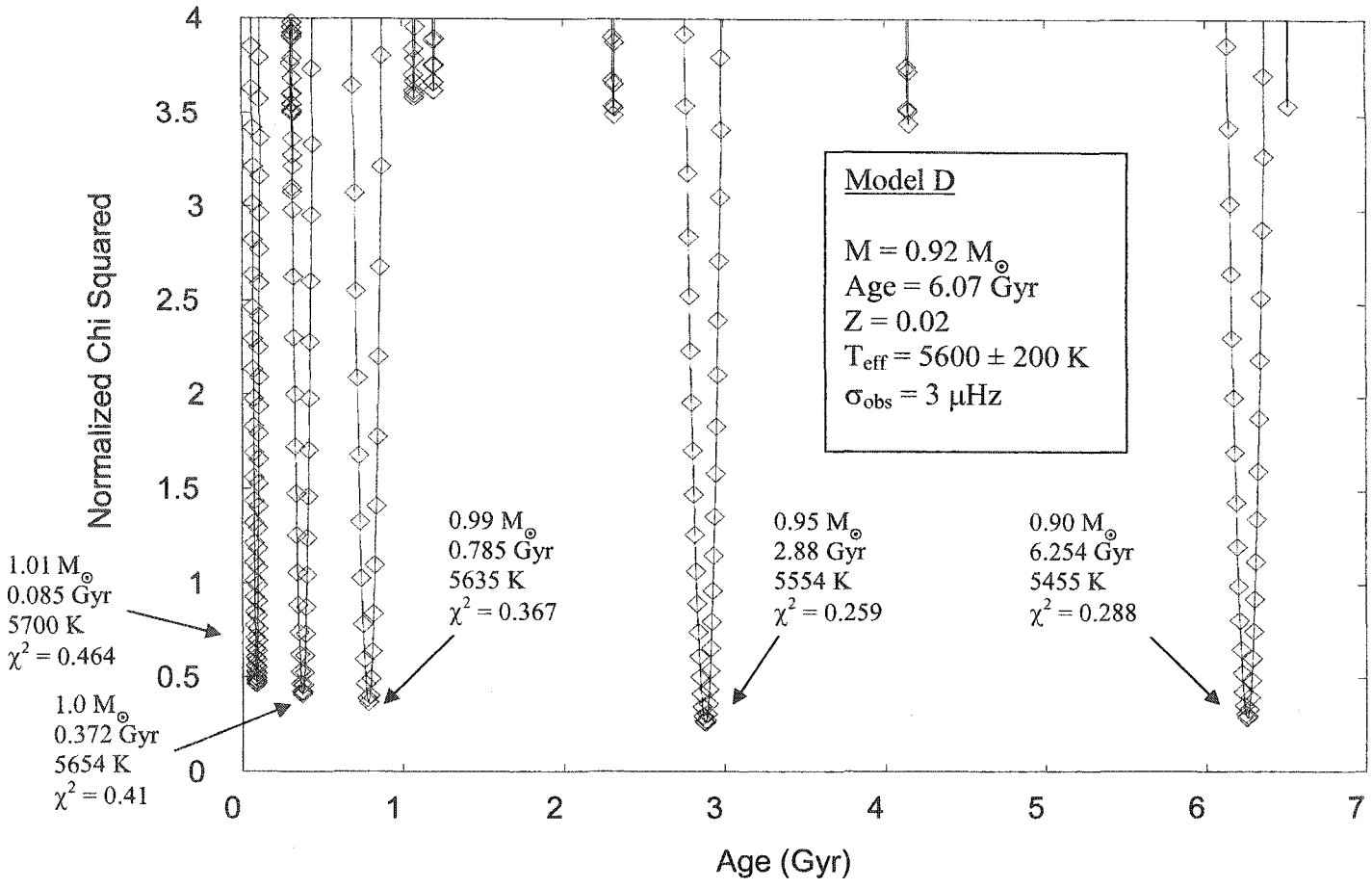

Figure 3.21: Normalized χ^2 versus age SEARCH program results using 14 $l = 0$, 1 frequencies from the unknown model D (see table 3.3). Three minima are labelled along with mass, age, T_{eff} and normalized χ^2 values. The figure minimum is located at 0.95 $M_\odot$ and 2.88 Gyr. The inset box lists the actual mass, age, Z, T_{eff} and σ_{obs} values for model D. The frequency interpolation in age is set to 100 points.

Table 3.7: Model D matched frequency results for the minimum at 0.95 $M_{\odot}$ and 2.88 Gyr. Listed are observed frequencies, model frequencies, model l and n values, and matching differences between observed and model frequencies.

ν_{obs} (μHz)	ν_{model} (μHz)	l	n	$\Delta_{obs\text{-}model}$ (μHz)
1313.640	1310.326	0	7	3.314
1392.279	1390.506	1	7	1.773
1480.936	1481.555	0	8	0.619
1559.432	1560.345	1	8	0.913
1650.191	1651.858	0	9	1.667
1729.808	1729.549	1	9	0.259
1819.292	1818.776	0	10	0.516
1893.707	1895.566	1	10	1.859
1983.474	1983.156	0	11	0.318
2058.446	2057.88	1	11	0.566
2142.154	2143.986	0	12	1.832
2216.567	2218.434	1	12	1.867
2304.206	2303.382	0	13	0.824
2380.441	2377.907	1	13	2.534

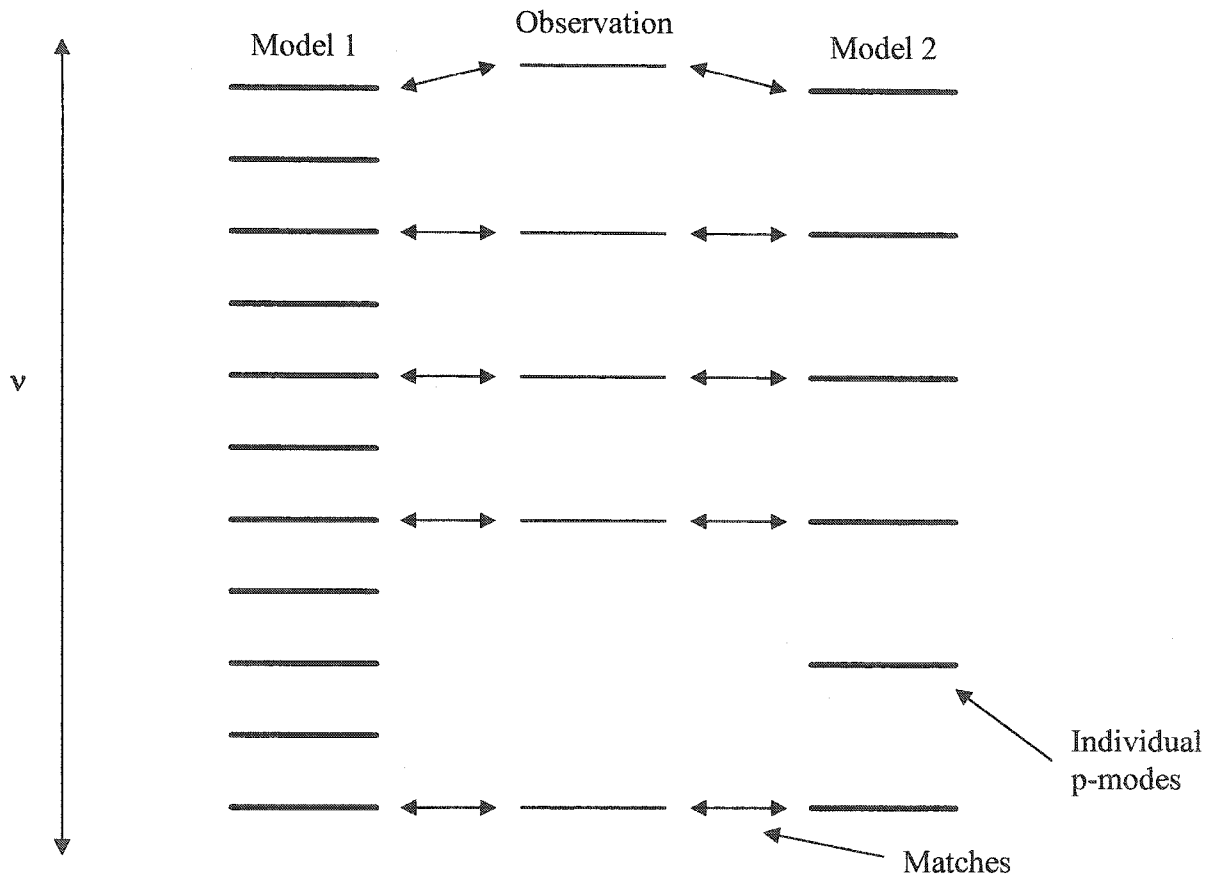

Figure 3.22: A schematic plot of frequency matching between an observed frequency spectrum and two different model spectra. This schematic illustrates the potential for an observed spectrum to be well matched to multiple model spectra (i.e. multi-valued). Such a case would require an additional constraint to determine the true best-fit model. This scenario did not arise during any testing conducted in this thesis.

Chapter 4

The Sun

4. Introduction

This chapter presents the testing results of the frequency search technique using observed solar p-mode frequencies. Observed solar p-mode frequencies are the most accurate observed stellar p-modes. Testing the frequency search technique using observed solar p-modes evaluates the technique under more realistic conditions.

Two tests of the frequency search technique are performed using observed solar p-modes. The first test compares observed solar p-mode frequencies with the calibrated solar model frequency grid from chapter 3. The second test compares observed solar p-mode frequencies with a model frequency grid constructed using standard solar model physics. This second test uses the optimal models for the frequency search technique summarized in § 3.8.

4.1. Forming a Solar Model Frequency Grid

Two solar model frequency grids are used for testing. The first grid uses the calibrated solar model frequency grid constructed in chapter 3. This model frequency grid was constructed around a calibrated solar model that does not include the gravitational settling of helium and heavy metals with a grey atmosphere in the Eddington approximation used to model the solar atmosphere. See table 3.1 to review the calibrated solar model frequency grid properties.

The second solar model frequency grid used for testing is constructed with the standard solar model as a central model. The standard solar model (used here) includes the of gravitational settling of helium and heavy metals, as well as a Krishna Swamy (1966) empirical fit to the observed solar T-τ to model the solar atmosphere. The central standard solar model is determined by evolving an appropriate solar ZAMS, 1 $M_{\odot}$ model to the current solar age, calibrated to the observed solar radius and luminosity to an accuracy of 1 part in 10^6. Calibration is achieved by allowing the variation of α the helium abundance in YREC until the desired accuracy is achieved. This standard solar model has been used successfully in previous works (e.g. see Brown et al. 2003). Resulting properties for the calibrated standard solar model, central model, are listed in table 4.1.

Table 4.1: The determined properties for the calibrated standard solar model, central model.

Parameters	Value
Mass	1.0 $M_{\odot}$
Age	4.55 Gyr
X_{ZAMS}	0.7063
Y_{ZAMS}	0.2737
Z_{ZAMS}	0.02
$L_{\odot}$	3.851×10^{26} W
T_{eff}	5780 K
α	2.086

Using the calibrated standard solar model values of X_{ZAMS} (hydrogen abundance), Y_{ZAMS} (helium abundance), Z_{ZAMS} (heavy metal abundance) and mixing length parameter, a grid of 11 standard solar model evolutionary tracks are calculated within the mass range 0.95 $M_{\odot}$ to 1.05 $M_{\odot}$, with a mass resolution of 0.01 $M_{\odot}$. All the

standard solar model evolutionary tracks are evolved from appropriate ZAMS models to the base of the giant branch in approximately 200 time steps per track. Maximum age values for the standard solar model evolutionary tracks range from 8.8 Gyr to 12.9 Gyr for mass of 1.05 $M_{\odot}$ and 0.95 $M_{\odot}$ respectively. The mass range was chosen to provide good coverage around the known mass of the Sun. The age range was chosen to be consistent with the calibrated solar model frequency grid from chapter 3.

Approximately 45 to 75 models per track are extracted at equal spacing along the 11 evolutionary tracks. Pulsation frequencies for l = 0, 1, 2 and n = 1 to 30 are calculated. The extracted models set the basic age resolution for the standard solar model pulsation spectra.

4.2. Testing Results Using the Calibrated Solar Model Frequency Grid

Observed solar p-mode frequencies were obtained from BiSON solar observations (Chaplin et al. 1999). Chaplin et al. (1999) identify 74 individual solar p-mode frequencies with l = 0, 1, 2, 3 and n = 8 to 28. The identified solar p-mode frequencies from Chaplin et al. (1999) are listed in table 4.2[27]. For this section, observed solar p-mode frequencies for l = 0, 1 and n = 8 to 25 are used.

Tests conducted with the calibrated solar model frequency grid use a frequency interpolation in age of 100 points between consecutive model spectra of constant mass. Figure 4.1 shows the SEARCH program results from the comparison the observed solar p-mode frequencies with the calibrated solar model frequency grid in a plot of normalized χ^2 versus age. Normalized χ^2 minima corresponding to solar models with

[27] Tables and figures are located at the end of this chapter.

mass values of 0.90 $M_\odot$ to 1.10 $M_\odot$ are identified. An identified figure minimum corresponds to the solar model with a mass of 0.90 $M_\odot$ and an age of 10.864 Gyr.

The identified minima of figure 4.1 have normalized χ^2 values ranging from 7 to 15, indicating that the observed solar p-mode spectra are matched to model spectra to values $> \left(\sigma_{Obs}^2 + \sigma_{Model}^2\right)^{1/2}$ ($\approx$ 1 μHz for this solar case). Frequency matching to $\leq$ 1 μHz is required to produce optimal normalized χ^2 results (values < 1) since the observed frequency uncertainties for the Sun are approximately 10 to 100 times smaller than the estimated model frequency uncertainties (therefore, only model frequency uncertainties dominate the normalized χ^2 results). Normalized χ^2 provides minima but does not confidently constrain any solar models (mass and age values).

Table 4.3 lists the solar model pulsation spectrum (M = 0.90 $M_\odot$, age = 10.864 Gyr) that best matched the observed solar p-mode spectrum. Matched observed and model frequencies, corresponding solar model *l* and *n* values, and the differences between the matched observed and model frequencies are listed. The solar model *l* and *n* values are consistent with the corresponding identified *l* and *n* values from table 4.2. Observed solar p-mode frequencies are matched to approximately < 1 μHz to 6 μHz.

The non-pulsation constraint of effective temperature is applied to the figure 4.1 results. The solar effective temperature of 5780 ± 20 K is used. Solar models within the mass and age range of 0.99 $M_\odot$ to 1.01 $M_\odot$ and 4.020 Gyr to 5.084 Gyr, respectively, are constrained by the solar effective temperature.

Additional testing using the calibrated solar model frequency grid is conducted by excluding observed solar p-mode frequencies with $n > 20$. The test is performed to explore the fact that high p-mode frequencies are poorly determined within stellar

models. Figure 4.2 shows the SEARCH program results of the comparison of the calibrated solar model frequency grid with observed solar p-mode frequencies ($n \leq 20$) in a plot of normalized χ^2 versus age. Normalized χ^2 minima are identified for solar models with masses of 0.90 $M_\odot$ to 1.10 $M_\odot$. A figure minimum is identified which corresponds to a solar model with a mass of 0.90 $M_\odot$ and an age of 10.846 Gyr. The identified minima of figure 4.2 have normalized χ^2 values between approximately 2 to 7, indicating that the exclusion of higher frequencies results in a better matching between observed and model frequencies. The normalized χ^2 results indicate that the observed and model frequencies are matched to values $> \left(\sigma_{Obs}^2 + \sigma_{Model}^2\right)^{1/2}$.

Table 4.4 lists the solar model pulsation spectrum (M = 0.90 $M_\odot$, age = 10.846 Gyr) that best matches the observed p-mode solar spectrum ($n < 20$). The solar model l and n values are consistent with the corresponding identified l and n values from table 4.2. Observed solar p-mode frequencies are matched to values of < 1 μHz to 3 μHz.

The non-pulsation constraint of effective temperature is applied to the figure 4.2 results. Solar models within the mass and age range of 0.99 $M_\odot$ to 1.01 $M_\odot$ and 4.002 Gyr to 5.070 Gyr, respectively, are constrained by the solar effective temperature.

The testing results using the calibrated solar model frequency spectrum (figures 4.1 and 4.2) do not correspond to the actual Sun indicating the use of the calibrated solar model frequency grid in the frequency search technique fails. The addition of the non-pulsation constraint of effective temperature limits possible matches (solar models) to values which straddle the properties of the actual Sun; however, this result is meaningless due to the failure of the calibrated solar model frequency grid.

4.3. Testing Results using the Standard Solar Model Frequency Grid

The second test involves the comparison of observed solar p-mode frequencies to the standard solar model frequency grid. This grid is an improvement over the calibrated solar model frequency grid which has higher mass resolution, more complete stellar physics and additional model p-mode frequencies. Fifty-one observed solar p-mode frequencies with $l = 0, 1, 2$ and $n = 8$ to 28 are used for the test. Figure 4.3 shows the SEARCH program in a plot of normalized χ^2 versus age. Normalized χ^2 values corresponding to standard solar models with masses of 0.95 $M_\odot$ to 1.05 $M_\odot$ are shown. The identified figure minimum corresponds to a standard solar model with a mass of 0.98 $M_\odot$ and an age of 5.486 Gyr.

The normalized χ^2 values for the minima in figure 4.3 range from approximately 3 to 5. These values are greater than 1 which is consistent with the fact that the solar frequencies are not matched to ≤ 1 μHz, the requirement to produce optimal normalized χ^2 results (values < 1).

Table 4.5 lists the standard solar model spectrum (M = 0.98 $M_\odot$, age = 5.486 Gyr) that best matches the observed solar p-mode spectrum. The standard solar model l and n values are consistent with the identified l and n values listed in table 4.2. Observed solar p-mode frequencies are matched to values of < 1 μHz to 4 μHz.

The non-pulsation constraint of the solar effective temperature is applied to the figure 4.3 results. Standard solar models within the mass and age range of 0.99 $M_\odot$ to 1.01 $M_\odot$ and 4.150 Gyr to 5.022 Gyr, respectively are constrained. The figure 4.3 minimum lies outside the range of models constrained by the observed solar effective temperature.

Additional testing of the standard solar model frequency grid is conducted by excluding observed solar p-mode frequencies with $n > 20$ to determine the affects of poorly determined high p-mode frequencies. Figure 4.4 shows the normalized χ^2 versus age SEARCH program results of the comparison of 36 observed solar p-mode frequencies ($n \leq 20$) with the standard solar model frequency grid. Normalized χ^2 values corresponding to standard solar models with masses of 0.95 $M_\odot$ to 1.05 $M_\odot$ are indicated. The identified figure minimum corresponds to a standard solar model with a mass of 0.99 $M_\odot$ and an age of 5.013 Gyr. The normalized χ^2 minima values range from 0.5 to 2 indicating that the observed frequencies are matched to $\approx\left(\sigma_{obs}^2 + \sigma_{model}^2\right)^{1/2}$.

Table 4.6 lists the standard solar model spectrum (M = 0.99 $M_\odot$, age = 5.013 Gyr) that best matches the observed solar p-mode spectrum. The standard solar model l and n values are consistent with the corresponding identified l and n values from table 4.2. Observed solar p-mode frequencies are matched to values ranging from « 1 μHz to 2 μHz.

The non-pulsation constraint of the solar effective temperature is applied to figure 4.4. Standard solar models within the mass and age range of 0.99 $M_\odot$ to 1.01 $M_\odot$ and 4.140 Gyr to 5.013 Gyr, respectively are constrained. The figure 4.4 minimum lies within the range of models constrained by the observed solar effective temperature.

The testing results in figures 4.3 and 4.4 show the use of a standard solar model frequency grid with the optimal requirements for the frequency search technique succeed in matching the observed Sun. The results of both figures (as well as figures 4.1 and 4.2) reemphasize the problem of inadequate modeling of the solar atmosphere.

4.4 Overall Results

The evaluation of the frequency search technique using observed solar p-mode frequencies produces some overall results. The overall results for chapter 4 are:

1. Testing of the frequency search technique using the calibrated solar model frequency grid failed to reproduce the observed Sun. This failure is the result of insufficient frequency resolution in mass which is confirmed independently (Guenther, private communication).
2. Testing of the frequency search technique using the standard solar model frequency grid was successful in reproducing the observed Sun.
3. Accurate modelling of stellar atmospheres within stellar models is necessary to produce accurate matches to higher observed p-mode frequencies.
4. The non-pulsation constraint of effective temperature is helpful in eliminating unphysical models from the results of a frequency search technique analysis. Effective temperature was applied successfully in the tests of this chapter.

Table 4.2: Observed solar p-mode frequencies and uncertainties from Chaplin et al. (1999). Frequencies with values of $l = 0$, 1, 2 and $n = 8$ to 25 are used in chapter 4. (With permission, from the *Monthly Notices of the Royal Astronomical Society*, Volume 308, © 1999, by Monthly Notices of the Royal Astronomical Society)

n	$l = 0$ (μHz)	$l = 1$ (μHz)	$l = 2$ (μHz)	$l = 3$ (μHz)
8	------	------	1394.659 ± 0.008	------
9	------	1472.828 ± 0.007	1535.857 ± 0.012	------
10	1548.328 ± 0.037	1612.715 ± 0.009	1674.543 ± 0.015	------
11	1686.570 ± 0.019	1749.303 ± 0.019	1810.350 ± 0.039	1865.289 ± 0.038
12	1822.227 ± 0.034	1885.112 ± 0.029	1945.740 ± 0.038	2001.200 ± 0.050
13	1957.407 ± 0.027	2020.794 ± 0.030	2082.052 ± 0.051	2137.804 ± 0.057
14	2093.494 ± 0.046	2156.760 ± 0.051	2217.743 ± 0.052	2273.471 ± 0.065
15	2228.696 ± 0.040	2291.954 ± 0.047	2352.162 ± 0.052	2407.722 ± 0.073
16	2362.824 ± 0.042	2425.617 ± 0.046	2485.874 ± 0.055	2541.657 ± 0.068
17	2496.172 ± 0.048	2559.139 ± 0.047	2619.724 ± 0.059	2676.242 ± 0.062
18	2629.680 ± 0.048	2693.310 ± 0.040	2754.374 ± 0.053	2811.426 ± 0.058
19	2764.088 ± 0.041	2828.058 ± 0.042	2889.556 ± 0.042	2946.981 ± 0.049
20	2898.953 ± 0.036	2963.393 ± 0.039	3024.662 ± 0.042	3082.252 ± 0.068
21	3033.749 ± 0.040	3098.111 ± 0.042	3159.918 ± 0.042	3217.814 ± 0.060
22	3168.527 ± 0.038	3233.222 ± 0.049	3295.088 ± 0.059	3353.381 ± 0.100
23	3303.480 ± 0.052	3368.586 ± 0.063	3430.979 ± 0.088	3489.528 ± 0.137
24	3438.973 ± 0.073	3504.038 ± 0.087	3567.071 ± 0.126	3626.061 ± 0.191
25	3574.987 ± 0.121	3640.307 ± 0.104	3703.208 ± 0.207	3762.638 ± 0.372
26	3710.664 ± 0.216	3776.859 ± 0.151	3840.098 ± 0.307	3900.509 ± 0.528
27	3847.579 ± 0.300	3913.392 ± 0.251	3977.242 ± 0.653	------
28	3984.403 ± 0.722	------	------	------

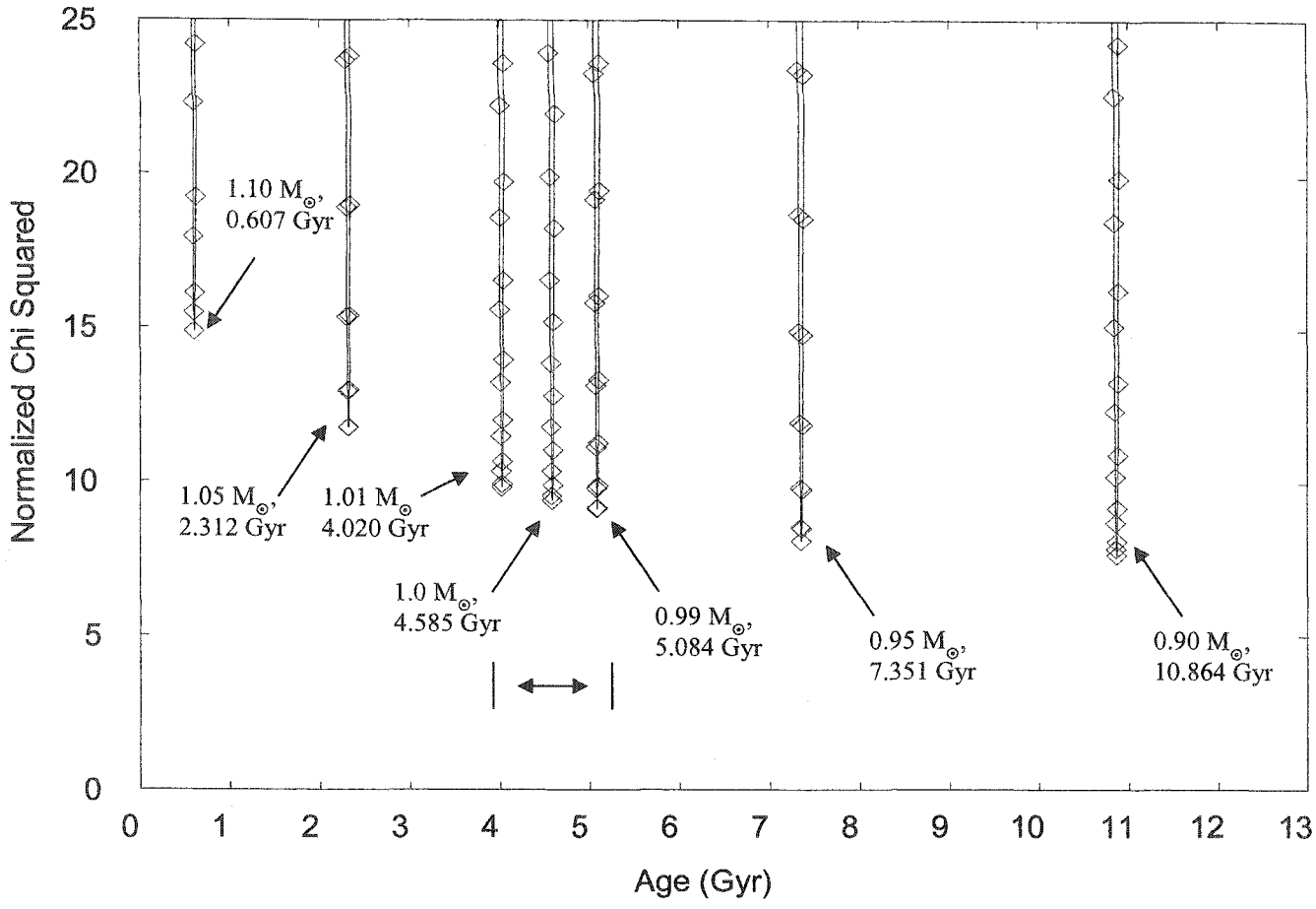

Figure 4.1: Normalized χ^2 versus age results from the comparison of the calibrated solar model frequency grid with 33 observed solar p-mode frequencies ($l = 0, 1$) from table 4.2. Normalized χ^2 minima of constant mass are labelled. A figure minimum is located at 0.90 $M_\odot$ and 10.864 Gyr. The denoted range identifies stellar models constrained by the effective temperature of the Sun (5780 ± 20 K). The constrained range in mass is 0.99 to 1.01 $M_\odot$ and in age is 4.020 to 5.084 Gyr.

Table 4.3: Model spectra (figure 4.1; M = 0.90 $M_{\odot}$, age = 10.864 Gyr) from the calibrated solar model frequency grid that best matches the 33 l = 0, 1 observed solar frequencies from table 4.2. Listed are the observed solar p-mode frequencies, model frequencies, model l and n values, and differences between the matched observed and model frequencies.

ν_{obs} (μHz)	ν_{model} (μHz)	l	n	$\Delta_{obs-model}$ (μHz)
1472.282	1471.555	1	9	1.273
1548.328	1548.539	0	10	0.211
1612.715	1610.554	1	10	2.161
1686.570	1684.756	0	11	1.812
1749.303	1746.642	1	11	2.661
1822.227	1820.055	0	12	2.172
1885.112	1882.026	1	12	3.086
1957.407	1955.393	0	13	2.014
2020.794	2018.328	1	13	2.466
2093.494	2090.751	0	14	2.743
2156.760	2154.090	1	14	2.670
2228.696	2225.731	0	15	2.965
2291.954	2288.687	1	15	3.267
2362.824	2359.392	0	16	3.432
2425.617	2422.721	1	16	2.896
2496.172	2492.766	0	17	3.406
2559.139	2556.817	1	17	2.322
2629.680	2627.137	0	18	2.543
2693.310	2691.819	1	18	1.491
2764.088	2762.201	0	19	1.886
2828.058	2827.629	1	19	0.429
2898.953	2897.612	0	20	1.341
2963.393	2963.389	1	20	0.004
3033.749	3033.292	0	21	0.457
3098.111	3099.286	1	21	1.175
3168.527	3169.043	0	22	0.516
3233.222	3235.662	1	22	2.440
3303.480	3305.319	0	23	1.839
3368.586	3372.341	1	23	3.755
3438.973	3442.165	0	24	3.192
3504.038	3509.471	1	24	5.433
3574.987	3579.226	0	25	4.239
3640.307	3646.986	1	25	6.679

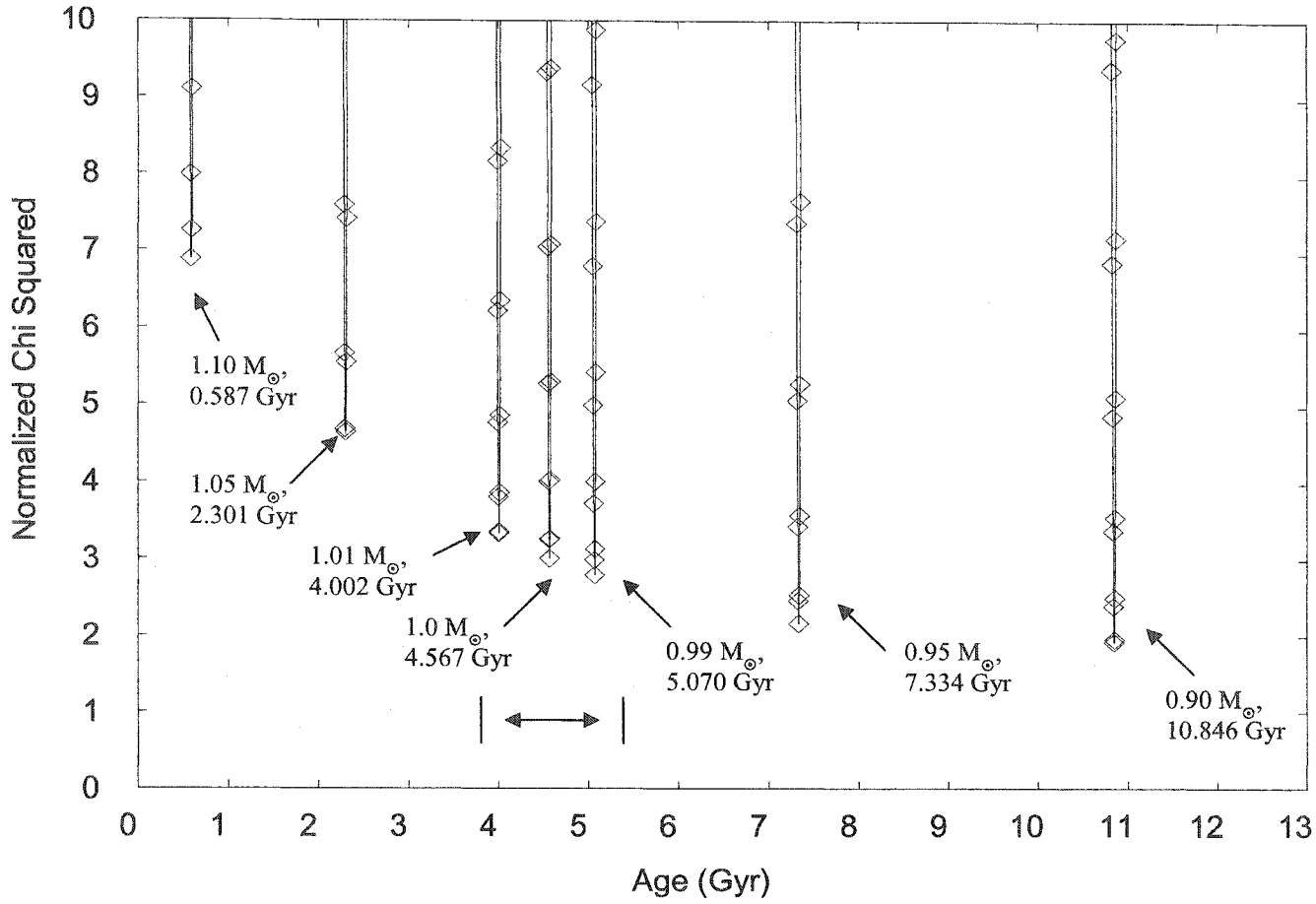

Figure 4.2: Normalized χ^2 versus age results from the comparison of the calibrated solar model frequency grid with 25 observed solar p-mode frequencies ($l = 0$, 1 and $n = 8$ to 20) from table 4.2. Normalized χ^2 values of constant mass are labelled. A figure minimum is located at 0.90 $M_\odot$ and 10.846 Gyr. The denoted range identifies stellar models constrained by the solar effective temperature (5780 ± 20 K). The constrained range in mass is 0.99 $M_\odot$ to 1.01 $M_\odot$ and in age is 4.002 to 5.022 Gyr.

Table 4.4: Model spectra (figure 4.2; M = 0.90 $M_{\odot}$, age = 10.846 Gyr) that best matches the 25 l = 0, 1 and n = 8 to 20 observed solar p-mode frequencies from table 4.2. Listed are observed solar p-mode frequencies, model frequencies, model l and n values, and differences between the matched observed and model frequencies.

ν_{obs} (μHz)	ν_{model} (μHz)	l	n	$\Delta_{obs\text{-}model}$ (μHz)
1472.828	1472.815	1	9	0.013
1548.328	1549.855	0	10	1.527
1612.715	1611.946	1	10	0.769
1686.570	1686.203	0	11	0.366
1749.303	1748.156	1	11	1.147
1822.227	1821.622	0	12	0.605
1885.112	1883.658	1	12	1.454
1957.407	1957.070	0	13	0.333
2020.794	2020.077	1	13	0.717
2093.494	2092.551	0	14	0.943
2156.760	2155.956	1	14	0.804
2228.696	2227.654	0	15	1.042
2291.954	2290.676	1	15	1.278
2362.824	2361.433	0	16	1.390
2425.617	2424.826	1	16	0.791
2496.172	2494.923	0	17	1.249
2559.139	2559.032	1	17	0.107
2629.680	2629.405	0	18	0.275
2693.310	2694.145	1	18	0.835
2764.088	2764.581	0	19	0.493
2828.058	2830.067	1	19	2.009
2898.953	2900.107	0	20	1.154
2963.393	2965.941	1	20	2.548

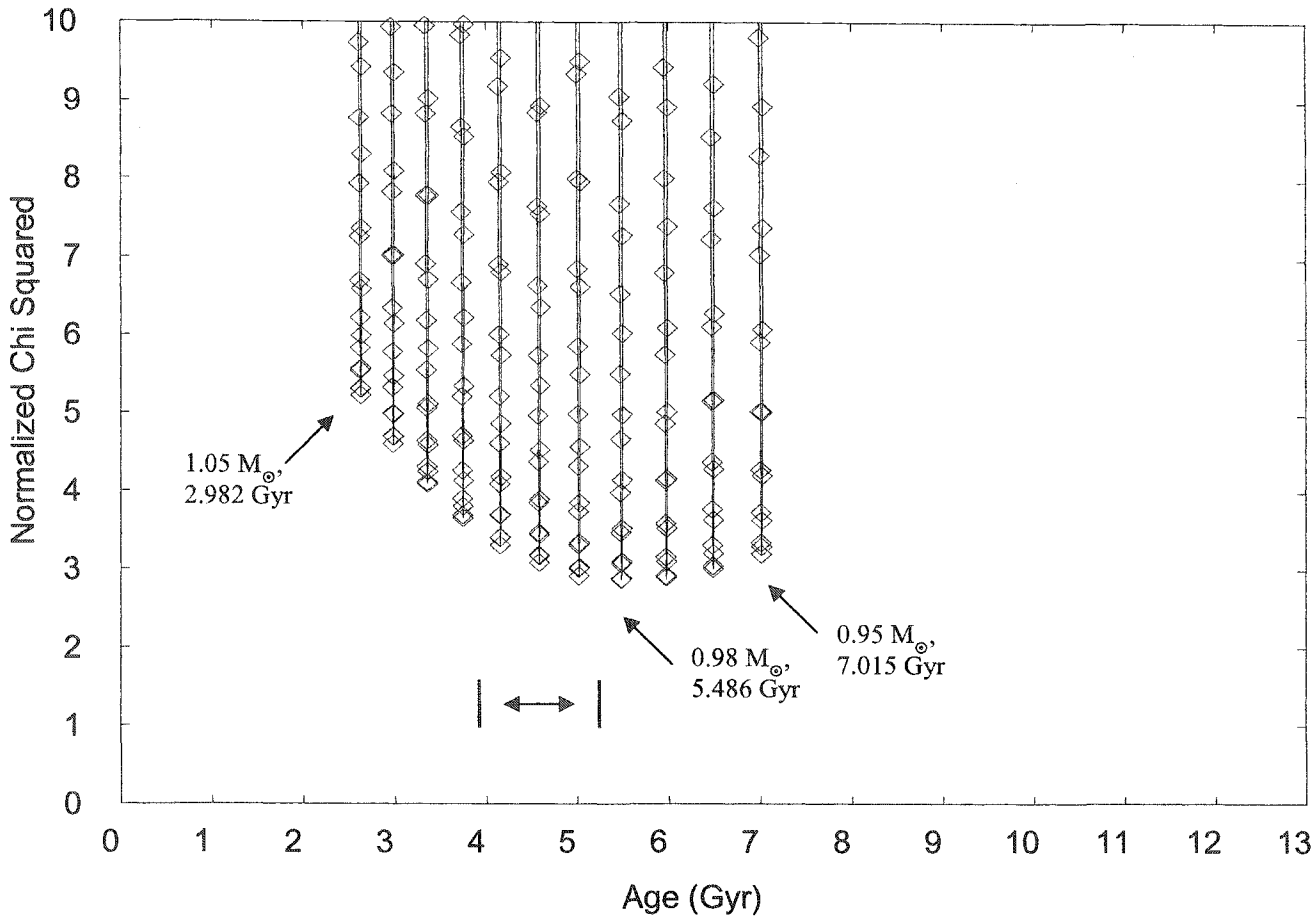

Figure 4.3: Normalized χ^2 versus age results for the comparison of the standard solar model frequency grid with 51 observed solar p-mode frequencies ($l = 0, 1, 2$) from table 4.2. The normalized χ^2 for the maximum and minimum mass results as well as the figure minimum at 0.98 $M_\odot$ and 5.486 Gyr are identified. The denoted range identifies the stellar models constrained by the solar effective temperature (5780 ± 20 K). The constrained range in mass is 0.99 to 1.01 $M_\odot$ and in age is 4.15 to 5.022 Gyr. The mass resolution for the results is 0.01 $M_\odot$.

Table 4.5: The model spectra (figure 4.3; M = 0.98 $M_{\odot}$, age = 5.486 Gyr) that best matches 51 $l = 0$, 1, 2 and $n = 8$ to 25 observed solar p-mode frequencies from table 4.2. Listed are observed solar p-mode frequencies, model frequencies, model l and n values, and differences between the matched observed and model frequencies.

ν_{obs} (μHz)	ν_{model} (μHz)	l	n	$\Delta_{obs-model}$ (μHz)
1394.659	1394.712	2	8	0.053
1472.828	1471.983	1	9	0.845
1535.857	1535.449	2	9	0.408
1548.328	1547.532	0	10	0.796
1612.715	1611.477	1	10	1.238
1674.543	1673.660	2	10	0.883
1686.570	1685.254	0	11	1.316
1749.303	1747.682	1	11	1.621
1810.350	1809.231	2	11	1.119
1822.227	1820.638	0	12	1.589
1885.112	1883.417	1	12	1.695
1945.740	1944.669	2	12	1.071
1957.407	1955.752	0	13	1.655
2020.794	2019.117	1	13	1.677
2082.052	2080.869	2	13	1.182
2093.494	2091.639	0	14	1.854
2156.760	2154.857	1	14	1.903
2217.743	2216.248	2	14	1.495
2228.696	2226.652	0	15	2.043
2291.954	2290.001	1	15	1.953
2352.162	2350.827	2	15	1.335
2362.824	2360.726	0	16	2.098
2425.617	2423.767	1	16	1.850
2485.874	2484.813	2	16	1.061
2496.172	2494.393	0	17	1.779
2559.139	2557.691	1	17	1.448
2619.724	2618.937	2	17	0.787
2629.680	2628.220	0	18	1.460
2693.310	2692.418	1	18	0.892
2754.374	2754.225	2	18	0.149
2764.088	2763.165	0	19	0.922
2828.058	2827.577	1	19	0.481
2889.556	2889.777	2	19	0.221
2898.953	2898.424	0	20	0.528
2963.393	2963.174	1	20	0.219
3024.662	3025.345	2	20	0.683
3033.749	3033.645	0	21	0.104
3098.111	3098.697	1	21	0.586
3159.918	3161.227	2	21	1.309

3168.527	3169.216	0	22	0.689
3233.222	3234.366	1	22	1.144
3295.088	3297.205	2	22	2.117
3303.480	3304.940	0	23	1.460
3368.586	3370.638	1	23	2.052
3430.979	3433.712	2	23	2.733
3438.973	3441.153	0	24	2.180
3504.038	3507.067	1	24	3.030
3567.071	3570.570	2	24	3.500
3574.987	3577.766	0	25	2.779
3640.307	3643.833	1	25	3.527
3703.208	3707.477	2	25	4.269

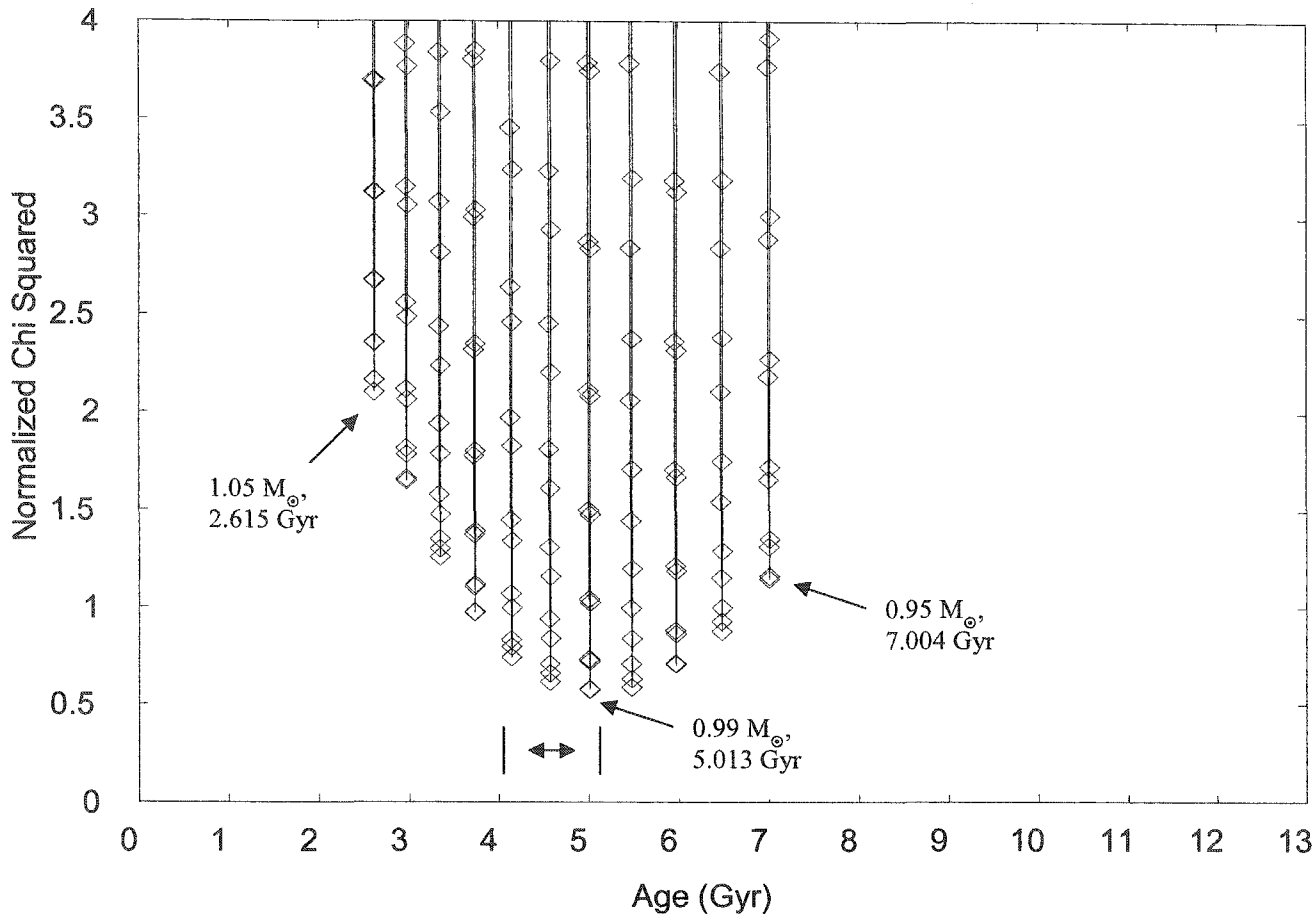

Figure 4.4: Normalized χ^2 versus age results for the comparison of the standard solar model frequency grid with 36 observed solar p-mode frequencies (l = 0, 1, 2 and n = 8 to 20) from table 4.2. The normalized χ^2 results for the maximum and minimum mass results as well as the figure minimum at 0.99 $M_\odot$ and 5.013 Gyr are identified. The denoted range identifies the stellar models constrained by the solar effective temperature (5780 ± 20 K). The constrained range in mass is 0.99 to 1.01 $M_\odot$ and in age is 4.14 to 5.013 Gyr. The mass resolution of the results is 0.01 $M_\odot$.

Table 4.6: The model spectra (figure 4.4; M = 0.99 $M_{\odot}$, age = 5.013 Gyr) that best matches 36 l = 0, 1, 2 and n = 8 to 20 observed solar p-mode frequencies from table 4.2. Listed are observed solar p-mode frequencies, model frequencies, model l and n values, and differences between the matched observed and model frequencies.

ν_{obs} (μHz)	ν_{model} (μHz)	l	n	$\Delta_{obs-model}$ (μHz)
1394.659	1394.686	2	8	0.027
1472.828	1472.468	1	9	0.360
1535.857	1535.680	2	9	0.177
1548.328	1547.953	0	10	0.375
1612.715	1612.047	1	10	0.668
1674.543	1674.109	2	10	0.434
1686.570	1685.955	0	11	0.615
1749.303	1748.479	1	11	0.823
1810.350	1809.710	2	11	0.640
1822.227	1821.370	0	12	0.857
1885.112	1884.252	1	12	0.860
1945.220	1945.740	2	12	0.520
1957.407	1956.561	0	13	0.845
2020.794	2019.873	1	13	0.921
2082.052	2081.437	2	13	0.615
2093.494	2092.531	0	14	0.963
2156.760	2155.829	1	14	0.931
2217.743	2216.949	2	14	0.794
2228.696	2227.669	0	15	1.027
2291.954	2291.076	1	15	0.878
2352.162	2351.739	2	15	0.423
2362.824	2361.970	0	16	0.854
2425.617	2424.939	1	16	0.678
2485.874	2485.748	2	16	0.126
2496.172	2495.984	0	17	0.488
2559.139	2558.971	1	17	0.168
2619.724	2619.889	2	17	0.165
2629.680	2629.513	0	18	0.167
2693.310	2693.596	1	18	0.286
2754.374	2755.212	2	18	0.838
2764.088	2764.531	0	19	0.443
2828.058	2828.852	1	19	0.794
2889.556	2890.798	2	19	1.242
2898.953	2899.836	0	20	0.882
2963.393	2964.571	1	20	1.178
3024.662	3026.505	2	20	1.842

Chapter 5

α Centauri A

5. Introduction

This chapter presents the testing results of the frequency search technique using observed stellar p-mode frequencies identified from α Cen A. Testing of the frequency search technique using observed stellar p-mode frequencies further evaluates the frequency search technique under more realistic conditions.

The α Cen binary system provides an excellent test-bed because the stellar properties of the system are well established. Observed stellar p-mode frequencies from α Cen A are compared with a model frequency grid appropriate to α Cen A. These tests use the optimal requirements for a model frequency grid summarized in § 3.8.

5.1. Forming a Model Frequency Grid for α Cen A

A model frequency grid based around a central model appropriate to α Cen A is required. The central model for the α Cen A model frequency grid is determined using model parameters from the analysis of α Cen A performed by Guenther and Demarque (2000).

The central model for the α Cen A model frequency grid is calculated for a 1.10 $M_{\odot}$ star, calibrated to the observed luminosity and effective temperature of α Cen A (see table 2.2). The age of α Cen A is uncertain due to uncertainties as to whether or not the

star possesses a convective core (see Guenther and Demarque 2000); hence, age is not used as a constraining parameter. The gravitational settling of helium and heavy metals are included in the α Cen A central model and a grey atmosphere in the Eddington approximation is used to model the stellar atmosphere.

Using YREC, a 1.10 $M_\odot$ ZAMS model was evolved to the observed luminosity and effective temperature of α Cen A, calibrated through variation of mixing length parameter and the helium abundance. Table 5.1 lists the determined properties for the calibrated α Cen A central model.

Table 5.1: The determined properties for the calibrated α Cen A central model.

Parameter	Value
Mass	1.10 $M_\odot$
X_{ZAMS}	0.686
Y_{ZAMS}	0.280
Z_{ZAMS}	0.034
L	1.575 ± 0.063 $L_\odot$
T_{eff}	5770 ± 50 K
α	2.043

Using the calibrated α Cen A model parameters of X_{ZAMS} (hydrogen abundance), Y_{ZAMS},(helium abundance), Z_{ZAMS} and mixing length parameter, a grid of 21 evolutionary tracks are calculated within the mass range of 1.0 $M_\odot$ to 1.2 $M_\odot$, with a mass resolution of 0.01 $M_\odot$. All α Cen A evolutionary tracks are evolved from appropriate ZAMS models to the base of the giant branch in approximately 225 time steps per evolutionary track. Maximum age values for the evolutionary tracks range from 6.8 Gyr and 13.2 Gyr for 1.2 $M_\odot$ and 1.0 $M_\odot$ respectively. The mass and age

ranges were chosen to provide sufficient coverage of the observed mass and predicted age range (evolutionary state) of α Cen A for the model frequency grid.

Pulsation frequencies are calculated from approximately 50 to 75 models per track extracted at equal spacing along the 21 evolutionary tracks. These extracted models set a basic age resolution for the α Cen A model pulsation spectra. Frequencies for $l = 0, 1, 2$ and $n = 1$ to 30 are calculated.

5.2. Testing Results using the α Cen A Model Frequency Grid

Observed p-mode frequencies for α Cen A were obtained from observations of α Cen A performed by Bouchy and Carrier (2002) (see § 1.5.1). Bouchy and Carrier (2002) identify 28 individual p-mode frequencies with $l = 0, 1, 2$ and $n = 15$ to 25. The l, n identifications for the observed α Cen A p-mode frequencies were determined using asymptotic theory for p-modes and should be regarded with caution. The observed frequency uncertainty is ± 0.46 μHz. The identified p-mode frequencies for α Cen A are listed in table 5.2[28].

Comments by Thoul et al. (2002) suggest that the α Cen A p-mode frequencies identified by Bouchy and Carrier (2002) are contaminated by 1 and 2-day aliasing. This contamination would make the identification (and detection) of $l = 2$ p-mode frequencies difficult and unreliable.

Due to the comments of Thoul et al. (2002), two tests of the comparison of the α Cen A model frequency grid with the observed p-mode frequencies for α Cen A are

[28] Tables and figures are located at the end of this chapter.

performed. Both tests use a frequency interpolation in age of 100 points between consecutive model spectra of constant mass.

The first test uses all 28 observed α Cen A p-mode frequencies listed in table 5.2 to compare with the α Cen A model frequency grid. Figure 5.1 shows the SEARCH program results in a plot of normalized χ^2 versus age. Normalized χ^2 minima are identified which correspond to α Cen A models with masses of 1.0 $M_\odot$ to 1.2 $M_\odot$. The identified figure minimum corresponds to the α Cen A model with a mass of 1.16 $M_\odot$ and an age of 5.07 Gyr.

Table 5.3 lists the model spectrum from the α Cen A model frequency grid that best matches the 28 observed α Cen A p-mode frequencies. The minimum for figure 5.1 has a normalized χ^2 value of 1.5. Observed and model frequencies are matched to an average value of ≈ 1 μHz (< 1 to 3.6 μHz) which is $\approx\left(\sigma_{Obs}^2+\sigma_{Model}^2\right)^{1/2}$ (≈ 1.1 μHz for this case). α Cen A model *l* and *n* values correspond to the identified *l* and *n* values for the matched α Cen A model pulsation spectrum. Normalized χ^2 results for α Cen A models with masses of 1.06 $M_\odot$ to 1.2 $M_\odot$ have values ranging from 1.5 to ~ 3, indicating these points are matched to values $\geq \left(\sigma_{Obs}^2+\sigma_{Model}^2\right)^{1/2}$.

The non-pulsation constraint of effective temperature is applied to figure 5.1. The effective temperature of α Cen A is 5770 ± 50 K, which constrains α Cen A models with a mass and age ranges of 1.06 $M_\odot$ to 1.14 $M_\odot$ and 5.73 Gyr to 8.372 Gyr. The figure minimum corresponding to 1.16 $M_\odot$ and 5.07 Gyr lies outside this constrained range.

Effective temperature constrains a range of α Cen A models which are consistent with the observed values for α Cen A; however, the figure minimum is inconsistent with the effective temperature constraints. This suggests there may be a problem with the observed α Cen A p-mode frequencies or with the α Cen A model frequency grid.

The second test of this chapter uses only l = 0, 1 observed α Cen A p-mode frequencies from table 5.2, to test the comments of Thoul et al. (2002). Figure 5.2 shows the SEARCH program results. Normalized χ^2 minima corresponding to the α Cen A models with masses of 1.0 $M_\odot$ to 1.2 $M_\odot$ are shown. The identified figure minimum corresponds to the α Cen A model with 1.08 $M_\odot$ and 7.836 Gyr. The normalized χ^2 results for the masses 1.0 $M_\odot$, 1.05 $M_\odot$ to 1.2 $M_\odot$ have values of less than ~ 2, which indicates the model spectra corresponding to these minima have matched the observed α Cen A p-mode frequencies to $\approx \left(\sigma_{Obs}^2 + \sigma_{Model}^2\right)^{1/2}$.

Table 5.4 lists the model spectrum that best matches the observed α Cen A p-mode frequencies. Observed and model frequencies for the figure minimum are matched to an average value of ≈ 0.7 μHz (< 1 to 2.3 μHz) which is $\leq \left(\sigma_{obs}^2 + \sigma_{\mathrm{mod}\,el}^2\right)^{1/2}$. The normalized χ^2 value for this minimum is 0.79. Matched model frequencies correspond to the identified n values for the observed α Cen A p-mode frequencies, but do not exactly match the identified l values. Three observed l = 0 p-modes of higher frequency are matched with l = 2 model frequencies (see table 5.4).

The non-pulsation constrain of effective temperature is applied to figure 5.2. The effective temperature of α Cen A constrains α Cen A models with mass and age values of 1.06 $M_\odot$ to 1.14 $M_\odot$ and 5.72 Gyr to 8.36 Gyr. The α Cen A model

corresponding to the minimum for figure 5.2 lies within the constrained mass and age range. These mass and age results are consistent with current stellar evolution models of α Cen A (e.g. see Guenther and Demarque 2000; Morel et al. 2001, Thévenin et al. 2002).

Better matching results between the α Cen A observed and model frequencies are achieved by the elimination of the observed α Cen A $l = 2$ p-modes which may suggest there has been a misidentification of the $l = 2$ frequencies in the Bouchy and Carrier (2002) results. The minimum of figure 5.2 plus the constrained mass range are consistent with observed values for α Cen A.

The results for α Cen A presented in this chapter are based on the assumed properties of the central model of the α Cen A model frequency grid obtained from Guenther and Demarque (2000). Any discrepancies in the α Cen A modelling of Guenther and Demarque (2000) will translate into the α Cen A testing discussed here.

5.3 Overall Testing Results

The application of the frequency search technique on observed α Cen A p-mode frequencies yields the following conclusions:

1. Tests of the frequency search technique using α Cen A observed p-mode frequencies were successful. The determined best models are consistent with observed values for α Cen A.
2. The non-pulsation constraint of effective temperature is required to eliminate unphysical models from the results of a frequency search technique analysis.

3. Better matching results were achieved after the elimination of $l = 2$ α Cen A observed p-mode frequencies. This suggests there may by a misidentification of $l = 2$ frequencies present in the results of Bouchy and Carrier (2002).
4. Note that this analysis using α Cen A observed frequencies does not constitute a rigorous analysis of the observed α Cen A p-mode spectrum. The goal of this analysis was to determine if the frequency search technique is able to produce useful results when using observed stellar p-modes.

Table 5.2: Observed p-mode frequencies from observations of α Cen A (Bouchy and Carrier 2002). (With permission, from *Astronomy & Astrophysics*, Volume 390, © 2002, by Astronomy & Astrophysics)

	$l = 0$ (μHz)	$l = 1$ (μHz)	$l = 2$ (μHz)
$n = 15$	--------	--------	1833.1
$n = 16$	1841.3	1887.4	1934.9
$n = 17$	--------	1991.7	2041.5
$n = 18$	--------	2095.6	2146.0
$n = 19$	2152.9	2202.8	2251.4
$n = 20$	2258.4	2309.1	2358.4
$n = 21$	2364.2	2414.3	2464.1
$n = 22$	2470.0	2519.3	2568.5
$n = 23$	2573.1	2625.6	--------
$n = 24$	2679.8	2733.2	2782.9
$n = 25$	2786.2	2837.6	2887.7

Table 5.3: The model spectrum (figure 5.1; M = 1.16 $M_{\odot}$, age = 5.075 Gyr) that best matches all 28 observed α Cen A p-mode frequencies from table 5.2. Listed are observed frequencies, model frequencies, model *l* and *n* values, and differences between the matched observed and model frequencies.

ν_{obs} (μHz)	ν_{model} (μHz)	*l*	*n*	$\Delta_{obs-model}$ (μHz)
1833.1	1831.050	2	15	2.050
1841.3	1837.727	0	16	3.573
1887.4	1885.981	1	16	1.418
1934.9	1935.331	2	16	0.431
1991.7	1990.492	1	17	1.208
2041.5	2040.099	2	17	1.401
2095.6	2095.913	1	18	0.313
2146.0	2145.973	2	18	0.027
2152.9	2151.653	0	19	1.247
2202.8	2201.753	1	19	1.047
2251.4	2252.024	2	19	0.624
2258.4	2257.328	0	20	1.072
2309.1	2307.935	1	20	1.165
2358.4	2357.964	2	20	0.436
2364.2	2362.818	0	21	1.382
2414.3	2413.890	1	21	0.410
2464.1	2464.142	2	21	0.042
2470.0	2468.564	0	22	1.436
2519.3	2519.920	1	22	0.620
2568.5	2570.278	2	22	1.778
2573.1	2574.296	0	23	1.196
2625.6	2626.455	1	23	0.855
2679.8	2680.351	0	24	0.551
2733.2	2733.010	1	24	0.190
2782.9	2783.671	2	24	0.771
2786.2	2786.816	0	25	0.616
2837.6	2839.828	1	25	2.228
2887.7	2890.337	2	25	2.637

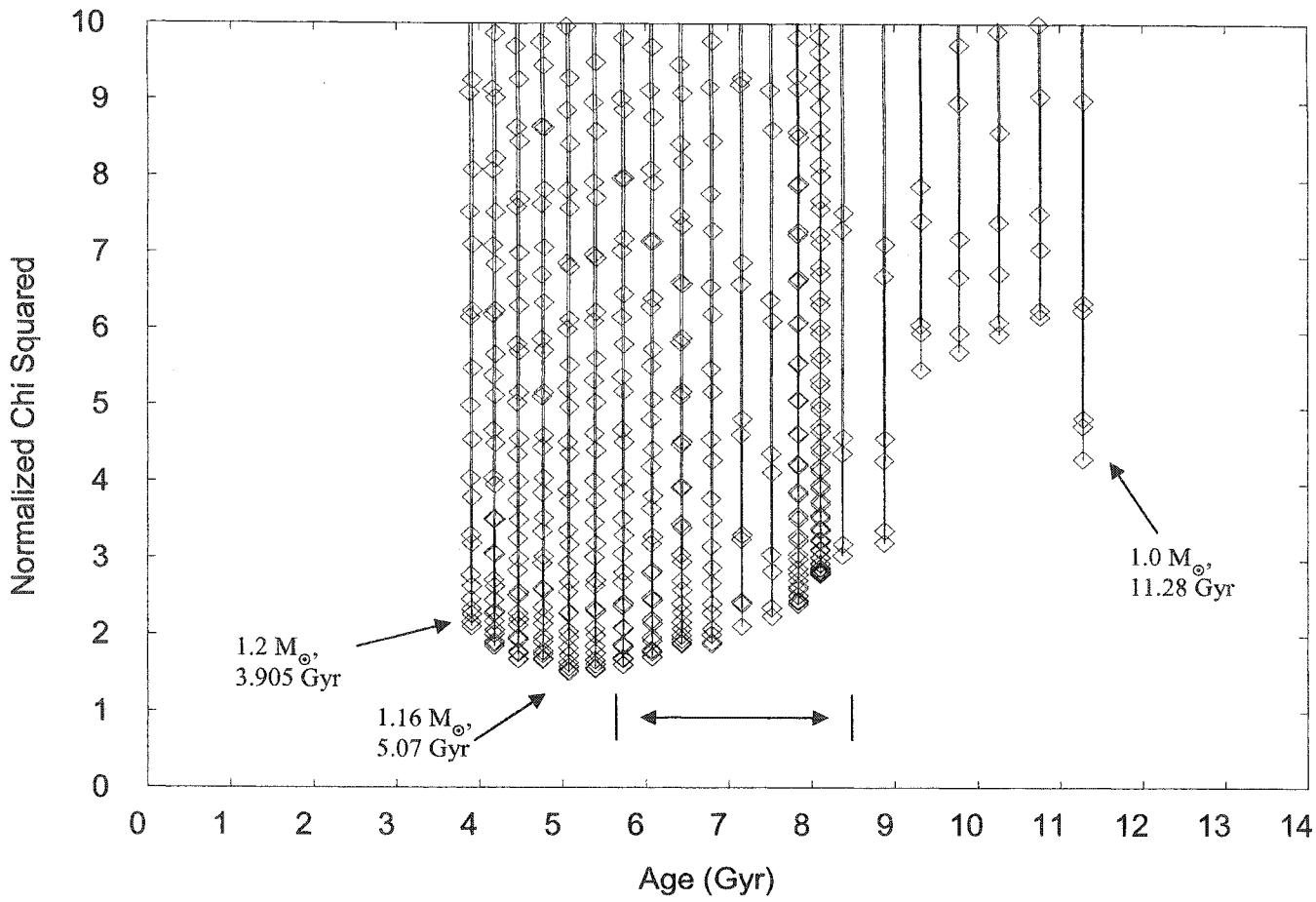

Figure 5.1: Normalized χ^2 versus age results using all 28 observed α Cen A p-mode frequencies from table 5.1. The normalized χ^2 results for the maximum and minimum mass values as well as the figure minimum at 1.16 M and 5.07 Gyr are identified. The denoted range identifies the α Cen A models which correspond to the effective temperature of α Cen A (5770 ± 50 K). The constrained range in mass is 1.06 $M_\odot$ to 1.14 $M_\odot$ and in age is 5.73 Gyr to 8.37 Gyr. The results have a mass resolution of 0.01 $M_\odot$.

Table 5.4: The model spectrum (figure 5.2; M = 1.08 $M_{\odot}$ and 7.836 Gyr) that best matches the l = 0, 1 observed α Cen A p-mode frequencies. Listed are observed frequencies, model frequencies, model l and n values, and differences between the matched observed and model frequencies.

ν_{obs} (μHz)	ν_{model} (μHz)	l	n	$\Delta_{obs\text{-}model}$ (μHz)
1841.3	1838.999	0	16	2.301
1887.4	1886.083	1	16	1.316
1991.7	1991.005	1	17	0.695
2095.6	2096.343	1	18	0.743
2152.9	2153.351	0	19	0.451
2202.8	2202.155	1	19	0.645
2258.4	2258.504	0	20	0.105
2309.1	2308.033	1	20	1.067
2364.2	2363.890	0	21	0.310
2414.3	2413.722	1	21	0.578
2470.0	2469.637	0	22	0.363
2519.3	2519.977	1	22	0.677
2573.1	2572.829	2	22	0.271
2625.6	2626.614	1	23	1.014
2679.8	2679.512	2	23	0.288
2733.2	2733.097	1	24	0.103
2786.2	2786.410	2	24	0.210
2837.6	2839.871	1	25	2.272

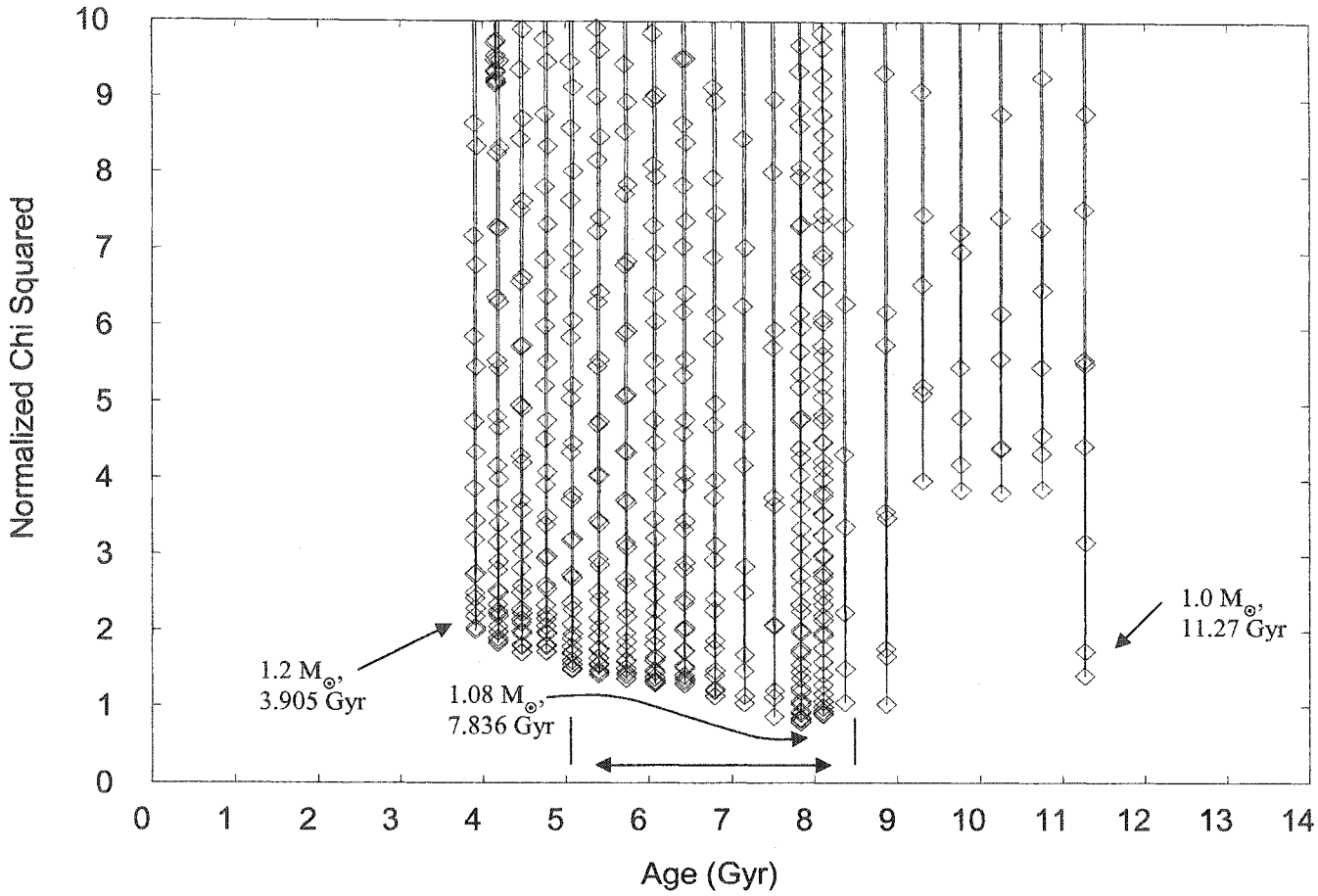

Figure 5.2: Normalized χ^2 versus age results using $l = 0$, 1 observed α Cen A p-mode frequencies from table 5.1. The normalized χ^2 values for the maximum and minimum masses as well as the figure minimum at 1.08 $M_\odot$ and 7.836 Gyr are identified. The denoted range indicates the α Cen A models which correspond to the effective temperature of α Cen A (5770 ± 50 K). The constrained range in mass is 1.06 $M_\odot$ to 1.14 $M_\odot$ and in age is 5.72 Gyr to 8.36 Gyr. The results have a mass resolution of 0.01 $M_\odot$.

Chapter 6

Summary and Conclusions

Chapters 3 presents the testing results of the frequency search technique using model generated p-mode frequencies. Chapters 4 and 5 present the results of tests on the observed p-mode frequencies of the Sun and α Cen A, respectively. The following sections summarize the key results from chapters 3, 4 and 5, and provide general conclusions for this thesis.

6.1. Computation and Testing Results

In chapter 3, the frequency search technique proved capable of determining the stellar model whose pulsation spectrum best matched an observed pulsation spectrum through tests using model generated pulsation spectra. A set of optimal requirements for the creation of a model frequency grid and for the frequency search technique were summarized. These requirements are:

1. A high frequency resolution in mass ($\leq$ 0.01 $M_{\odot}$) is required for a model frequency grid. This may be accomplished by creating a sufficiently dense grid of evolutionary tracks in mass or by applying frequency interpolation in mass.
2. Frequency interpolation in age is required to provide the necessary resolution in the normalized χ^2 to identify individual minima for constant masses. The level

of interpolation required for a model frequency grid will vary depending on the initial age resolution of the calculated model pulsation spectra.

3. For the 2-D case of evaluating the mass and age of a stellar model whose pulsation spectrum best matches an observed pulsation spectrum, the value of heavy metals must be well determined for the central model of any model pulsation grid.
4. Low observed frequency uncertainties are desirable. A low set of observed frequency uncertainties will decrease the denominator in the calculation of the χ^2. Therefore, any match with a low χ^2 value will have a higher degree of confidence.
5. Large numbers of observed p-mode frequencies are desirable. Determined matches with more observed p-mode frequencies will increase the confidence in a normalized χ^2 result.
6. Additional constraints are required to interpret the matching results of the frequency search technique. Effective temperature provides a readily observable non-pulsation constraint parameter and is a possible indicator of a problem with the basic properties of a central model for a model frequency grid.
7. No assumptions are made about the amplitudes or lifetimes of the observed p-mode frequencies when used with this technique.

6.2. Solar Testing Results

In chapter 4, the frequency search technique was tested with observed solar p-mode frequencies using the calibrated solar model and standard solar model frequency

grids. The optimal model frequency grid requirements summarized in chapter 3 were incorporated into the standard solar model frequency grid. A summary of the results of the tests of chapter 4 are:

1. Tests using the calibrated solar model frequency grid failed to reproduce the observed Sun. This failure is the result of insufficient model resolution in mass which is confirmed independently (Guenther, private communication).
2. Testing using the standard solar model frequency grid succeeded in matching the observed Sun. This success is due to the application of the optimal resolution in mass to the standard solar model frequency grid.
3. Accurate modelling of stellar atmospheres within stellar models is necessary to produce accurate matches to higher observed p-mode frequencies. Better matching results were achieved after the elimination of higher frequency observed solar p-modes ($n > 20$) from the tests.
4. The non-pulsation constraint of effective temperature is required to eliminate unphysical models from the results of a frequency search technique analysis. Effective temperature was applied successfully in the tests of this chapter.

6.3. α Cen A Testing Results

In chapter 5, the frequency search technique was tested using the stellar p-mode frequencies obtained from observations of α Cen A. This testing was only an exploratory analysis of the α Cen A observed pulsation spectrum. A summary of the test results for chapter 5 are:

1. The testing of the frequency search technique using the α Cen A observed p-mode frequencies was successful in determining a range of α Cen A models that best match the p-mode observations.
2. Better matching results were achieved after the elimination of $l = 2$ α Cen A observed p-mode frequencies. This suggests there may by a misidentification of $l = 2$ frequencies present in the results of Bouchy and Carrier (2002).

6.4. General Conclusions and Future Work

The frequency search technique is a useful research tool to determine stellar properties from observed p-mode frequencies. The frequency search technique is able to constrain the mass and age of a star using only the oscillation frequencies.

A practical application of the frequency search technique would involve the construction of an extensive model frequency grid (a mega-grid), covering the entire mass, age and appropriate composition range for stars predicted to exhibit solar-type oscillations. This mega-grid would include the optimal requirements summarized in § 3.6 and § 6.1. Using such a mega-grid to compare with any p-mode observations from a solar-type star would enable the immediate constraint of a best fit stellar model and corresponding stellar properties.

The frequency search technique offers many avenues for improvement and expansion. The following summarizes some key points for continued work with the frequency search technique:

1. The inclusion of frequency interpolation in mass for a model frequency grid is warranted.

2. The generalization of the frequency search technique to include variation of heavy metals, helium abundance and mixing length parameter.
3. The exploration of the use of other non-pulsation constraints (e.g. Luminosity).
4. The inclusion of more rigorous stellar atmospheric modelling.
5. Explore the benefit of using other best fit parameters to evaluate the comparison of observed and model spectra.

Appendix A

This appendix contains the complete code and documentation for the SEARCH program used and developed for this thesis. The SEARCH code was written in FORTRAN 77.

```
C
C       Program Search2b
C
C
C       This program is designed to test ideas of interpolation and
C       using Chi Squared when comparing grids of model data with
C       observed oscillation frequencies.  The program will read in
C       a grid of models, a set of observed frequencies and will
C       peroform both an interpolation and computation of chi
C       squared values. The program will output mass, age, and chi
C       squared information.
C
C       Created: July 15, 2002
C
C       Last Revised: August 27, 2002
C

        Program Search2b

        implicit none

        Integer a,b,i,j,c,z,x,y,ii,g,lambdamax,m,aa,q,r,t,s,u,p,w,t2,
     1  kk,n(10000),l(10000),lambda(10000),nA(1000),nB(1000),bb,
     2  lA(1000),lB(1000),NN(10000),LL(10000),matchedN,matchedL,
     3  modeldata2(2,500,500),zzz(100)

        Real age(10000),modelerror,modeldata1(2,500,500),LLL,
     1  lspace(10000),xage(1000),xlambda(1000),larges(1000),
     2  Largespace(1000),RR,deltaAge,Amodel(1000),AgeA,AgeB,
     4  vmodelB(1000),Bmodel(1000),chisquared(1000),delta,
     6  deltav(10000),Ivmodel(10000),vmodelA(1000),cutoff,
     7  matchedv,matchedLarge

        Real*8 rchi,fchi,IAge,vobs(100),vobserror(100),vmodel(10000)

        Character*80 file1(100)

        Character*5 mass(100)

C       The following sets rules for matched frequencies. RR sets the
C       percent of observed frequencies that must be matched. LL sets
C       the value which defines a clear match. LLL is the percent of
C       the large spacing which the difference between the observed
C       frequency and the model frequency must be less than in order to
C       be a match.

C       Cutoff for matches... 80%.

        RR=0.8

C       Cutoff for match... 1/4 large spacing.

        LLL=0.25

C       Number of interpolations between model A and model B.
```

```
        aa=99

C       Cutoff for Chisquared values.

        cutoff=20000

C       Value for model error used in chi squared calculation.

        modelerror=1

C
C       Program Begins.
C

        print *,' '
        print *,'Program Search2b'
        print *,' '

C       Open file containing all relevant model frequency data.

        print *,'Flag 1'

      open(11,file='C:/Research/MScThesis/alphacendata.txt',
     1  status='old')

C       Count and read all data from above file.

        a=0

      print *,'Flag 2'

      do 10 i=1,100
        read(11,*,end=15) file1(i), mass(i)
        a=a+1
        print *, mass(i)
10     continue
15     continue

       close(11)

C      Open file containing observed frequency data.

       print *,'Flag 3'

       open(22,file='C:/Research/MScThesis/alphacenobs.txt',
     1  status='old')

C      Count and read all data from above file.

       b=0

       print *,'Flag 4'

       do 20 i=1,100
         read(22,*,end=25) vobs(i), vobserror(i)
         b=b+1
20     continue
```

```
25      continue

        bb=b

        close(22)

C       Open file for output of modeldata1(...), modeldata2(...)
C       information.  This file will contain frequency data binned by
C       age.

        print *,'Flag 5'

        open(33,file='C:/Research/MScThesis/modeldata.txt',
     1  status='old')

C       Open file for output of matched n, l, frequency values. This
C       file will also contain chi squared, delta and the number of
C       matches.

        open(44,file='C:/Research/MScThesis/match.txt',status='old')

C       Open file for output of results. This file will contain mass,
C       age, weighted chi squared and the total number of frequencies.

        open(55,file='C:/Research/MScThesis/results.txt',status='old')

C       Title information for results.txt.

        write(55,*) '# Mass     Age     Weighted Chi2'
        write(55,*) ' '

C
C       Begin the main loop for this program.  Begin looping through all
masses
C       and associated data.
C

        do 50 j=1,a

        print *,'Beginning data scan...'

C       Open file containing model data information for mass value
specified
C       above.

        open(66,file=file1(j),status='old')

C       Count and read all relevant data from the mass file opened above.

        c=0

        do 75 i=1,10000

        read(66,*,end=80) n(i), l(i), lambda(i), age(i), vmodel(i),
     1  lspace(i)
        c=c+1
```

```
75      continue
80      continue

        close(66)

C       Find the maximum lambda/age value in the data set.  This will
set the
C       upper range limit for the binning of data according to age/arc
length.
C       Arc length is used since it is already in integer form.  The arc
length
C       values are consistent for each mass data set, but are not
compatable
C       between different masses.

        lambdamax=lambda(1)

        do 100 i=2,c
          if(lambdamax.lt.lambda(i))then
          lambdamax=lambda(i)
          endif
100     continue

C       Begin binning the mass data in common ages/arc lengths.
C       z represents the number of data points in each bin.
C       g represents the number of age bins.


        g=0

        print *,'Mass=',mass(j)

        do 150 x=0,lambdamax

        z=0

        g=g+1

        do 200 i=1,c-1

          if(lambda(i).eq.x)then

          z=z+1

          ii=i

          xage(g)=age(i)
          xlambda(g)=lambda(i)

          modeldata1(1,z,g)=vmodel(i)
          modeldata2(2,z,g)=n(i)
          modeldata2(1,z,g)=l(i)
          modeldata1(2,z,g)=lspace(i)

        do 225 y=ii+1,c

          if(lambda(i).eq.lambda(y))then
```

```
          z=z+1


          modeldata1(1,z,g)=vmodel(y)
          modeldata2(2,z,g)=n(y)
          modeldata2(1,z,g)=l(y)
          modeldata1(2,z,g)=lspace(y)

          endif

225       continue

          goto 230

          endif

200       continue

230       continue

          zzz(g)=z

C         Output modeldata information into output file to view.
C         This can be commented out when it is known that everything
C         works okay.

          write(33,*) 'Mass=',mass(j)
          write(33,*) 'Age=',xage(g)
          write(33,*) 'Arc Length=',xlambda(g)
          write(33,*) 'Number of data points=',zzz(g)
          write(33,*) 'Vmodel    n       l      Large Spacing'
          write(33,*) ' '

          do 250 m=1,z

          write(33,*) modeldata1(1,m,g), modeldata2(2,m,g),
        1  modeldata2(1,m,g), modeldata1(2,m,g)

250       continue

          write(33,*) ' '

150       continue

          print *,'Binning complete...'

C
C         This represents the break in the program between the binning of
C         the model data and the subsequent interpolations, matching and
C         determinations of the chisquared.
C
C         Begin interpolation and determination of chi squared.
C         The following puts the first age group into A and the second
C         age group into B.
C
```

```
      do 275 q=1,g-1

      do 300 r=1,zzz(q)

      vmodelA(r)=modeldata1(1,r,q)
      nA(r)=modeldata2(2,r,q)
      lA(r)=modeldata2(1,r,q)
      Largespace(r)=modeldata1(2,r,q)

      vmodelB(r)=modeldata1(1,r,q+1)
      nB(r)=modeldata2(2,r,q+1)
      lB(r)=modeldata2(1,r,q+1)

300   continue

C     The following matches corresponding n and l values for the
C     model datagroups.  This is done in order to interpolate the
C     model data between bins A and B.

      t=0

      AgeA=xage(q)
      AgeB=xage(q+1)

      deltaAge=ABS(AgeA-AgeB)

      do 325 r=1,zzz(q)

      do 350 s=1,zzz(q)

      if((nA(r).eq.nB(s)).and.(lA(r).eq.lB(s)))then

C     t counts the number of matches.

      t=t+1

      Amodel(t)=vmodelA(r)
      Bmodel(t)=vmodelB(s)

      larges(t)=Largespace(r)

      NN(t)=nA(r)
      LL(t)=lA(r)

      goto 325

      endif

350   continue
325   continue

C     The following will perform an interpolation between bins A and
C     B.


      print *,'Beginning Interpolation/Matching...'
```

```
C       Reset all Chisquared values to zero.

        do 430 kk=1,1000
        chisquared(kk)=0
430     continue

C       The following loops through the interpolation governed by "aa".

        do 375 u=0,aa

        t2=0

C       The following performs an interpolation in age.

        IAge=deltaAge*(dble(u)/100.0D0)+AgeA

C       Title information for match.txt.

        write(44,*)
        write(44,*) 'Mass=',mass(j)
        write(44,*) 'Age=',IAge
        write(44,*) 'Vobs    Vmodel     l     n     ChiSquared'

C       The following performs an interpolation in frequency.

        do 400 p=1,t

        deltav(p)=ABS(Amodel(p)-Bmodel(p))

        Ivmodel(p)=-deltav(p)*(dble(u)/100.0D0)+Amodel(p)

C        print *,Ivmodel(p), Amodel(p)

400     continue

C       The following will determine the difference between matched
C       model and observed frequencies.

        do 425 w=1,b

        matchedN=NN(1)
        matchedL=LL(1)
        matchedv=Ivmodel(1)
        matchedLarge=larges(1)

C        print *,vobs(w)

        delta=ABS(vobs(w)-Ivmodel(1))

        do 450 p=1,t-1

        if(delta.gt.ABS(vobs(w)-Ivmodel(p+1)))then

        delta=ABS(vobs(w)-Ivmodel(p+1))

        matchedN=NN(p+1)
```

```
        matchedL=LL(p+1)
        matchedv=Ivmodel(p+1)
        matchedLarge=larges(p+1)

        endif

450     continue

C       The following will determine if the matching between the
C       observed and model frequency is within the value LLL of the
C       large spacing.

        if(delta.gt.LLL*matchedLarge)then
        goto 425
        endif

C       t2 counts the number of true matches.

        t2=t2+1

C       The following calculates the chisquared and sets the upper
C       limit at cutoff.

        chisquared(t2)=((delta)**2)/((vobserror(w))**2+(modelerror)**2)

        if(chisquared(t2).gt.cutoff)then
        chisquared(t2)=cutoff
        endif

C       The following writes matching information to the file
C       match.txt.

        print *,'Flag 6'

        write(44,*) matchedL, matchedN, matchedv, vobs(w),
     1  chisquared(t2), t2, delta

425     continue

C       The following determines the summed chisquared for all the
C       matched frequencies.

        print *,'Determining Chi2...'

        fchi=0

        do 475 i=1,t2

        fchi=fchi+chisquared(i)

475     continue

C       The following determines the weigthed chisquared. The
C       chisquared is weighted by the number of matches set by
C       the value LLL.

        rchi=fchi/dble(t2)*(1+(dble(bb)-dble(t2)))
```

```
C       The following sets an upper limit at cutoff for the summed
C       chisquared.

        if(rchi.gt.cutoff)then
        rchi=cutoff
        endif

C       The following sets a minimum on the number of matched observed
C       frequencies that defines a good chi squared.

        if(t2.lt.RR*b)then
        rchi=cutoff
        endif

C       The following writes the final data for the file results.txt.

        write(55,*) mass(j), IAge, rchi, t2, t

        print *,' Scan complete.'

375     continue

275     continue

C       Mass file loop ends

50      continue

        stop

        end

C       Program Ends
```

References

Alexander, D.R., & Ferguson, J.W. 1994, *ApJ*, 437, 879-891.

Antia, H.M., & Basu, Sarbani. 1994, *ApJ*, 426, 801-811.

Baglin, A., et al. 1998, In: Deubner, F-L., Christensen-Dalsgaard, J., Kurtz, D.W. (eds.) Proc. IAU Symp. 185, *New Eyes to See Inside the Sun and Stars*, 301, Kluwer, Dordrecht, see also http://www.astrsp-mrs.fr/projets/corot/

Bahcall, J.N., Pinsonneault, M.H., & Wasserburg, G.J. 1995, *Rev. Mod. Phys.*, 67, 781-808.

Bahcall, J.N., Pinsonneault, M.H., & Basu, Sarbani. 2001, *ApJ*, 555, 990-1012.

Barban, C., et al. 1999, *A&A*, 350, 617-625.

Basu, Sarbani. 1997, *MNRAS*, 288, 572-584.

Basu, Sarbani., Antia, H.M. 1998, *The Structure and Dynamics of the Interior of the Sun and Sun-Like Stars*, ESA Publications.

Bedding, T.R., Kjeldsen, H., Reetz, J., & Barbuy, B. 1996, *MNRAS*, 280, 1155-1161.

Bedding, T.R., Kjeldsen, H., & Christensen-Dalsgaard, J. 1997, astro-ph/ No. 9709005, v1. 1 Sept. 1997.

Bedding, T.R., Butler, R.P., Kjeldsen, H., Baldry, I.K., O'Toole, S.J., Tinney, C.G., Marcy, G.W., Kienzle, F., & Carrier, F. 2001, *ApJ*, 549, L105-L108.

Bedding, T.R. et al. 2002, astro-ph/ No. 0209359, v1. 18 Sept. 2002.

Bedford, D.K., Chaplin, W.J., Davies, A.R., et al. 1993, GONG 1992: *Seismic Investigation of the Sun and Stars*, A.S.P. Conf. Ser. Vol. 42, Brown, T.M., ed., Brigham Young, Utah, pp. 383.

Bell, R.A. 1993, *MNRAS*, 264, 345.

Bell, R.A. & Gustafsson, B. 1989, *MNRAS*, 236, 653-707.

Belmonte, J.A., Jones, A.R., Palle, P.L., & Roca Cortes, T. 1990a, *ApJ*, 358, 595-609.

Belmonte, J.A., Perez Hernandez, F., Roca Cortes, T. 1990b, *A&A*, 231, 383-390.

Böhm-Vitnese, E. 1958, *Zs. Ap.*, 46, 108.

Bonnell, J.T., & Bell, R.A. 1993, *MNRAS*, 264, 334.

Bouchy, F., & Carrier, F. 2001, *A&A*, 374, L5-L8.

Bouchy, F., & Carrier, F. 2002, *A&A*, 390, 205-212.

Brown, K.I.T., Butler, M.N., & Guenther, D.B. 2003, astro-ph/ No. 0207008 3 July 2002.

Brown, T.M., & Gilliland, R.L. 1990, *ApJ*, 350, 839-845.

Brown, T.M., & Gilliland, R.L. 1994, *ARA&A*, 32, 37-82.

Brown T.M., Christensen-Dalsgaard, J., Weibel-Mihalas, B., & Gilliland, R.L. 1994, *ApJ*, 427, 1013-1034.

Brown, T.M., Gilliland, R.L., Noyes, R.W., & Ramsey, L.W. 1991, *ApJ*, 368, 599-609.

Brown, T.M., Kennelly, E.J., Korzennik, S.G., Nisenson, P, Noyes, R.W., & Horner, S.D. 1997, *ApJ*, 475, 322.

Burki et al., 2002, http://obswww.unige.ch/gcpd/ph13.html

Buzasi, D., Catanzarite, J., Laher, R., Conrow, T., Shupe, D., Gautier III, T.N., Kriedl, T., & Everett, D. 2000, *ApJ,* 532, L133-L136.

Carrier, F., et al. 2001, *A&A*, 378, 142-145.

Carroll, B.W. & Ostlie, D.A. 1996, *An Introduction to Modern Astrophysics*, Addison-Wesley, Inc.

Chaboyer, B., Demarque, P., & Guenther, D.B. 1999, *ApJ*, 525, L41-L44.

Chaplin, W.J., Elsworth, Y., Howe, R., Isaak, G.R., McLeod, C.P., Miller, B.A., van der Raay, H.B., Wheeler, S.J., & New, R. 1996, *Solar Phys.*, 168, 1-18.

Chaplin, W.J., Elsworth, Y., Isaak, G.R., Millar, B.A., & New, R. 1999, *MNRAS*, 308, 424-430.

Chou, D.-Y., Sun, M.-T., Huang, T.-Y., et al. 1995, *Solar Physics*, 160, 237-243.

Christensen-Dalsgaard, J. 1988, *A HR Diagram for Stellar Oscillations. Advances in Helio- and Astroseismology*, IAU Symp. No. 123, Kluwer, Dordrecht, pp. 295.

Christensen-Dalsgaard, J. 1993, in GONG 1992: *Seismic Investigations of the Sun and Stars*. ASP Conference Series, Vol. 142, ed. T.M. Brown.

Christensen-Dalsgaard, J. 1998, *Lecture Notes on Stellar Oscillations*, Fourth Edition.

Christensen-Dalsgaard, J. 2001, *MONS on the Danish Romer Satellite: Measuring Oscillations in Nearby Stars*, In: Proc. of the 1st Eddington Workshop on Stellar Structure and Habitable Planet Finding, 11-15 June 2001, Cordoba, Spain, (eds.) B. Ballrick, F. Favata, W. Roxburgh, D. Galadi, ESA SP-485, Noordwijk, ESA Publications Division, pp. 25-34.

Christensen-Dalsgaard, J. 2002, *Rev. Mod. Phys.*, 74, 1073-1129.

Christensen-Dalsgaard, J., & Berthomeiu, G. 1991, in Solar Interior and Atmosphere. ed. A.N. Cox, W.L. Livingsten, M.S. Matthews, (University of Arizona Press, Tuscon) p. 401.

Christensen-Dalsgaard, J. & Frandsen, S. 1983, *Solar Physics*, 82, 165-204.

Christensen-Dalsgaard, J., Gough, D.O., & Thompson, M.J. 1991, *ApJ*, 378, 413-437.

Christensen-Dalsgaard, J., Bedding, T.R., & Kjeldsen, H. 1995, *ApJ*, 443, L29-L32.

Clayton, D.D. 1968, *Principles of Stellar Evolution and Nucleosynthesis*, McGraw-Hill, Inc.

Cox, J.P. 1980, *The Theory of Stellar Pulsation*, New Jersey, Princeton University Press.

Dappen, W., & Gough, D.O. 1986, In: NATO ASI Ser. C 169, Seismology of the Sun and the Distant Stars, ed. D.O. Gough (Dordrecht: Reidel), p.275.

Demarque, P., Guenther, D.B., & van Altena, W.F. 1986, *ApJ*, 300, 773-778.

Demarque, P., & Guenther, D.B. 1999, *Proc. Natl. Acad. Sci.* USA, 96, 5356-5359.

Di Mauro, M.P., & Christensen-Dalsgaard, J. 2001, Proceedings of the SOHO 10/GONG 2000 Conference, ed. A. Wilson, SP-464, 373.

Domingo, V., Flecke, B. & Poland, A.I. 1995, *Solar Physics*, 162, 1-37.

Drake, J.J., & Smith, G. 1993, *ApJ*, 412, 797-809.

Dravins, D., Lindegren, L., Nordlund, A., & VandenBerg, D.A. 1993a, *ApJ*, 403, 385-395.

Dravins, D., Linde, P., Fredga, K., & Gahm, G.F. 1993b, *ApJ*, 403, 396-411.

Dravins, D., Linde, P., Ayres, T.R., Lindsky, J.L., Monsignori-Fossi, B., Simon, T., & Wallinder, F. 1993c. *ApJ,* 403, 412-425.

Dravins, D., Lindegren, L., & Vandenberg, D.A. 1998, *A&A*, 330, 1077-1079.

Duvall, T.L., Jr. 1995, in Proceeding of the 4th SOHO Workshop: Helioseismology, ESA SP-376, vol. 1, ed. J.T. Hoeksema, V. Domingo, B. Fluet, B. Bathrell, (ESA Publication Division, Noordwijk, The Netherlands), p. 107-111.

Dziembowski, W.A., Gough, D.O., Houdek, G., & Sienkiewcz, R. 2001, *MNRAS*, 328, 601-610.

Edmonds, P.D. 1993, PhD Thesis, University of Sydney.

Edmonds, P.D., & Cram, L.E. 1995, *MNRAS*, 276, 1295.

Edmonds, P.D., Cram, L.E., Demarque, P., Guenther, D.B., & Pinsonneault, M. 1992, *ApJ*, 394, 313-319.

Edmonds, P.D., Gilliland, R.L. 1996, *ApJ*, 464, L157.

European Space Agency (Hipparcos). 1997, *The Hipparcos and Tycho Catalogue*, ESA Publications Division, Noordwijk, The Netherlands.

Fossat, E. 1991, *Solar Physics*, 133, 1-12.

Frandsen, S. 1987, *A&A*, 181, 289-292.

Gelly, G., Grec, G., & Fossat, E. 1986, *A&A*, 164, 383.

Girard, T.M., Wu, H., Lee, J.T., & Dyson, S.E. 1996, *BAAS*, 28, 919.

Gough, D. 1987, *Nature*, 326, 257-259.

Gough, D. 1993, in Les Houches Session XLVII: Astrophysical Fluid Dynamics, ed. J.-P. Zahn, and J. Zinn-Justin, (Elsevier, Amsterdam), p. 399-560.

Gough, D. 1996, in Proceedings of the VI IAC Winter School "The Structure of the Sun," ed. T. Roca Cortes and F. Sanchez, (Cambridge University Press, Cambridge, England), p. 141-228.

Gough, D., & Thompson, M.J. 1991, in Solar Interior and Atmosphere, Space Science Series, ed. A.N. Cox, W.L. Livingston, M. Matthews, (University of Arizona Press, Tucson), p. 519-561.

Gray, D.F. 1992, *The Observation and Analysis of Stellar Photospheres*, 2nd Ed., Cambridge Univeristy Press.

Gray, D.F. & Brown, K. 2001, *PASP*, 113, 723-735.

Griffin, R.E.M., & Lynas-Gray, A.E. 1999, *AJ*, 117, 2998-3006.

Guenther, D.B. 1994, *ApJ*, 422, 400-411.

Guenther, D.B. 1998, in Proceedings of the SOHO 6/GONG 98 Workshop, 'Structure and Dynamics of the Interior of the Sun and Sun-like Stars', Boston, USA, 1-4 June 1998, ESA SP-418, October 1998.

Guenther, D.B. 2002, *ApJ*, 569, 911-940.

Guenther, D.B., & Demarque, P. 1986, *ApJ*, 301, 207.

Guenther, D.B., Demarque, P., Kim, Y.-C., & Pinsonneault, M.H. 1992a, ApJ, 387, 372-393.

Guenther, D.B., Demarque, P., Pinsonneault, M.H., & Kim, Y.-C. 1992b, *ApJ*, 392, 328-336.

Guenther, D.B., & Demarque, P. 1993, *ApJ*, 405, 298-306.

Guenther, D.B., & Demarque, P. 1996, *ApJ*, 456, 798.

Guenther, D.B., Kim, Y.-C., & Demarque, P. 1996, *ApJ*, 463, 382.

Guenther, D.B., & Demarque, P. 1997, *ApJ*, 484, 937.

Guenther, D.B., & Demarque, P. 2000, *ApJ*, 531, 503-520.

Guenther, D.B., Krauss, L.M., & Demarque, P. 1998, *ApJ*, 498, 871-876.

Guenther, D.B., et al. 2000, *ApJ*, 530, L45-L48.

Hart, A.B. 1954, *MNRAS*, 114, 17.

Hart, A.B. 1956, *MNRAS*, 116, 38.

Harvey, J.W., Hill, F., Hubbard, R.P., et al. 1996, *Science*, 272, 1284-1286.

Hatzes, A.P., & Cochran, W.D. 1994a, *ApJ*, 422, 366-373.

Hatzes, A.P., & Cochran, W.D. 1994b, *ApJ*, 432, 763-769.

Heasley, J.N., Janes, K., Guenther, D., Mickey, D., & Demarque, P. 1996, *PASP*, 108, 385.

Houdek, G., Balmforth, N.J., Christensen-Dalsgaard, J., & Gough, D.O. 1999, *A&A*, 351, 582-596.

Iglesias, C.A., & Rogers, F.J. 1996, *ApJ*, 464, 943.

Innis, J.L., Isaak, G.R., Speake, C.C., Brazier, R.I., & William, H.K. 1991, *MNRAS*, 244, 643-653.

Irwin, A.W., Fletcher, J.M., Yang, S.L.S., Walker, G.A., & Goodenough, C. 1992, *PASP*, 104, 489-499.

Isaak, G.R., & Isaak, K.G. 2001, *Stellar Seismology, Stellar Ages and the Cosmological Constant*, In: Astrophysical Ages and Time Scales, ASP Conf. Series, vol. 245, (eds.) T. von Hippel, N. Manset, C. Simpson.

Kawaler, S. 1998, in Proceedings of IAU Symp. 185, New Eyes to See inside the Sun and other Stars, 261, ed. F.L. Deubner, J. Christensen-Dalsgaard, D.W. Kurtz, (Dordrecht, Kluwer).

Kim, Y.-C., & Chen, K.L. 1998, *ApJ*, 496, L121-L124.

Kjeldsen, H., & Bedding, T.R. 1995, *A&A*, 293, 87-106.

Kjeldsen, H., Bedding, T.R., Viskum, M., & Frandsen, S. 1995, *AJ*, 109, 1313-1319.

Kjeldsen, H, Bedding, T.R., Christensen-Dalsgaard, J. 2000, In: Szabados, L., Kurtz, D. (eds.) IAU Colloquium 176: The Impact of Large-Scale Surveys on Pulsating Star Research, Vol. 203, 73, ASP Conf. Ser., see also http://astro.ifa.au.dk/MONS

Kjeldsen, H., & Bedding, T.R. 2001, Proc. of the SOHO 10/GONG 2000 Workshop: Helioseismology & Astroseismology at the dawn of the millennium, 2-6 Oct. 2000, ESA Publications, pg. 361-366.

Krishna Swamy, K.S. 1966, *ApJ*, 145, 174.

Kurucz, R.L. 1979, *ApJS*, 40, 1-340.

Ledoux, P., & Walraven, T. 1958, "*Variable Stars*" Handbok der Physik, vol. 51, chapter IV, (Springer, Berlin), p. 352-604.

Leibacher, J., & Stein, R.F. 1971, *ApJL*, 7, 191-192.

Leighton, R.B., Noyes, R.W., & Simon, G.W. 1962, *ApJ*, 135, 474.

Libbrecht, K.G. 1988, IAU Symp. 132, The Impact of Very High S/N Spectroscopy on Stellar Physics, eds., Cayrel de Strobel, G., Spite, M., Kluwer, Dortrecht, pp. 83.

MacDonald, P.A. 2001, M.Sc. Thesis, Saint Mary's University.

Martic, M., et al. 1999, *A&A*, 351, 993-1002.

Martic, M., Lebrun, J.C., Schmitt, J., Appourchaux, T., & Bertaux, J.L. 2001, *Observing Solar-like Oscillations: α CMi, η Cas, ζ Her.*, ed. Wilson, A., ESA Publications Division, ESA SP-464, pp. 431.

Matthews, J.M., et al. 2000, In: Szabados, L., Kurtz, D. (eds.) IAU Colloquium 176: The Impact of Large-Scale Surveys on Pulsating Star Research, Vol. 203, 74, ASP Conf. Ser., see also http://www.astro.ubc.ca/MOST

Michaud, G. 1970, *ApJ*, 160, 641.

Michaud, G. 1986, *ApJ*, 302, 650-655.

Morel, P, Berthomieu, G., Provost, J., & Thevenin, F. 2001, *A&A*, 379, 245-256.

Morel, P., Provost, J., Lebreton, Y., Thevenin, F., & Berthomieu, G. 2001, *A&A*, 363, 675-691.

Neuforge-Verheecke, C., & Magain, P. 1997, *A&A*, 328, 261-268.

Nordlund, A.A., & Stein, R.F. 1996, In: Proceedings of the 32nd Liege Colloquium, eds., Noels, A., Fraipont-Caro, D., Gabriel, M., Grevesse, N., & Demarque, P., University of Liege Press, pp. 75.

Noyes, R.W., Baliunas, S.L., Belserene, E., et al. 1984, *ApJ*, 285, L23-L26.

Pinsonneault, M.H. 1988, Ph.D. Thesis, Yale University.

Plaskett, H.H. 1916, *ApJ*, 43, 145.

Poretti, E., Buzasi, D., Laher, R., Catanzarite, J., & Conrow, T. 2002, A&A, 382, 157-163.

Pottasch, E.M., Butcher, H.R., & van Hoesel, F.H.J. 1992, A&A, 264, 138-146.

Pourbaix, D., et al., 2002, *Constraining the difference in convective blueshift between the components of α Cen with precise radial velocities*, astro-ph/ No. 0202400, v1., 21 Feb. 2002.

Prather, M. 1976, Ph.D. Thesis, Yale University.

Retter, A, Bedding, T.R., Buzasi, D., & Kjeldsen, H. 2002, astro-ph/ No. 0208518 v1. 28 August 2002.

Richard, O., Dziembowski, W.A., Sienkiewicz, R., & Goode, P.R. 1998, *The Structure and Dymanics of the Interior of the Sun and Sun-like Stars*, ESA Publications.

Rogers, F.J. 1986, *ApJ*, 310, 723-728.

Rogers, F.J., Swenson, F.J., & Iglesias, C.A. 1996, *ApJ,* 456, 902.

Schou, J., & Buzasi, D.L. 2000, *AAS*, 197, 4604S.

Soderblom, D.R., & Dappen, W. 1989, *ApJ*, 342, 945-950.

Tassoul, M. 1980, *ApJS*, 43, 469-490.

Taylor, B.J. 1999, *A&AS*, 134, 523-524.

Thevenin, F., Provost, J., Morel, P., Berthomieu, G., Bouchy, F., & Carrier, F. 2002, *Asteroseismology and calibration of the α Cen binary system*, astro-ph/ No. 0206283, v1. 17 Jun. 2002.

Thoul, A., Scuflaire, R., Vatovez, B., & Noels, A. 2002, *Asteroseismology across the HR-Diagram*, CAUP. Porto (Portugal), 1-5 July, 2002.

Tilton, G.R. 1988, *Meteorites and the Early Solar System*, University of Arizona Press.

Tomczyk, S., Streander, K., Card, G., Elmore, D., Hull, H., & Cacciani, A. 1995, *Solar Physics,* 159, 1-21.

Toutain, T., & Frohlich, C. 1992, *A&A,* 257, 287-297.

Ulrich, R.K. 1970, *ApJ*, 162, 993.

Ulrich, R.K. 1986, *ApJ*, 306, L37-L40.

Unno, W., et al. 1989, *Nonradial Oscillations of Stars*, 2nd edition, (University of Tokyo, Tokyo).

Vauclair, C. 1997, in Proceedings of IAU Symp. 181, Sounding Solar and Stellar Interiors, 367, ed. J. Provost, F.X. Schmider, (Dordrecht: Kluwer).

Curriculum Vitae

Kevin I. T. Brown

Education:

2003-
Ph.D. in Astronomy, UWO, London, ON.

2000-2003
M.Sc. in Astronomy, February 2003, Saint Mary's University, Halifax, NS.

1995-2000
B.Sc. in Astronomy & Geophysics, Honours, UWO, London, ON.

1990-1995
Ontario Secondary School Diploma, Honours, St. Clair Secondary School, Sarnia, ON.

Relevant Experience:

2001-2002
Part-time instructor for the Astronomy & Physics department at Saint Mary's University.

2001-2002
Graduate student representative for Astronomy & Physics department at Saint Mary's University.

2001-2002
Canadian Astronomical Society (CASCA) graduate student representative for the Astronomy & Physics department at Saint Mary's University.

2001-2002
Performed public tours at Saint Mary's University's Burke-Gaffney Observatory.

2000-2002
Teaching Assistant for first year Astronomy and Physics courses at Saint Mary's University. This involved preparing and overseeing labs, marking for courses and being available for student inquiries.

1998-2000
Research Assistant under the supervision of Prof. David F. Gray at UWO. This position involved performing observations of F, G & K type stars using the high resolution spectrograph at UWO's Elginfield Observatory, the analysis of the resulting data as well as performing general maintenance for the telescope.

1998-2000
Performed public tours at UWO's Cronyn Observatory.

1997-1999
Teaching Assistant for first year Astronomy courses at UWO. This involved the marking of course work.

Awards:

2000-2002
Saint Mary's University Graduate Student Award

2000
NSERC Undergraduate Summer Research Award

1995-1996
UWO Entrance Scholarship

Publications:

Full Refereed Journal Articles

Brown, K.I.T, Butler, M.N. & Guenther, D.B. 2002. "Constraints on proton-proton fusion from helioseismology." Submitted to Phys. Rev. C.

Gray, D.F. & Brown, K. 2001 "Line-depth ratios: Temperature indices for giant stars." Publications of the Astronomical Society of the Pacific. 113: 723-735.

Gray, D.F, Tycner, C. & Brown, K. 2000. "Spectral-line profiles in the daytime sky." Publications of the Astronomical Society of the Pacific. 112: 328-334.

Conference Proceedings

Brown, K.I.T, Butler, M.N. & Guenther, D.B. 2002. "Using the accuracy of helioseismology to constrain proton-proton fusion." CASCA 2002. Penticton, BC. May 11-14, 2002. (talk)

References:

ANNUAL REVIEWS
A NONPROFIT SCIENTIFIC PUBLISHER
www.annualreviews.org
4139 El Camino Way, P. O. Box 10139
Palo Alto, California 94303-0139 USA
Fax 650.855.9815

Laura Folkner
Permissions Department
Lfolkner@annualreviews.org
650.843.6636

October 18, 2002

TO:

Ref: Your e-mail of 10/8/02

FROM: Laura Folkner, Permissions Department Laura Folkner

Thank you for your request for permission to reprint the following material:

Brown & Gilliland: Fig. 2, page 46, *Annual Review of Astronomy & Astrophysics*, Vol. 32, 1994

We are happy to grant you permission to use this material in your Master of Science thesis. Please use the following acknowledgment:

"With permission, from the *Annual Review of Astronomy & Astrophysics*, Volume 32, © 1994, by Annual Reviews www.annualreviews.org"

This permission to reprint is for a one-time usage only and any subsequent use of this material requires submission of a new permission request.

Fees for this noncommercial usage have been waived for you. If I can be of further assistance, please do not hesitate to contact me.

INSTITUT FOR FYSIK OG ASTRONOMI
AARHUS UNIVERSITET
Institute of Physics and Astronomy, University of Aarhus

16 December 2002

Dear Kevin,

With this letter I grant you permission to use Figure 12 of my paper 'Helioseismology', published in *Rev. Mod. Phys.*, vol. 74 (Oct. 2002).

Yours sincerely,

Jørgen Christensen-Dalsgaard

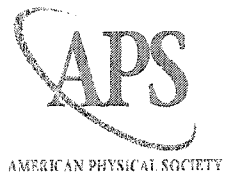

AMERICAN PHYSICAL SOCIETY

October 9, 2002

Attn: Kevin Brown

Re: **Your request as a non-author to reprint an abstract, figure, table, graph or excerpt**

Article(s): Figure 12, Christensen-Dalsgaard, J. 2002, Rev. Mod. Phys., 74, 4, October 2002

The American Physical Society is pleased to grant you a one-time permission to reproduce the above referenced material in your upcoming publication. You must also obtain permission from at least one of the authors for each separate work. The authors' name and addresses can be found on the first page of the published article.

On all copies of the Article, please cite the original publication in full in the copyright credit line as follows:

> Authors names, journal title, volume number, page number and year of publication. Copyright (YEAR) by the American Physical Society.

For example:

> Damien Challet and Neil F. Johnson, Physical Review Letters, 89, 028701, (2002). Copyright 2002 by the American Physical Society

Sincerely,

Anita Wiley
APS Customer Service

The University of Sydney

School of Physics

Faculty of Science
College of Sciences and Technology

NSW 2006 AUSTRALIA

9 October 2002

Dear Kevin,

I am happy to give my permission for you to reproduce figures from the paper by Bedding et al. 2001, March 1 ApJ, 549: L105-L108. Good luck with your thesis and please do send me a copy.

Yours sincerely,

Dr Timothy R. Bedding
(Senior Lecturer)

Blackwell Publishing

RE: Table 1, Chaplin WJ et al. 1999. MNRAS.

Dear Kevin Brown,

Thank you for your email request. Permission is granted for you to use the material above for your thesis subject to the usual acknowledgements and on the understanding that you will reapply for permission if you wish to distribute or publish your thesis commercially.

Good Luck!

Best wishes,
Lindsay

Lindsay Doyle
Permissions Controller
Blackwell Publishing

Am
Ber
Bost
Copenhag
Edinbur
Melbou
Oxf
P
Tok
Vier

Registered off
108 Cowley Road, Oxf
OX4 1JF,
Registration numb
0180277 Engl

www.blackwellpublishing.c

To: Kevin Brown · wo.ca>
Subject: Re: Permission to reproduce figures

Hello there,

Please feel free to use the pictures.

Cheers,
Bernard McCarty

On Tue, 8 Oct 2002, Kevin Brown wrote:

> To whom it may concern,
>
> My name is Kevin Brown and I am currently a graduate student at the
> University of Western Ontario. I am currently finishing my Master of
> Science thesis in the research field of astroseismology. I am emailing
> BISON in order to ask permission to reproduce two figures from your website
> and include them within my thesis. These two figures include:
>
> - The 7-year BISON power spectrum, from the BISON home page
> - The pictorial examples of spherical harmonics, from the BISON background
> page.
>
> My university requires a letter of permission for each copyrighted figure
> used in my thesis. If you wish to give me permission to use the two
> figures discussed above, I ask that you please sent me a letter of
> permission to the address below.
>
> Thank you for your time.
>
>
> Sincerely,
>
> Kevin Brown
>
>
>
>
>
>
>
>
>
>
>
>
>
>

To: "Kevin Brown"
Subject: Re: Permission to reproduce figure and table

Dear Sir,

In answer to your request, we are pleased to inform you that you are authorized to reproduce :

Fig 2, Table 2, from Astronomy & Astrophysics, 390, 205-212 (2002)

The references of the source must be given. (title, year, issue)

Yours sincerely,

Permission dept

-----Message d'origine-----

>

To whom it may concern,

My name is Kevin Brown and I am currently a graduate student at the University of Western Ontario. I am currently finishing my Master of Science thesis in the research field of astroseismology. I am emailing the Astronomy & Astrophysics Journal in order to ask permission to reproduce a figure and table, and include them within my thesis. The figure and table are from:

Bouchy, F., & Carrier, F. 2002, A&A,"The Acoustic Spectrum of Alpha Cen A," 390, 205-212.
Figure #2
Table #2

My university requires a letter of permission for each copyrighted figure and table used in my thesis. If you wish to give me permission to use the figure and table discussed above, I ask that you please sent me a letter of permission to the address below.

Thank you for your time.

In

Sincerely,

Kevin Brown